



HAL
open science

Establishement of high-throughput in situ diffraction data measurement methods applied to biological samples

Igor Chaussavoine

► **To cite this version:**

Igor Chaussavoine. Establishement of high-throughput in situ diffraction data measurement methods applied to biological samples. Structural Biology [q-bio.BM]. Institut Polytechnique de Paris, 2020. English. NNT : 2020IPPAX015 . tel-03378798

HAL Id: tel-03378798

<https://theses.hal.science/tel-03378798>

Submitted on 14 Oct 2021

HAL is a multi-disciplinary open access archive for the deposit and dissemination of scientific research documents, whether they are published or not. The documents may come from teaching and research institutions in France or abroad, or from public or private research centers.

L'archive ouverte pluridisciplinaire **HAL**, est destinée au dépôt et à la diffusion de documents scientifiques de niveau recherche, publiés ou non, émanant des établissements d'enseignement et de recherche français ou étrangers, des laboratoires publics ou privés.



INSTITUT
POLYTECHNIQUE
DE PARIS

NNT : 2020IPPAX015

Thèse de doctorat



Establishment of high-throughput in-situ diffraction data measurement methods applied to biological samples

Thèse de doctorat de l'Institut Polytechnique de Paris
préparée à l'École polytechnique

École doctorale n°626 Ecole Doctorale de l'Institut Polytechnique de Paris (ED IP
Paris)

Spécialité de doctorat : Physique

Thèse présentée et soutenue à Gif-sur-Yvette, le 31 mars 2020, par

IGOR CHAUSSAVOINE

Composition du Jury :

Jean-Baptiste Charbonnier Cadre scientifique des EPIC, Université Paris-Saclay (IBC)	Président
Mirjam Czjzek Directeur de recherche, Sorbonne Université	Rapporteur
Stéphane Veesler Directeur de recherche, CINaM-CNRS	Rapporteur
Linda Miallau PhD, Institut de Recherche NovAliX	Examineur
Ahmed Haouz Directeur de plateforme, Institut Pasteur	Examineur
Gilles Ferry Chef du département de Chimie des Protéines, Institut de Recherche Servier	Examineur
Monica Spano Maître de Conférences, Université Grenoble Alpes (Institut de Biologie Structurale)	Examineur
Matthieu Réfrégiers Responsable de Ligne, École Polytechnique	Directeur de thèse
Léonard Chavas Responsable de Ligne, Université Paris Saclay	Co-directeur de thèse

Establishment of microfluidic-based high-throughput *in situ* diffraction data measurement methods applied to biological samples

Igor Chaussavoine

ABSTRACT (Fr)

Titre

Mise en place d'un système microfluidique de mesures de données de diffraction *in situ* à haut débit sur des échantillons biologiques

Mots clés

Microfluidique, diffraction, synchrotron, cristallographie, *in situ*

Résumé

Dans le domaine de la compréhension des molécules biologiques, la cristallographie aux rayons X est une des méthodes majeures. Elle permet de rapidement obtenir une structure 3D d'une molécule ou d'un assemblage de molécules en faisant interagir un cristal de cette molécule avec un faisceau de rayons X. Bien que l'opération soit d'une grande complexité, l'évolution de la technique depuis ses débuts à permis à des outils tels que la ligne de lumière PROXIMA-1 du synchrotron SOLEIL d'obtenir la structure 3D de centaines de molécules biologiques ou assemblages de molécules biologiques.

Cette méthode nécessite différentes étapes cruciales pouvant rendre difficile l'approche de certaines molécules. Parmi ces méthodes, l'expérience de cristallographie est cruciale. Elle fait interagir un faisceau de rayons X ionisant avec un cristal biologique extrêmement précieux et fragile. Cette étape est une course contre la montre entre la récolte des données et la destruction inévitable de l'échantillon. Pour permettre au cristal de survivre les quelques secondes / minutes de la collecte, ceux-ci sont refroidis à l'aide d'azote à des températures cryogéniques pour ralentir la diffusion de l'ionisation destructrice de symétries dans le cristal. La congélation de ces échantillons aqueux nécessite l'ajout de molécules qui protègent l'intégrité du cristal de l'expansion des molécules d'eau lors de leur congélation. L'ajout de cette molécule peut toutefois rendre difficile voir impossible la complexe étape de cristallisation des molécules. Pour contourner la cryogénéisation et les dommages de radiation, les expériences sont effectués sans cryogénéisation, dites *in-situ* et la course entre collecte et destruction est gagnée en effectuant des collectes sur un grand nombre de cristaux puis assembler les données obtenues jusqu'à obtenir la structure de la molécule.

Les méthodes actuellement utilisées, dite de serial crystallography, récupèrent une fraction infime des données requises sur chacun des cristaux, ce qui amène à une forte consommation d'échantillons difficiles à se procurer. Cette thèse présente une approche utilisant la microfluidique, permettant de placer et collecter automatiquement les cristaux biologiques sur un angle permettant de réduire drastiquement l'utilisation d'échantillons. Le but des travaux présentés est de mettre en place un système de mesures in

situ à haut débit, en tirant avantage des nouvelles avancées en développements de puces microfluidiques adaptées à des échantillons biologiques cristallins, en complément des approches robotiques mises en places sur la ligne PROXIMA-1. Les puces devront être munies de qualités particulières qui devront favoriser un chargement d'échantillons cristallins avec un minimum de stress externe ; supporter les environnement chimiques des échantillons ; disposer de manière périodique les cristaux tout au long de la puce ; être usinée dans un matériau permettant la prise de collectes de clichés de diffraction avec un minimum d'absorption et de diffusion en bruit de fond ; être adaptées au robot de changement d'échantillons opérationnel sur la ligne.

Les travaux présentés vérifient les capacités de la puce à répondre à certaines difficultés actuelles de la cristallographie, comme la sensibilité de certains échantillons ou l'acquisition expérimentale de la phase. De plus, elle examine les rapports directs que cette technologie pourrait avoir sur le domaine : Le trempage automatique de ligands, utiliser la maîtrise offerte par la microfluidique sur les mouvements de fluide et sur la mixité de ceux-ci est un plus permettrait un trempage précis et automatique des cristaux. Le confinement des échantillons, utiliser la puce microfluidique pour isoler la molécule du milieu extérieur permettrait une étude de molécules sensibles à l'oxygène par exemple, mais surtout permettrait une couche de protection primordiale permettant d'étudier des échantillons dangereux comme des virus. L'acquisition de donnée de diffraction d'échantillons in-cellulo, pour bénéficier de l'apport des mécanisme cellulaire de cristallisation de molécules.

ABSTRACT (EN)

Title

Establishment of microfluidic-based high-throughput in situ diffraction data measurement methods applied to biological samples

Keywords

Microfluidic, diffraction, synchrotron, crystallography, *in situ*

Abstract

In the field of biological crystallography, the solution commonly adopted to protect fragile samples from the X-ray beam is the freezing of the samples. Chemical treatment prevents water crystallisation, therefore the destruction of samples, but can be an obstacle to the crystallization of sensitive molecules. To circumvent this difficulty, the experiments are carried out at room temperature called *in-situ* using data coming from a large number of samples to circumvent the difficulties of radiation damage. The methods currently used, called serial crystallography, recover a tiny fraction of the data required on each of the crystals, which leads to a high consumption of rare samples. This thesis presents an approach, using microfluidics, allowing to automatically place and collect biological crystals on an angle allowing to drastically reduce the sample consumption. The aim of the work presented is to set up a high-throughput in situ measurement system, taking advantage of new advances in the development of microfluidic chips adapted to crystalline biological samples, in addition to the robotic approaches implemented on the PROXIMA-1 beamline. The chips will have to be provided with particular qualities which will favor a loading of crystalline samples with a minimum of external stress; withstand the chemical environment of the samples; periodically arranging the crystals throughout the chip; be machined from a material allowing the taking of diffraction collections with a minimum of absorption and background noise diffusion; be adapted to the operational sample changing robot on the line. The work presented verifies the capabilities of the chip to respond to certain current difficulties in crystallography, such as the sensitivity of certain samples or the experimental acquisition of the phase, and examines the direct contributions that this technology could have on the field, such as automatic soaking of ligands, confinement of samples, or allow acquisition of diffraction data on *in-cellulo* samples.

CONTENTS

Abstract (Fr)	2
Titre	2
Mots clés	2
Résumé	2
Abstract (En)	3
Title	3
Keywords	3
Abstract	3
Contents	4
Introduction	10
Actual state of macromolecular crystallography	10
Serial crystallography	11
Interest provided by microfluidic in macromolecular crystallography	14
Benefits of wedged serial crystallography	16
Material and Methods	19
Serial crystallography	19
Macromolecular crystallography	19
Proteins	19
Crystals of proteins	19
Protein crystallisation	20
Reference proteins	20
A glance in the crystallisation theory	20
Vapour diffusion	21
Batch crystallisation	22
X-ray crystallography	22
PROXIMA-1 beamline	24
X-ray source	24
Mechanic of synchrotrons	25
Generalities on a synchrotron	25
Synchrotron SOLEIL	27
PROXIMA-1 specificities	27

Experimental environment	29
Sample environment	29
Sample handling	31
Control command : MXCuBE	32
Data treatment : XDSme	32
Microfluidics	32
Theory	33
Laminar flow	33
Pressure drop	33
Hydro resistance	33
Analogy with electronic	34
Chip principle	34
Crystal trapping principle	36
Crystals	37
Chip creation	37
Instrumentation	37
Laserwriter	37
KloéDesign software	38
Plasma chamber	39
Corona ioniser	39
Pattern designs	40
Materials	40
Manufacturing steps	40
Spin-coating	41
Plasma bonding	41
Detailed procedure	42
Mold preparation	44
Chip characteristics	44
Sample injection	45
Constraints during injection	45
Injection techniques	45
Pressure controller	45
Depressurised and capillary injection	46
Peristaltic pump	46
Injection protocol	46
Chemical tests	47
Injection of coloured chemicals	47
Injection of glass beads	47
Injection protocols	47

Permeability towards oxygen	48
Chemical tests	48
Control experiments with ChipX3	48
Optional design for ligand injection	50
Specific microfluidic requirements	50
Chip modifications	51
Optional designs for cell trapping	52
Grid cell trapping	52
Adapted strategy for trapping	52
Chip preparation	52
Line cell placing	54
Design presentation	54
CATS chip manipulation	55
X-ray data collection	56
Chip mounting on the goniometer	56
In-situ Geometrically Optimised Raster scanning	56
Goal of the I.G.O.R. scanning	56
Scripted procedure	57
Coding details	58
MXCuBE implementations	60
Data collection	61
Chip Design, Tests and Results	63
Introduction	63
Design of the chip pattern	63
Improvement of the chip molding	64
Window creation	64
External mold	66
Thinner chips	66
Improvement of the chip environment	67
Chip handling	67
Chip support frame	67
Absorption studies	68
Preliminary absorption studies	68
Chip thickness	69
PDMS mount	70
Beam impact	71
Chip validation	71
Beam transmittance vs incoming beam intensity	72

Beam transmittance vs beam energy	72
Chip angle	73
In chip transmittance information	73
Validation of chip design	74
Chemical tests	74
Strategy for the tests	75
Effects of the chemicals on trapping	75
Permeability towards oxygen	76
Experiment on a kapton-PDMS chip V9	76
Control experiments with ChipX3	77
Conclusions	78
Ligand soaking microfluidic preliminary experiment for ligand screening	79
Interest of in-chip ligand soaking	79
Ligand soaking injection experiment	79
Results	79
Conclusions	80
General Issues	81
Injection process	81
Plunging challenges	81
Sedimentation issues	82
Challenges in crystal sampling	83
Challenges with the injection	84
Channel filling	84
Preloading	85
Unplugging	86
Annexe problems	87
Injection of air bubbles	87
Crystal clogging	88
Beamline adaptations	89
Beamstop and capillary	89
Cryostream	90
Three-points centering	90
Conclusions	91
Crystallography applications	92
Introduction	92
Wedge serial crystallography on test sample	93
Lysozyme	93
Crystallisation	93

Crystal loading	93
Data collection	94
Data processing and structure determination	94
Conclusions	96
Insulin	96
Crystallisation	96
Crystal loading	98
Data collection	98
Data processing and structure determination	98
Conclusions	98
Anomalous phasing using Insulin as an example	99
Contextual setting	99
Data collection	100
Data processing and structure determination	100
Conclusions	101
In vivo macromolecular crystallography	101
General context	101
Classical trapping	103
Crystal loading	103
Data collection	104
Data processing and structure determination	104
Conclusions	104
Alternative trapping results	105
Grid cell trapping	105
Line cell placing	106
Conclusions	107
Conclusions	107
Handling sensitive samples, example of Ribosome	108
Contextual setting	108
Crystallisation	108
Crystal loading	109
Data collection	110
Specific issues with Ribosome crystals	111
Conclusions	112
Protein/Ligand complex formation	113
human Quinone reductase 2	113
Contextual settings	113
Crystallisation approach	113
Crystal loading	115

Data collection	116
Data processing and structure determination	116
Conclusions	118
Conclusions	118
Conclusions and Perspectives	119
Annexes	123
Crystallisation solutions	123
hQr2 crystallisation tests	123
Commercial screens for chemical tests of chips	124
Protocols for chemical tests	125
Long injection protocol	125
Fast injection protocol	126
Tests on sample stability	128
Ribosomes injection experiment results	128
Tests against dissolution	128
Injection protocols	128
Absorptions studies	129
Chip Transmittance of the different chips	129
Chip transmittance depending on the position in the chip	130
List of chip patterns	131
Terminology and summary	131
Pattern V9	132
Pattern V11 : high trap density	133
Pattern V12 : variation in trap size	133
Pattern V13 : in-chip ligand injection	134
Pattern V14-V17 : ostromer-kapton chips	135
Pattern V18 : adaptation for needle objects	136
Pattern V19 : standardisation of the chip	137
Patterns V20-V22 : design optimisation	138
Injections difficulties during chemical tests	139
Proxima-1 beamline technical overview	140
List of Figures	141
List of Tables	144
Bibliography	145

INTRODUCTION

1. Actual state of macromolecular crystallography

In the context of molecular biology, the three dimensional structure of biological macromolecules is vital to identify their mechanical functions and interactions with their surrounding elements. As of 2020, more than 89% of the registered macromolecular structures in the protein data bank [[Protein Data Bank](#)] were obtained using X-ray crystallography (Fig. 1.1). Prior to these experiments, samples need to be prepared through a series of steps generally organised as follows (Fig. 1.2). First, the protein sample of interest needs to be produced, using majoritarily bacteria transformed by a DNA plasmid that will overexpress the protein of interest. In a second step, the molecules are purified from the other constituents of the production process. The homogeneous sample is then submitted to crystallisation screening, in order to identify conditions where the molecules are packed in a coherent periodic arrangement with 3D symmetries. Finally, the crystallised samples can be submitted to X-ray diffraction during crystallography experiments, consisting in exposing to a coherent monochromatic X-ray beam the crystalline sample. This produces a diffraction pattern, typically recorded at different angles to obtain near-atomic information on the three-dimensional conformation of the protein after structure determination.

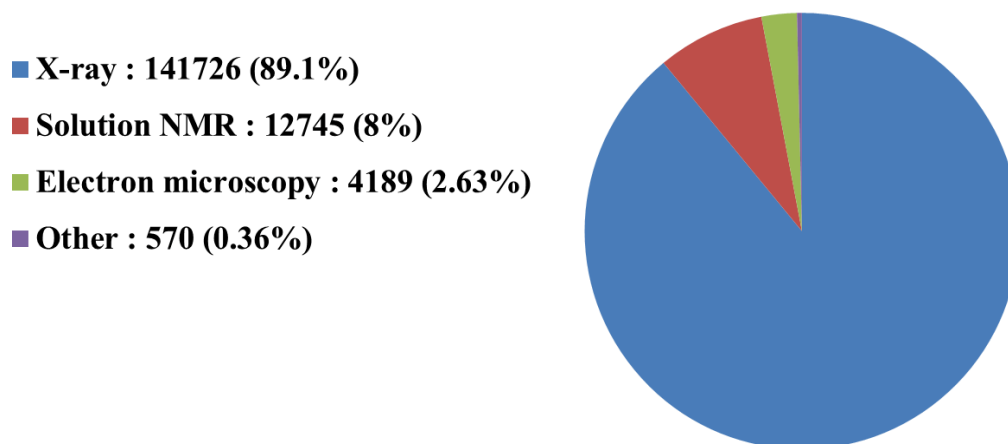
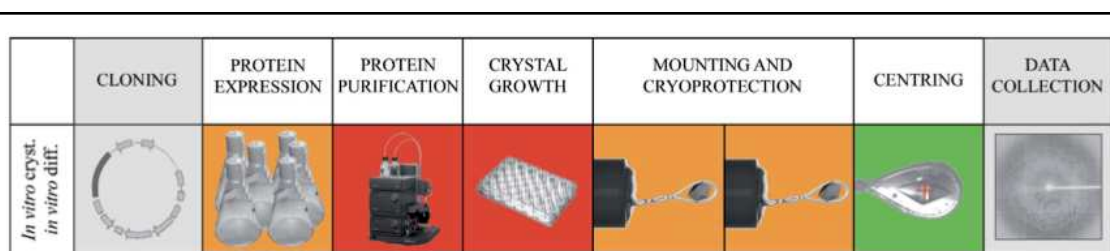


Figure 1.1 : PDB data distribution by experimental methods.

The graph shows the PDB statistics as of 13/01/2020 [[Protein Data Bank](#)].

The diversity and particular specificity of biological macromolecules regularly prevent one of the sample preparation or acquisition steps, caveat for the acquisition of data and resolution of their 3D structures. Among these issues, the chemical fragility of the molecules poses difficulties for the X-ray diffraction

step. The free radicals locally generated after the interaction of the X-rays with biological molecules propagate inside the crystal, eventually affecting the intermolecular contacts involved in the crystal lattice, thus destroying to some extents the symmetries within the crystal, which will participate in the degradation of the diffracting power of those crystals. To bypass this difficulty, the crystals are classically frozen to cryogenic temperatures in order to reduce the propagation of free radicals for the time of the experiment. Although radiation damages are mitigated when experimenting at lower temperatures, freezing crystalline samples may end up with the destruction of the crystal lattice due to the expansion of the water molecules during the freezing process. As a consequence, an additional preparation step emerges where the crystals need to be cryoprotected using specific chemicals. Eventually, the physical equilibrium of the macromolecules forming the crystal lattice may be altered, yet again degrading the diffraction power of the crystal, leading to a decrease in data quality or even the complete destruction of the crystal.



Inspired from Boudes et al Acta Crystallogr D Struct Biol 2016 fig. 1.

Figure 1.2 : Overall view of a classical sample preparation pipeline.

The table shows the common sample preparation steps towards macromolecular crystallography data collection. The color code indicating the overall success rate of the different steps shows *green* for high success rate, *orange* for medium success rate and *red* for low success rate, respectively (Bourne et al. 2016).

2. Serial crystallography

The macromolecular X-ray crystallography (MX) experiments require the acquisition of a large angle with a high angular resolution, leading to the recording of a magnitude of thousand images, mostly depending on the crystal symmetries. Originally defined for X-ray Free-Electron Laser (XFEL) sources, Chapman *et al.* developed and proposed a strategy of data collection that took into consideration the destructive power of the FEL X-ray pulses [Chapman]. In this approach, hundreds of thousands of crystals are exposed to X-rays, with only one diffraction image recorded *per* crystal. X-ray pulses at XFELs are very brilliant and less than 100 femtoseconds in length, faster than the propagation in the crystal of the free radicals generated by the X-ray pulses [Neutze]. Consequently, in this approach the XFEL beam interacts with the crystal, which diffracts before being damaged. The principle is referred to as *diffraction before destruction*, as it takes full advantage of the highly intense X-ray photon beam, with an average brilliance of $1.6 \times 10^{25} \text{ ph.s}^{-1}.\text{mm}^2.\text{mrad}^2$ (0.1% bandwidth) for the European XFEL, 10 000 times more brilliant than at synchrotrons. Such a high density of photons physically destroys the sample, however it also permits to obtain a signal over noise ratio from smaller crystals sufficient for data collection, even with small crystals and fewer symmetries. A direct consequence of the enormous amount

of diffraction images accumulated in this technique lies in the difficulties in analysing the data. Classically, it requires between 100 000 and several million crystal diffraction images to confidently pretend to solve a macromolecular structure. The advances and developments in the last decades of state-of-the-art technologies targeted towards these crystallographic measurements participated in the increase by several orders of magnitude of the data acquisition and data processing speeds. A non-exhaustive list of the equipment that benefited from these developments include an explosion in the data acquisition frequency of the X-ray detectors ; the quality and stability of the photon sources ; the power and calculation speeds of the processing computers. These evolutions now permit to record large amounts of data in order to obtain a crystal structure, and eventually to collect data on crystals at room temperature, opened to structure determination from multiple crystals and partially answering to the needs of serial crystallography.

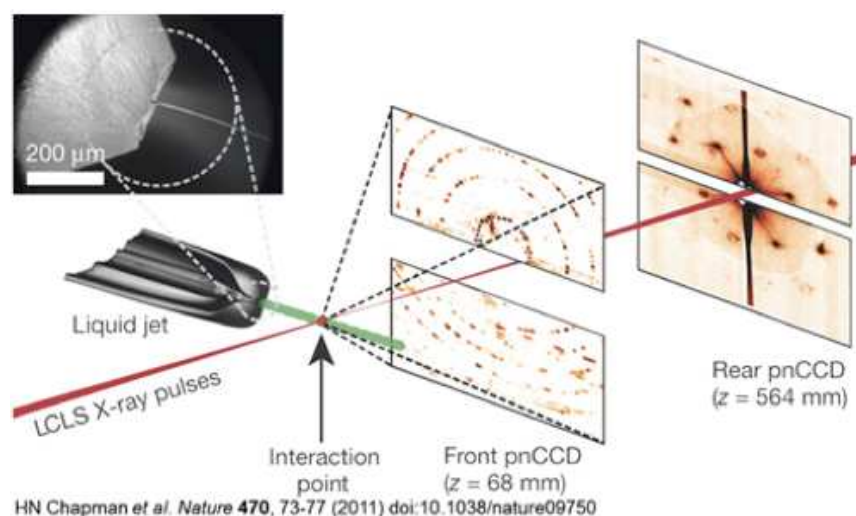


Figure 1.3 : Gas-dynamic virtual nozzle liquid jet for serial crystallography at XFELs.

A high pressure liquid jet brings micron-sized macromolecular crystals in the focus of a femtosecond pulsed coherent X-ray beam. The diffraction spots are here recorded on a CCD detector [[Chapman](#)].

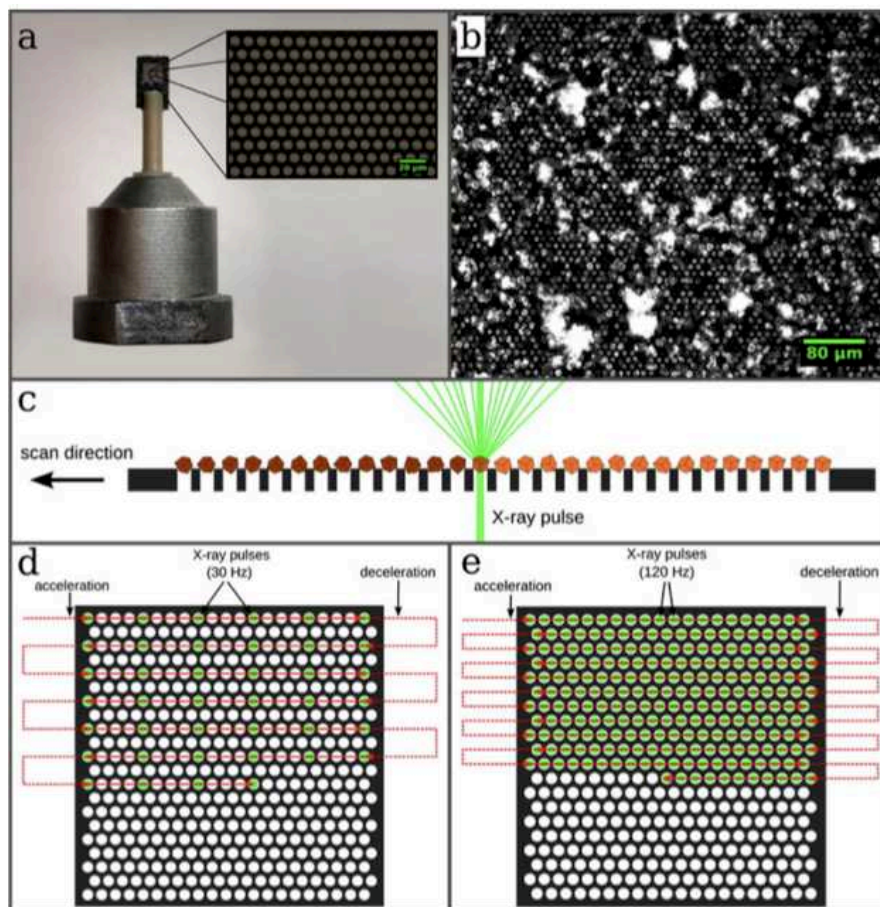
Considering the complexity of the experiments, and in order to properly bring the sample in focus with the X-ray beam, several delivery methods have been developed. The initial SFX experiments at XFELs involved the so-called gas-dynamic virtual nozzle (GDVN, [[DePonte](#)]) sample injector (Fig. 1.3), which presents the crystals in a thin liquid jet made of their growing medium surrounded by high pressure gas. The technique allows constantly delivering the crystalline sample at high speed, yet with a very small ratio of diffracted over injected crystals, typically less than one percent. Of serious advantage, the GDVN injection setup permits to perform time-resolved experiments when coupled with a visible light laser pump activating the samples before the X-ray intersection point, therefore prior to the diffraction process. A non-exhaustive list of sample delivery methods effective in 2015 include GDVN jet [[DePonte](#)], Electrospun jet [[Sierra](#)], LCP jet [[Weierstall](#)], Micromesh, acoustic delivery [[Roessler](#)] and micropattern chip [[Roedig](#)]. The common flag within these delivery techniques targets a reduction in crystal consumption (Table 1.2).

Some of these methods are of interest for synchrotron-based serial crystallography experiments, and have already been tested and implemented on multiple synchrotron sites. The method from Roedig *et al.* [Roedig] is developed upon a high speed fixed-target of a silicium-based microfluidic chip (Fig. 1.4). The principle is to synchronise a fast and precise goniometer to a high frequency pulse delivery X-ray source in order to diffract samples fixed within these targets. In order to place the samples in the beam focus, a drop containing the crystals is deposited at the top of the chip positioned horizontally. The crystals then fill the places in the grid by sedimentation. The chip is then mounted on a goniometer for later synchronisation with the X-ray beam. Through this method, when the X-ray beam interacts with multiple crystals, the information recorded show difficulties to be efficiently processed, pushing for the requirement to optimise the experimental procedure with the exposed locations within the chip that would need to contain only one crystal. In this specific design, the crystal placement method is stochastic, leading to the need for an optimised concentration to maximise the number of patterns occupied by only one crystal. In realistic cases, the crystal repartition leads to a hit rate at room temperature of 2% to 10%.

ADVANTAGES	DRAWBACKS
High throughput : 33.6 images second	Specific goniometer
Still images : low impact of radiation damages	Need hardware adaptations on the beamline
Adapted to synchrotron and FEL sources	Evaporation difficulties
Adapted to microcrystals	Still images : extended amount of data needed
Can operate with or without cryogenisation	Complexity in synchronising X-ray pulses with crystal patterns according to chip design
Low background images	Small crystal size range

Table 1.1 : Advantages and drawbacks of Roedig *et al.* in chip serial crystallography [Roedig].

The technique shows a high *crystal placed over crystal diffracted* ratio compared to the other sample delivery approaches mentioned above. Furthermore, it allows to experiment on either cryo-cooled crystals or at room temperature. It is a good representation of the design tendencies behind chip-based serial crystallography. Table 1.1 summarises the advantages and drawbacks of the technique compared to other crystallography methods. In order to improve data quality and open the field to a larger set of samples, we have chosen to concentrate on yet another method for crystal delivery, based on handling the samples through microfluidic devices.



Roedig et al, Nat Methods 2017 Aug; doi: 10.1038/nmeth.4335 fig.2

Figure 1.4 : Design of the micro-patterned silicon chip and data collection strategy [Roedig].

(a) The chip is attached to a plastic rod for the purpose of thermal isolation. The membrane part within the outer frame consists of micropores with diameters of typically 4 μm - 8 μm , which are arranged in a triangular grid. (b) The chip acts as a sample holder for more than 20 000 microcrystals, which largely organise themselves according to the pore pattern. (c) After being loaded, the microcrystals are scanned through the X-ray beam. By shooting through the micropores in the chips the interaction of the X-rays with any support material is further minimised. (d, e) Scanning strategies for measurements performed at room temperature and cryogenic temperatures, respectively.

3. Interest provided by microfluidic in macromolecular crystallography

Among the different sample delivery methods, a microfluidic sample delivery [Lyubimov] technique reduces the crystal consumption to the minimum necessary for collecting self-sufficient data sets. The technique consists in placing the crystals at known positions using a microfluidic trapping array (Fig. 1.5). It drastically enhances the crystal consumption efficiency while preventing the dehydration of the samples and performing the experiments at room temperature. As the technique only requires a small X-ray beam, it can be applied to either synchrotron or XFEL sources.

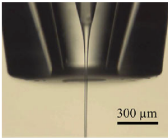
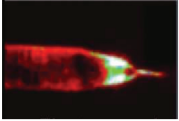
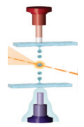
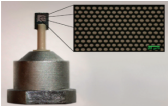
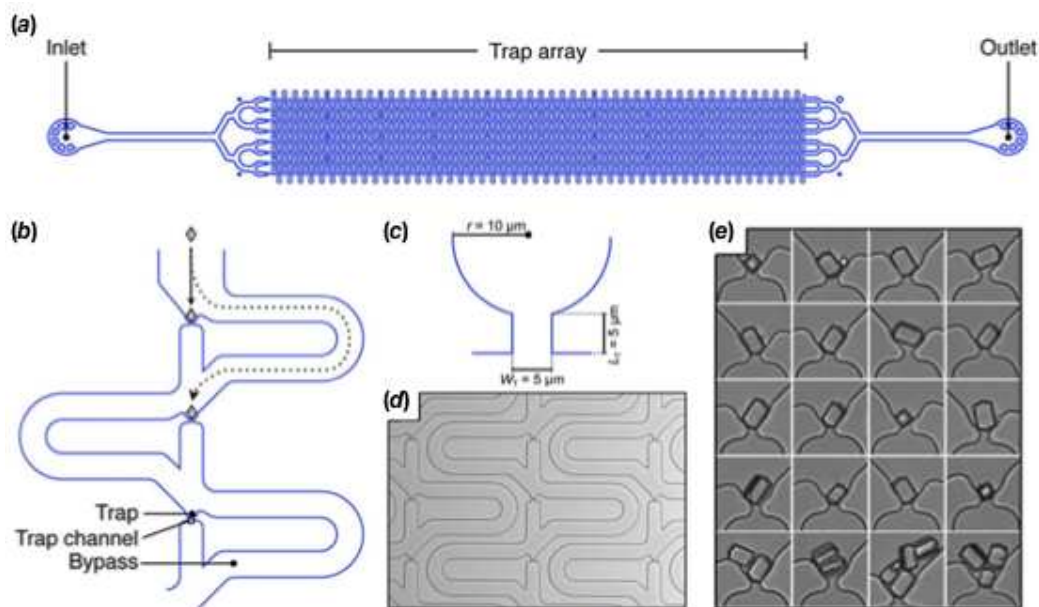
METHOD	EFFICIENCY	ADVANTAGES	LIMITATIONS
 GDVN jet	25 000 [DePonte]	Low background, crystals in native buffer	High sample consumption, possible clogging and bubbles, possible crystal damage
 Electrospun jet	500 [Sierra]	Low background, low flow rate	Require glycerol, impacts electrostatic charge on crystals
 LCP jet	500 [Weierstall]	Low background, low flow rate, lipidic cubic phase	Crystals must grow in lipidic cubic phase
 Micromesh	N/D	Rapid data collection, small sample size, fits standard goniometer	Freezing and cryopreservation required, need multiples devices for complete data set
 Drop-on-demand	2 [Roessler]	Precise sample delivery, crystals in native buffer	Solvent background scattering, evaporation
 Micropattern chip	11 [Roedig]	Precise sample delivery, crystals in native buffer	Evaporation

Table 1.2 : Sample delivery methods for serial crystallography experiments.

A comparative summary (inspired from [Lyubimov]) is shown for various existing liquid-jet and fixed-target sample-delivery methods used for serial femtosecond crystallography at X-ray sources. The column *Efficiency* represents an estimation of the average number of crystals *per* integrated images based on the information provided in the indicated references.

4. Benefits of wedged serial crystallography

As described above, *in situ* serial crystallography is a solution towards structure determination of macromolecular crystals while circumventing the difficulties emerging during cryoprotection and fishing of the crystalline objects. When applied at XFELs, it is common to sacrifice for the experiments large amounts of sample, which limits the access to critical and rare samples.



Lyubimov et al 2015. Acta Cryst. D71, 928-940. doi:10.1107/S1399004715002308 Fig.3

Figure 1.5 : A microfluidic trap array for protein crystals.

(a) Schematic representation of a microfluidic design for trapping crystals. (b) Close-up view of the general scheme for trap-and-bypass hydrodynamic crystal capture. (c) Schematic of a single hydrodynamic trap [labeled in (b); W_t stands for the width of the trap channel and L_t for the length of the trap channel]. (d) Representative section of a fabricated crystal-trapping chip. (e) Light-micrograph series showing single and multiple HEWL microcrystals immobilized in hydrodynamic traps.

The access to the microfluidic sample delivery method to acquire wedges of images *per* crystal forms a tempting option. In this approach, instead of obtaining one single still image *per* crystal, as it is common practice with most of the other sample delivery techniques, the microfluidic placement combined with precise handling of the chip at the beamline, would open to possibilities in recording complete wedges for each crystal, reducing by such the required amount of sample for obtaining a complete data set, thus minimising crystal consumption. To comply with these requirements, the chips will need to present specific qualities that will favor loading of the crystalline samples with a minimum of external stress ; have the crystals periodically placed throughout the chip ; be machined in a material allowing data collection of diffraction patterns with minimum absorption and scattering from the background ; be adapted to the operational sample exchange robot on the beamline and open to

possibilities of small molecule and ligand soaking of crystals, leading field in industrial pharmaceutical applications.

During preliminary studies, the proof-of-principle of the wedged-serial crystallography at synchrotrons was introduced [[Chaussavoine](#)], opening the beamline towards complementary sample delivery techniques. The current work was performed at the PROXIMA-1 beamline, fulfilling its requirements in terms of sample environment setup. In this context, a large part of the studies built upon the different advantages that the microfluidic wedged serial macromolecular crystallography could bring on different biological issues. Among these scientific issues, five case studies were approached.

- Molecules sensitive to manual handling, chemical variations or temperature drifts bring their own difficulties in the preparation steps prior to X-ray diffraction experiments. Microfluidic-based serial crystallography can assist in resolving the destruction processes and therefore permit optimising sample preparation conditions at a later stage.
- Diffraction experiments gather information on the 3D structure of a macromolecule, but lack the phase information crucial to calculate the structure. Various methods lead to the obtention of the phase information. Among them, the anomalous dispersion phasing access to the information by using small intensity differences between data acquired at selected energies. As the microfluidic add diffusion and absorption disrupting the information quality, it is of interest to measure the impact of the microfluidic chip on the anomalous data acquisition.
- The *in cellulo* crystal growing approach is one of the state-of-the-art technology for the crystallisation of biomolecules directly from their natural environment. In this approach, only a small percentage of cells witness these crystal growing events, leading to difficulties isolating the crystal-containing cells prior to perform MX experiments. Here, microfluidics could help in screening a large amount of samples, hence circumventing the difficulties in isolating cells.
- Molecules sensitive to external stresses would benefit from microfluidic handling. As an example, crystals of large macromolecular complexes are often suffering physical and chemical manipulation while being prepared for cryo-protection and cryo-conservation prior to the X-ray diffraction experiments; microfluidic-based handling would avoid stringent stress on those samples. Similarly, oxygen sensitive molecules could be prepared in a concealed environment prior to transport to the beamline and diffraction experiments, and virus manipulation on the beamline would be facilitated with a sealed sample delivery device.
- In an attempt to engineer new therapeutics, or with the goal to gain further medical knowledge on the structural conformation behind complex formation between a macromolecule and its ligand partner, the technique of ligand screening appears as a common method to confirm the interaction mode of a particular protein with a series of potential target molecules, applying crystallography towards the end of the pipeline for the structure determination. In this repeated process where each protein-ligand complex has to be manually handled and prepared for X-ray diffraction

experiments, microfluidic chips can drastically automate the technique when performing in-chip crystal soaking with several ligands.

The above questions are broad and much too complicated to be fully answered in a single thesis. Yet, while investigating the potential application of the microfluidic devices developed at PROXIMA-1 compelling results were obtained confirming the strong expectations manifested towards the field of microfluidics. The current works on microfluidic driven XFEL crystal delivery [[Martiel, Grünbein, Ren](#)], on crystal growth within microfluidic chips [[Dhouib, Wijn](#)] or on plate screening [[Bingel-Erlenmeyer, Le Maire](#),] would yet be another field of interest for the crystallographic community. The topic being vast and largely explored, we decided to concentrate on developing a method using microfluidic and automation for samples already crystallised and readily available for optimised serial crystallography experiments on synchrotron beamlines.

MATERIAL AND METHODS

1. Serial crystallography

1.1. *Macromolecular crystallography*

1.1.1. Proteins

Proteins are biological macromolecules formed by chains of amino acids. By regulating a plethora of cellular events, proteins are considered as highly important molecules within the cells. A second key function of proteins lies in their structural or mechanical properties. Proteins maintain the architecture and the internal organisation of cells, notably permitting intracellular dynamical events (*e.g.* movements of compartments), or even pushing the cells to move in their surroundings. A protein can also take the role of an antibody, transport others proteins, and many more functions too numerous to be detailed here. The diversity and the multiple roles of proteins for the survival of cells make them an essential category of molecule to study. Moreover, the absence or malfunction of essential proteins eventually bring cellular anomalies, making them a potential target of modern medicine. The specific three dimensional folding of proteins dictates their shape and related functions. Where in enzymes it will bring close together catalytic residues, the folding will open pores for creating fluid channels in membrane proteins. As a consequence, the study of the three dimensional structure of proteins becomes crucial in order to better understand their function. The structural characterisation of a macromolecule at sub-nanometric resolutions emerged from the developments of several methods, among which nuclear magnetic resonance (NMR) spectroscopy, cryo-electron microscopy, and X-ray crystallography. In the current studies, we will focus on the applicability of microfluidic devices for macromolecular X-ray crystallography.

1.1.2. Crystals of proteins

A crystal is a periodical arrangement of motifs distributed in three dimensions. The motif could be an atom, a small molecule made of multiple atoms, or bigger organic molecules such as proteins, protein complexes or even viruses. Depending on the nature of the motif composing the crystal, various panels of interactions are found such as covalent bonds (*e.g.* in diamond) or weaker interactions like in biological crystals. The weak crystal contacts encountered in protein crystals result in difficulties when crystallising and maintaining the crystals stable. Moreover, the protein crystal is also weakened by large solvent channels present between the proteins constituting the crystal. Practically, crystals have to be continuously restrained by a precipitant solution, without which the contacts among proteins become

loose, affecting their stability and the crystal contacts, therefore causing the crystals to lose their properties.

1.2. Protein crystallisation

1.2.1. Reference proteins

Microfluidic chips were developed for and tested with macromolecular crystals. For this purpose, three reference proteins were crystallised, as developed in the crystallisation protocols below.

Lysozyme is a well characterised protein, comfortable to work with due to its faculty to crystallise in various conditions, including the batch method. Lysozyme is considered as the standard when developing new diffraction techniques or new crystal handling approaches. As such, it appears as a good choice for the present studies and for the proof of principle.

Insulin is also well characterised. The protein crystallises in batch, and presents some naturally occurring heavy atoms. Using Insulin, anomalous data collection and structure determination can be confirmed without further sample modification.

Qr2 is used as a reference protein for small molecule screening in pharmaceutical companies, notably at SERVIER. In the current studies, human Qr2 was used for testing the microfluidic chips targeting ligand screening. Additionally, *hQr2* crystals grow in needle shapes, yet another challenge for the crystal injection steps. Finally, *hQr2* crystallises better using the vapour diffusion method, in small drops. Thus, working with *hQr2* allows optimising the injection process from samples initially prepared in drops, a difficult task on its own.

1.2.2. A glance in the crystallisation theory

The process of crystal growth for macromolecules is complex but can be summarised in a sequence of two major events : nucleation and crystal growth. In practice, the molecule is first diluted in a solution where it remains soluble and stable. Some chaotropic agents, usually known as precipitants are then added to the solution, forcing the molecules to locally concentrate. The strategies towards proper crystal formation and further maturation will depend on the nature and fragility of the link among the biological molecules, the kinetic of the nucleation and crystal growth. Depending on how the molecule responds, different procedures are used to attain the supersaturated state and then the nucleation zone (Fig. 2.1). When the nuclei form, the crystals grow until the concentration of the molecules drops under the supersaturation state. Because of the high complexity of the macromolecules, precise theoretical solution models that would permit their crystallisation are impossible to establish. In order to estimate the nucleation conditions, large commercial screens are used to test a wide range of crystallisations solutions. When one condition shows nucleation, a series of surrounding conditions are then tested in order to optimise the crystal formation, growth and diffraction quality. Among the modified conditions are temperature, acidity, precipitant concentration, and molecule concentration [[Chayen](#)].

1.2.3. Vapour diffusion

Vapour-diffusion methods involve an aqueous drop containing the protein and the crystallisation agents in undersaturation. Typically, drops of 0.1 to 2 μL are set, depending on the crystallisation strategy adopted. After sealing the reservoir containing the precipitant solution, the volume of the drop will equilibrate against the concentrations in the reservoir solution. Consequently, the crystallisation condition will concentrate until equilibrium is reached. During the diffusion process (in which both chaotropic agents and protein concentrate), a single crystallisation trial proceeds through a range of conditions, thereby conducting to a self-screening process (Fig. 2.1, dashed curve B).

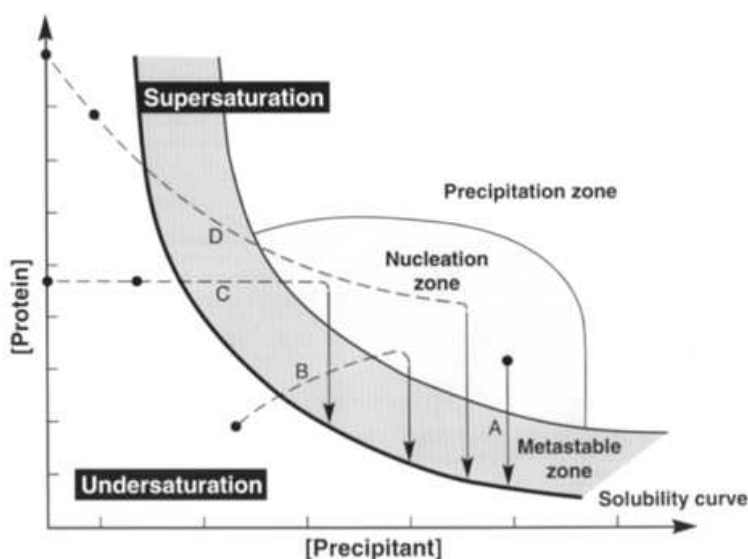


Figure 2.1 : A schematic drawing of a protein crystallisation phase diagram based on two of the most commonly screened parameters : proteins and precipitant concentrations.

The four major crystallisation methods, namely (A) batch crystallisation ; (B) vapour diffusion ; (C) dialysis ; and (D) free-interface diffusion (also known as liquid-over-liquid diffusion) are highlighted showing that in order to produce crystals, all the systems need to reach the same destination, namely the nucleation zone, after which they travel through the metastable zone and eventually arrive at the solubility curve. Each method achieves this journey *via* a different route. Filled dots (•) represent the starting conditions. In the case of dialysis and free-interface diffusion two alternative starting points are shown since the undersaturated protein solution can contain solely protein or alternatively, protein with a low concentration of precipitating agents [Chayen].

***hQr2* crystallisation.** The vapor diffusion method was applied on *hQr2* for crystallisation in plates using both the sitting and the hanging drop techniques. For the sitting drops, attempts of crystallisation were screened manually by mixing 1 μL of the crystallisation solution with 1 μL of the target molecule in IQ crystallisation plates (TTP labtech), after disposing 70 μL of the crystallisation solution into the reservoir. The Mosquito® (TTP labtech) crystallisation robot was also used for automated crystallisation setup, mixing 0.1 μL of the crystallisation solution with 0.1 μL of the target molecule. For the hanging drops, the VDX crystallisation plates (Hampton Research) were used for manually setting up drops of

1 μ L crystallisation solution and 1 μ L of the target molecule. The reservoirs were filled with 1 mL of crystallisation solution. All of the crystallisation screenings were realised and incubated at 20°C.

Two crystallisation conditions were refined for *hQr2*. *Condition A* consisted of a crystallisation solution composed of 1.4 M ammonium sulfate ; 100 mM Hepes or Bis-Tris, pH 7.0, mixed with the protein concentrated at 21 mg/mL (sample batch 6His-*hQr2*/pet28). *Condition B* consisted of a crystallisation solution composed of 1.645 M ammonium sulfate ; 100 mM Hepes, pH 7.25, mixed with the protein concentrated at 20 mg/mL (sample batch *hQr2*Pool2_01/20th/12).

1.2.4. Batch crystallisation

In the batch crystallisation method, the protein to be crystallised and the chaotropic agents are mixed to their final concentrations. Supersaturation is thus achieved upon mixing, and conditions only change as protein comes out of solution into the growing crystals. There is less exploration of the phase diagram, and consequently, several microbatch trials may be required to replace a single vapour-diffusion experiment. The batch method is associated with the use of large quantities of material, and hence it is not widely adopted. The introduction of the microbatch technique, where the crystallisation samples are dispensed as small drops under oil, has overcome the requirement for large quantities of materials, as well as some other difficulties (discussed below) arising from diffusion methods. The batch crystallisation method was applied to both Lysozyme and Insulin proteins.

Lysozyme crystallisation. Two solutions were mixed, consisting in a stock of Lysozyme (120 mg/mL w/v HEWL ; Sigma/Aldrich) diluted in 50 mM acetate and a precipitant solution made of 1 M NaCl ; 35% Ethylene Glycol ; 12.5% PolyEthylene Glycol-3350 ; and 50 mM NaOAc/HOAc, pH 3.5. The two solutions were incubated in ice before mixing a 1:3 ratio (typically 1 mL Lysozyme solution and 3 mL precipitant solution). The mixture was then incubated at 10°C for 15 hrs before being stored at -20°C after checking the size distribution of the crystals under a microscope.

Insulin crystallisation. The final crystallisation solution consisted of 10 mM HCl ; 50 mM Na Citrate ; 15% Acetone ; and 6 mM Zinc Sulfate. Insulin powder (2 mg ; Sigma/Aldrich) was dissolved in 400 μ L of the crystallisation solution lacking the 15% Acetone, and incubated at 50°C for 20 min. Acetone was then added to obtain the final 15% concentration. After a second incubation of the crystal solution at 50°C for 20 min, the reaction was quenched at 20°C for 6 hrs. The solution was then stored at 4°C.

1.3. X-ray crystallography

In order to determine the three dimensional arrangement and structure of the motif in a crystal (an atom, an ion or a macromolecule such as a protein), the approach favoured in these studies is X-ray diffraction, principle that obeys the Bragg's law (Fig. 2.2). In this technique, the crystals are irradiated with X-rays, resulting in the generation of a diffraction pattern composed of the incident beam and diffracting waves at various angles. The incoming X-rays will interact with the electrons of the atoms, diffusing in all directions with an intensity that will depend on the amount of electrons composing the

atoms, and the number of periodic entities making the plane. The diffusing X-rays interact with each others in a constructive interference when the conditions satisfy the Bragg's law :

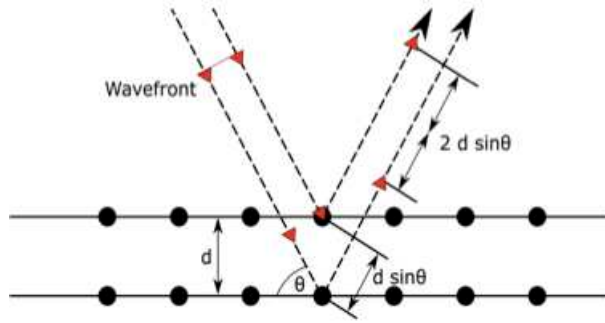


Figure 2.2 : Illustration of the Bragg's law.

The illustration is the classical Bragg representation of equation 2.1. In the figure, d stands for the distance between two lattice planes in a crystal ; and θ is the angle between the incident beam and the lattice plane.

$$n \lambda = 2d \sin \theta$$

(eq 2.1)

with n a natural number, λ the wavelength of the incoming wave, d the distance between two lattice planes, and θ the angle between the incident beam and the lattice plane.

In order to facilitate the representation and understanding of the diffraction principle, a geometric construct represented as a sphere (the Ewald sphere) takes into account the reciprocal lattice of the centered crystal. By definition, the Ewald sphere has a radius equal to the inverted wavelength $1/\lambda$. Through the Ewald sphere, and tightly related to the Bragg's law that defines the diffraction conditions, it is possible to determine the lattice planes that causes the diffracted signal for the wavelength used. Taking the above into account, diffraction will happen only for all the reciprocal lattice points sitting on the surface of the Ewald sphere.

Each recorded reflection will correspond to a precise point of the reciprocal lattice, thus representing a (diffracting) wave with an amplitude and a relative phase. The phase of the diffracted beams is directly related to the orientation of the crystal. While performing X-ray crystallography experiments, the diffracting photons are recorded and eventually counted on an X-ray detector, which will regroup all the amplitude information ; the phase-related information, however, is lost in the process. Moreover, due to the nature of the diffraction waves, the intensities and phases of the beams diffracted *via* the Bragg's law, correspond to the Fourier transform of the distribution of the electron density within the crystal. The electron density of a diffracting object can be described by a Fourier transform [Drenth] :

$$\rho(x, y, z) = \frac{1}{V} \sum_h \sum_k \sum_l |F(hkl)| \exp[- 2\pi i(hx + ky + lz) + i\alpha(h k l)]$$

(eq 2.2)

In equation 2.2, $\rho(x, y, z)$ represents the electron density ; V the volume of the crystal ; x, y, z the three space coordinates ; h, k, l the position of the molecule in the three axes of the crystal ; and $\alpha(hkl)$ the phase angle to be determined. $\rho(x, y, z)$ is expressed as a Fourier transformation of the structure factors $F(hkl)$. The amplitude of these structure factors is obtained from the intensity of the diffracted beam after application of certain correction factors :

$$I(hkl) \sim |F(hkl)|^2 \quad (\text{eq 2.3})$$

The remaining unknown, the phase $\alpha(hkl)$, can be retrieved by various approaches, the explanation of which are beyond the scope of this thesis. The main interest this work concentrates on is related to the quality of the structure factors that could be collected from macromolecular crystals, which will have a direct impact on the quality of the final structures that can be solved.

More specifically, the energy contained in each X-ray photon will be deposited on the crystal, and converted into entropic disruption of the crystal directly related to the brilliance of the incident beam and to its intensity and the incoming energy / wavelength. The degradation of the crystal and sample within will be proportional to the dose deposited. A direct consequence of these X-ray induced damages lies in the disruption of the crystalline arrangement, therefore affecting the diffraction capabilities of the crystal. Thus, to collect high quality structure factors will be a compromise between the number of photons interacting with the crystal and its sensitivity to X-ray. In order to reduce the speed of the expansion of the radiation-induced degradation, biological samples exposed to strong X-ray sources are classically handled at cryogenic temperatures. By doing so, the formation of free radicals that spread inside the crystal is locally restrained for longer time-scales usually sufficient to record useful X-ray diffraction data. Nevertheless, in addition to the fact that it does not prevail radiation damages to occur, prior to working at cryogenic conditions, crystals need to be treated adequately, often resulting in crystal lattice disruption.

2. PROXIMA-1 beamline

2.1. X-ray source

In order to generate the X-rays used in macromolecular crystallography, highly energised and charged particles are deviated, giving rise to a loss of energy in the domain of X-rays (in the present case). In X-ray tubes or in accelerators (linear or synchrotrons), electrons are accelerated and then deviated. A non-exhaustive list of the advantages of synchrotrons over the other techniques include the possibility to modulate the wavelength of the beam ; the low divergence ; and the high brilliance provided by these machines. Taken all together, the combination of these characteristics allows obtaining a virtually parallel X-ray beam, which permits studying large objects, notably important when performing diffraction-based experiments.

2.1.1. Mechanic of synchrotrons

A synchrotron is a particle accelerator arranged in a cyclic structure (Fig. 2.3). An initially charged particle is first accelerated close to the speed of light through a linear accelerator. The particle will then enter a storage ring, where it will be regularly accelerated within a straight section to gain energy, before being deviated from its forward direction to maintain a nearly circular shape. The geometry of the synchrotron permits to boost and recycle multiple times the charged particles using the same instruments. There are two major types of synchrotrons : colliders, such as the Large Hadron Collider developed for collision studies of two highly energetic particles ; and light sources that accommodate a series of equipment such as bending magnets, wigglers and undulators to accelerate electrons and optimise the use of the synchrotron effect that produces photons. When a charged particle is deviated from its linear trajectory, it will emit electromagnetic radiation waves that can be exploited at dedicated instruments developed for the studies of specific samples.

2.1.2. Generalities on a synchrotron

The synchrotron can be separated into several components as follows (and in reference to Fig. 2.3) :

1. **Electron gun.** The electrons used to form bunches are extracted from the combined action of heating a plate of heavy metal (tungsten at Synchrotron SOLEIL) and applying a strong electric field.
2. **Linear accelerator** or LINAC. The electrons are then packed in bunches and get their first acceleration, coming to a velocity near the speed of light before injection into the booster ring.
3. **Booster ring.** This ring consists of a small circular accelerator that boosts the bunches of electrons to a nominal energy in the order of GeV for third generation synchrotrons (2.75 GeV at Synchrotron SOLEIL).
4. **Storage ring.** This larger ring has two main purposes : to store electrons and preserve their energetic properties ; and to emit synchrotron light to dedicated instruments. The storage of the electrons is realised by running through three major components :
 - a. **Bending magnets** (*red* in Fig. 2.3) are used to bend the electron bunches coming out of straight lines. A direct consequence here is that the curving of the storage ring is not continuous but originates from a series of consecutive curved and straight lines. When passing through the bending magnets, the electrons change direction and emit synchrotron light of small brightness but over a large energy spectrum that can be used by some beamlines.
 - b. **Focusing magnets** (*green* in Fig. 2.3) are magnetic optics used to maintain the electron beam stable and focussed.
 - c. **Accelerating cavities** compensate the energy loss of the electron bunches after passing through the bending magnets, for the electrons to maintain their nominal velocity and

energy.

5. **Insertion devices.** These elements are classically made of series of alternate magnets in the middle of designated straight segments producing a sinusoidal magnetic field curving the electron path periodically and to emit intense synchrotron radiation. There are two types of insertion devices that differ from their magnetic geometry and therefore optical properties :
 - a. **Wigglers** oscillate the electrons over a large magnitude, resulting in a spectrum of wavelengths with a Gaussian distribution.
 - b. **Undulators** oscillate the electrons over a smaller magnitude when compared to wigglers. Coupled to a phenomenon of resonance among the emitted light, it results in the emittance of discrete wavelengths with high brilliance.
6. **Beamlines.** The instruments designed to take advantage of the beam generated by the insertion devices or bending magnets can be divided into three main sections :
 - a. **Optical hatch**, where optical equipments are used to craft the beam.
 - b. **Experimental hatch**, where the conditioned beam interacts with the sample studied.
 - c. **Control cabin**, where all the instruments can be remotely operated and the experiments piloted.

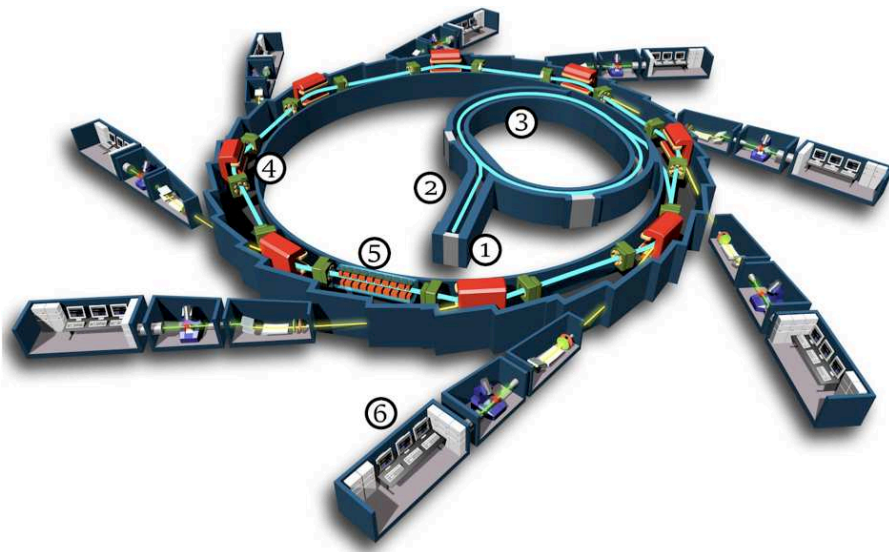


Figure 2.3 : Simplified scheme of a classical synchrotron layout [SOLEIL].

The critical parts are described in the text and consist of : (1) Electron gun ; (2) Linear accelerator or LINAC ; (3) Booster ring ; (4) Storage ring ; (5) Insertion devices ; (6) Beamlines.

2.1.3. Synchrotron SOLEIL

Synchrotron SOLEIL is the French synchrotron. The energy of the electron beam in the storage ring is 2.75 GeV. When compared to other synchrotron sources, Synchrotron SOLEIL is optimised for soft X-rays (10 eV to 10 KeV or 100 nm to 0.1 nm). Twenty-nine beamlines are distributed around the storage ring and provide access to wavelengths from the terahertz (~1 mm or 0.01 eV) to hard X-rays (100 keV or 0.01 nm). Each instrument or beamline is designed and optimised for particular types of experiments applying X-ray diffraction, spectrometry, imaging, etc.

BEAMLINER	PROXIMA-1 [Asconte]	PROXIMA-2A [Duran]	MASSIF-1 [Bowler]	I02 [Sandy]
Synchrotron	SOLEIL	SOLEIL	ESRF	DLS
Brilliance (v/ sec)	1.4×10^{11}	3.5×10^{12}	3×10^{12}	1.5×10^{12}
Divergence (μ rad)	< 350	< 350	< 104	< 100
Energy range (keV)	6.5 - 15.0	6.0 - 18.0	12.8	7.0 - 18.0
Beam size (μ m ²)	40 x 20	10 x 5	100 x 100	80 x 15
Max resolution (Å)	< 0.8	< 0.6	0.9	1.09
In situ access	Yes	Yes	No	Yes
Automation	Partial	Partial	Full	Full
Detector	EigerX-16M	EigerX-9M	Pilatus3-2M	Pilatus-6M
Image weight (Mb)	6	3	4	6
Collect speed (Hz)	100	40	31	13

Table 2.1 : PROXIMA-1 beamline compared to other representative beamlines.

2.1.4. PROXIMA-1 specificities

Macromolecular X-ray crystallography (MX) beamlines are specialized in measuring X-ray diffraction data from crystals for structural biology studies. The crystals are made of large molecules, like proteins, nucleic acid, alone or coordinating lipids and/or sugars, or complexes from combinations of

those. MX beamlines differ on specific implementations such as the beam size, divergence, or energy spectrum. Due to their success, MX beamlines are nowadays highly automated, taking advantage of diagnostics for beam stability and robot-assisted automation for sample replenishment. PROXIMA-1 (PX1, [Ascone]) is an MX beamline characterised by a nearly parallel X-ray beam and high-speed data collection (Table 2.1).

Diffraction experiments at PX1 and most other MX beamlines worldwide are performed under cryogenic conditions to delay the impact of radiation damage on the crystal. Furthermore, in order to collect sufficient data to cover a complete Ewald sphere, the sample must be rotated over a certain degree of oscillation, resulting in an acquisition time that takes a few minutes at the fastest. In order to manipulate the crystal at the beam interaction region, a 3-axes goniometer allows manipulating sample holders often from the SPINE European standard [Romoli] in which the crystals are usually held. Automation in sample mounting through the use of a robotised sample exchange system requires storing the cryogenized crystals in *UniPuck* storage cassettes [Cohen] kept in liquid nitrogen. The Dewar container permits to store up to three UniPucks (48 samples) in one round of experiments, certifying their cooling. On the goniometer, crystalline samples are kept under a flow of gas nitrogen at approximately 100 K.

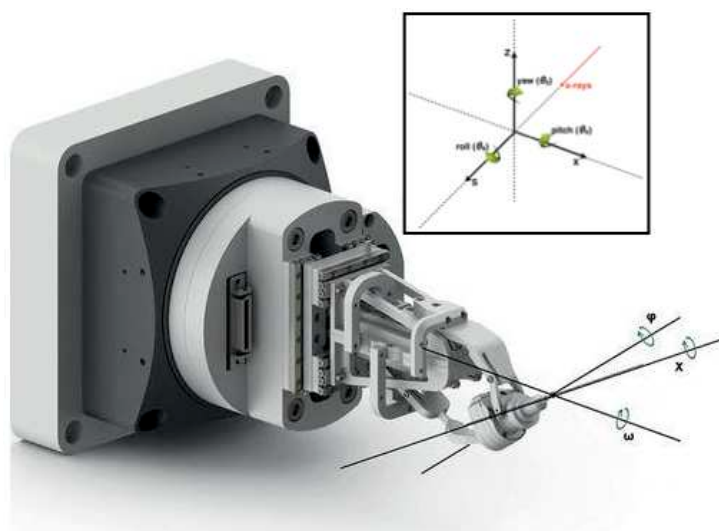


Figure 2.4 : Sketch of the SmarGon [SmarAct] goniometer with the different rotation axis.

The SmarGon can place a sample in the three X, Y and Z dimensions with a precision of ~ 5 nm. The sample can rotate through an ω rotation aligned with the X-axis. Two additional rotation axes are present : the φ axis co-directional to the ω rotation when the third rotation axis, χ , is equal to zero. Although ω and φ are open-loop rotation motors, χ is limited in its oscillation from the angle of 0° to 90° . The spheres of confusions for all the three rotation axes are below $3 \mu\text{m}$, and below $1 \mu\text{m}$ for the ω rotation.

2.2. Experimental environment

2.2.1. Sample environment

The sample environment is a critical part of the beamline directly surrounding the sample. In the following paragraphs, the components of the sample environment at PROXIMA-1 will be described ; different sample environments, more specific to other end-stations, will have complementary properties but are not developed here. For clarity purposes, the beamline orthogonal reference system will be used, with the S-axis representing the axis in the direction of the beam, the X-axis the horizontal axis perpendicular to the S-axis, and the Z-axis vertical (*inlet* in Fig. [2.4](#)). Only the beamline components used in these studies will be described (Fig. [2.5](#)).

Beam-stop : a tungsten bar accommodated in the beam path between the sample and the detector. The beam stop is used to stop the incident beam and therefore part of the air-diffusion that would happen would the incident beam propagate up to the surface of the detector. The size of the beamstop is optimised to block the incident beam, yet allowing to collect the low angles. Eventually, its angular size can be tuned by adjusting its distance from the sample position on the S-axis.

Capillary : a 0.2 mm inner diameter capillary is located as close as physically possible (typically 10 mm) of the sample, in the X-ray direction and before the sample position. The capillary is used to enhance the effects of the incident beam by removing most of the background generated by air scattering from the interaction of the incident beam with upstream equipment.

Goniometer : to facilitate sample positioning to the X-ray interaction point, the goniometry system at PROXIMA-1 adopts the Chi-geometry (Fig. [2.4](#)) to favour centring around three rotation axes. The goniometer consists of a clever combination of motors that will permit handling and manipulating the pin loops with high precision. The sample is secured on the goniometer head through an electromagnet that can carry objects weighing up to 50 g. Any sample holder fulfilling the mass limitations and presenting an adequate metallic connector [[SmarAct](#)] can be handled by the goniometer.

Sample exchange robot : robotised arm used to transfer the samples from their stored location to the goniometer head. The major application of the robot targets crystals mounted on pins, frozen and immersed into liquid nitrogen. At PROXIMA-1, the sample pins are kept in container cassettes of the *UniPuck* geometry [[Cohen](#)], with 16 pins *per* cassette that can be loaded. Three of these cassettes may be placed inside a Dewar storage accessible by the robot, providing a capacity to handle 48 pins for one Dewar loading. The robot has been developed to automatically pick a selected pin and mount it onto the goniometer head. Eventually, it will replace this pin with a fresh sample, always at cryogenic temperatures in order to avoid warming up the frozen crystals.

Cryostream : cold nitrogen stream focused onto the sample in order to maintain the temperature of the experiment constant and most of the time at around 100 K. To avoid cold-air turbulence, the nitrogen stream is surrounded by a thin film of dried-air at room temperature. The control of the nitrogen stream can be precisely tuned, eventually setting warm temperatures depending on the experiments. The position of the solid tip of the cryostream cane is adaptable to an optimised orientation, ideally aligned on the crystal and placed at around 7 mm of the sample. To adapt *in situ* experiments, a motorised axis removes the cane further away, allowing for mounting more voluminous sample holders on the goniometer head. Additionally, during *in situ* experiments, the cryostream temperature is classically tuned for room temperature and retracted in the far position to avoid condensation droplets on the chip.

On-axis visualisation camera (OAV) : camera mounted on a microscope centered at the focus point of the beamline. The OAV is placed in the path of the X-ray beam. A 45° holly mirror allows the camera to sit in the direction of the beam, thus to visualise the sample in the orientation it will be exposed to the X-rays, yet without interfering with the propagation of the direct beam. Light is illuminating the sample through the combination of LED blobs shining on a parabolic mirror to benefit from homogeneous illumination on the sample.

Initially designed for one type of sample holder [[Romoli](#)], the sample environment at PROXIMA-1 went through several iterations and optimisations that currently provides room for adapting various types of experiments. Thus, microfluidic chips surrounded by a 3D-printed frame have been designed to fit within the tight sample environment described above. The chip (dimensions of 30 x 40 x 5 mm³) should evolve with all the equipment necessary for the diffraction experiments yet without physically colliding with any of these components. While rotating around the X-ray interaction point, the chip will have to avoid the beam-stop, the capillary, the OAV and the cryostream nozzle. Their relevance during the diffraction experiments explain their absolute requirement, therefore causing the chip's handling to be delicate, which imposes strict protocols to apply, in order to prevent any unwelcome collision.

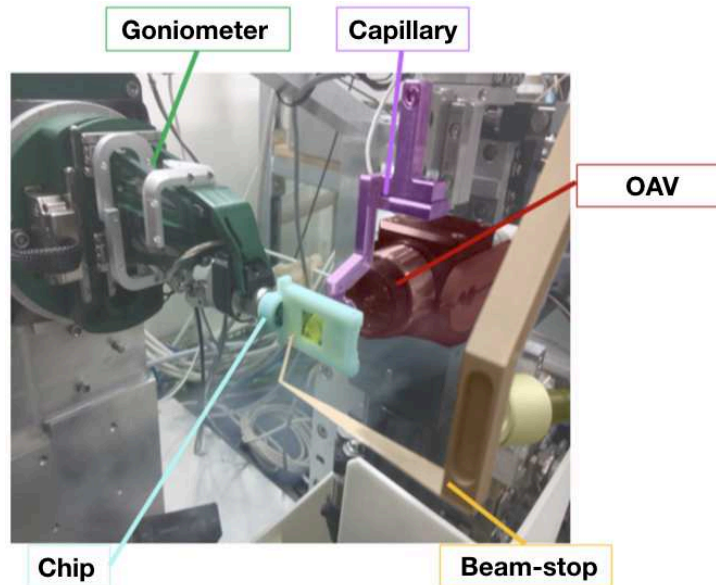


Figure 2.5 : PROXIMA-1 sample environment.

The picture shows a view of the PROXIMA-1 environment with a chip mounted on the goniometer. The capillary and the beamstop are inserted and the cryostream is retracted. The beamline is in position for the collection.

2.2.2. Sample handling

The Cryogenic Automated Transfer System (CATS, [[Jacquamet](#)]) sample exchange robot (*IRELEC*) corresponds to a 6-axis robotic arm equipped with an interchangeable gripper. At PROXIMA-1, it ensures the automation of the sample exchange between the goniometer and the storage place while maintaining the crystals in a cryogenic condition. With the evolution of the sample environment and related technologies, the robotic arm had to be adapted to the various changes to prevent any hardware collisions, to handle new types of gripper accessing different locations in the beamline and to follow the delicate repositioning of the goniometer.

The CATS uses space reference points to be parameterised. Each point is defined with its linear and angular coordinates related to the gripper. After teaching the robot with the exact locations of these points, it will automatically calculate all the trajectories and optimise the related motors to travel through the shorter path between each point of the trajectories. With this method, the robotic arm can manipulate safely any type of samples even in a tight hardware environment, using these complex yet precise trajectories between the sample holder and the goniometer head.

As explained above, the CATS robot has an interchangeable gripper that allows mounting various kinds of sample holders. The three grippers originally present at PROXIMA-1 consisted in a pin handler,

designed to safely bring the SPINE European standard [[Romoli](#)] for MX sample holder to the goniometer while preventing the sample to warm up ; a calibration tool developed to automatically teach the space positions of reference objects to the robot with micrometer precision ; a crystallisation plate handler to perform diffraction experiments directly using the robotic arm and without mounting the plate on the goniometer head. Too poorly characterised and used, this last type of gripper was not calibrated and abandoned for the microfluidic approach.

2.2.3. Control command : MXCuBE

The Macromolecular Crystallography Customized Beamline Environment (MXCuBE, [[Gabadinho](#)]) project started in 2005 at the ESRF, with the objective of providing crystallography beamline users an easy-to-use software platform to run their experiments. In 2010, a collaboration agreement was signed for the development of MXCuBE between the major synchrotron facilities in Europe. Today MXCuBE is actively supported by the following partners: ESRF, Synchrotron SOLEIL, MAX IV, HZB, EMBL, DESY, ALBA, and Global Phasing Ltd.

On the PROXIMA-1 beamline, the MXCuBE software permits users to handle their crystals from their storage cassettes (kept in nitrogen inside the main Dewar storage) to the goniometer head ; align the crystal to the X-ray interaction point ; define all the parameters for data collection ; and perform the collect. As a direct consequence, the users do not have to understand the complex setup of the beamline in order to use it. The MXCuBE interface brings a common tool to users across most European MX beamlines, allowing them to experiment on different synchrotron sites yet with similar feeling and efficiency.

2.2.4. Data treatment : XDSme

The program package *X-ray Detector Software* (*XDS*, [[Kabsch](#)]) was developed to convert information recorded from consecutive diffraction images on a single or multiple crystals and to produce a list of corrected integrated structure factors in a semi-automated manner. *XDSme* [[Legrand](#)] is an open-source list of Python scripts implemented for Linux platforms to ease the use of the *XDS* program package and optimise the data processing of X-ray diffraction data from macromolecular crystals.

3. Microfluidics

Microfluidics utilise state-of-the-art technological developments that bring new prospects to chemistry, biology, medicine and other science fields. It permits to increase the speed of reaction ; to decrease the volume of reactant ; to reach high levels of control of the reactions. A non-exhaustive list of examples includes microfluidic chips used to facilitate blood analysis ; micro-chemical reactions isolated in drops or even sorting nano-particles in sizes [[Abdallah](#)]. Some of the particularities of microfluidics, specifically used for the current project, include: the micrometer size of the channels and patterns constituting the microfluidic device that permits making multiple patterns within a restricted space and using small volumes of liquid ; and the small Reynolds number in water ($Re < 1 \ll 2000$), a

characteristic that allows using the laminar flow properties of liquids for different purposes such as isolating chemical reactions.

3.1. Theory

3.1.1. Laminar flow

The Reynolds number (equation [2.4](#)) is considered as of low values in the dimensions of microfluidics, and permits to stay in a laminar flow with no chaotic eddies or vortices. The major advantages can then be summarised as the possibility to reverse the flow and the absence of mixing. Furthermore, a direct consequence of laminar flow lies in the speed inside the channel that appears to be higher at the center of the fluid than at the edges.

$$Re = \frac{\rho v L}{\eta} \quad (\text{eq 2.4})$$

With Re the Reynolds number ; ρ the density of the fluid ; v the velocity of the fluid ; L the characteristic length ; and η the dynamic viscosity.

3.1.2. Pressure drop

The pressure drop as defined in microfluidics is the difference of pressure between two points in a fluid-carrying network. It is caused by the friction of the fluid, strongly influenced by its viscosity, and therefore linked to the resistance of the flow within the channel following the Hagen-Poiseuille's law (equation [2.5](#)).

$$\Delta P = Q R_H \quad (\text{eq 2.5})$$

With ΔP the pressure difference ; Q the volumetric flow ; and R_H the radius of the channel, or here the hydro resistance.

3.1.3. Hydro resistance

The hydro resistance R_H represents a force directed against the current flow. This value will depend on the geometry of the channel, when considering a cylindrical channel (equation [2.6](#)) or a rectangular section (equation [2.7](#)).

$$R_H = 8 \frac{\eta}{\pi} L R^{-4} \quad (\text{eq 2.6})$$

With R_H the hydro resistance in the case of a cylindrical channel ; and R the radius of the channel.

$$R_H = \frac{12 \eta L}{\omega h^3} \left[1 - \frac{h}{\omega} \left(\frac{192}{\pi} \sum_{n=1,3,5}^{\infty} \frac{1}{n^5} \tanh \frac{n\pi\omega}{2h} \right) \right]^{-1} \quad (\text{eq 2.7})$$

With R_H the hydro resistance in the case of a rectangular section ; and ω the width of the rectangle ; h the height of the rectangle [Hudson]. With simplification and in an arbitrary section, equation 2.7 can be simplified as follows :

$$R_H = \frac{12 \eta L}{1-0.63 \frac{h}{L}} \frac{1}{h^3} \approx A \frac{L}{\omega} \approx 2 \eta L \frac{P^2}{A^3} \quad (\text{eq 2.8})$$

For the present work and to simplify the calculations, the geometry of the channels will be approximated to be represented by rectangular sections of constant thickness.

3.1.4. Analogy with electronic

In microfluidics, several behaviours can be compared to electronics [Oh]. Thus, the difference in potential ΔU becomes the pressure difference ΔP , the intensity I is changed to the flow rate Q , and the resistance R is represented by the hydro resistance R_H . The following equations are representative of some analogies between microfluidics and electronics, notably with the Ohm's law (equation 2.9), the serial reliability (equation 2.10), and the parallel reliability (equation 2.11).

$$\Delta U = R I \rightarrow \Delta P = R_H Q \quad (\text{eq 2.9})$$

$$R_{eq} = R_1 + R_2 \rightarrow R_{H eq} = R_{H1} + R_{H2} \quad (\text{eq 2.10})$$

$$\frac{1}{R_{eq}} = \frac{1}{R_1} + \frac{1}{R_2} \rightarrow \frac{1}{R_{H eq}} = \frac{1}{R_{H1}} + \frac{1}{R_{H2}} \quad (\text{eq 2.11})$$

3.2. Chip principle

The different liquids containing the crystals are known as mother liquors. By definition, they have various compositions depending on the sample. The mother liquors are liquids that are different than pure water in terms of viscosity, hydro resistance, chemical activity, homogeneity and isotropy. Furthermore, mother liquors may contain semi-solid objects (impurities) that could have similar sizes than crystals, which may interfere with the trapping events.

The macromolecular crystals have unique and different mechanical and chemical properties. The crystals are sensitive to temperature, chemical equilibrium in the liquid, pressure and external stress depending on the nature and properties of the sample composing them. The holding process of the crystals inside the chip will be hereafter called the ‘trapping process’. For the rest of the chip principle, these different characteristics will be set aside, the liquid will be considered as water and the crystal a spherical object of infinite resistance and the same density as water, allowing to simplify the hypothesis and therefore prepare an experimental model. The different characteristics set aside will be discussed separately.

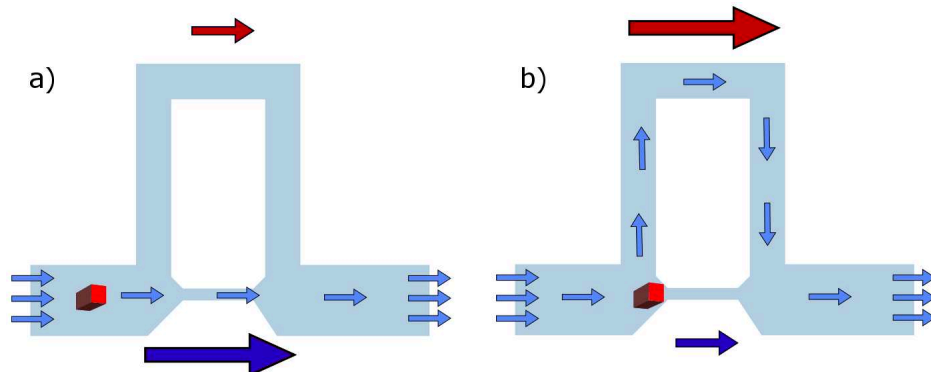


Figure 2.6 : Scheme of the trapping principle.

(a) Evolution of the liquid flow through a crystal-free trap. (b) Evolution of the liquid flow with a crystal trapped. *Red* arrows represent the large and long flow path. *Dark-blue* arrows represent the thin channels. *Light-blue* arrows represent the liquid flow preferential path.

In order to trap the crystals in predefined locations, the chips have been designed to accommodate different widths of the channels, going from wide (more than three times the diameter of the crystals, where it will freely circulate) to thin widths (less than half of the diameter of the crystals to facilitate trapping). Trapping several crystals is facilitated by taking advantage of the hydro resistance of the running liquid : at the point of intersection, the main and wide channel splits into two sub-channels, composed of the first (Fig. 2.6, *red* arrows) large and long channel expanded by the second (Fig. 2.6, *dark-blue* arrows) thinner channel. The second of the above-mentioned channels presents a lower resistance R_H than the first one, implying that the sample crystal will more likely go through the red channel for then being trapped later in the device. When trapped properly, the crystal will diminish access to the thinner channel therefore raising the hydro resistance locally, causing a preferential flow towards the larger channel. As the first crystal will be trapped, the next one and others will evolve within the larger channel up to the next trapping system following the inherent pressure of the liquid flow. In conditions where the direction of the liquid flow will be reversed, the crystal will offer no resistance to the flow, the wider channel will present a lower hydraulic resistance, and the crystal will be released from the trapping system. In the absence of liquid flow, the crystal will stay in position, and the low Reynolds number will favour minimum Brownian movements. Importantly, such a system may be replicated in parallel [[Sochol](#)] or in serial to multiply the trapping of crystals.

3.3. Crystal trapping principle

Using the system presented above in order to trap crystal samples at all the available positions, two fluidic constraints are necessary : all of the crystal-containing fluid needs to pass through the trapping systems ; and the fluid should be able to flow even when all the traps are occupied. Owing to the tendency of the fluid to progress as a laminar flow, the first condition can be fulfilled by passing more than 50% of the fluid through the channel making the trap, and then applying the same procedure in a mirror trapping pattern continuing on the other side of the trapping system. The symmetry of the flow within the channel network coupled to the low Reynolds number will ensure that all the liquid passes through the traps. The presence of the large channel (Fig. 2.6, red arrows) fulfils the second condition. Comparing the throughput between two channels of length L and width ω as referred to in equation 2.9, we end-up with the following equations :

$$\Delta P = R_H Q \Rightarrow Q = \frac{\Delta P}{R_H} \quad (\text{eq 2.12})$$

When applying some constant pressure in input and output, the pressure differential becomes constant such as $\Delta P = \text{Constant}$

$$Q_t > Q_0 \Rightarrow R_H > R_{H_0} \quad (\text{eq 2.13})$$

With the approximation of rectangular sections of identical thickness, the following estimation can be deduced :

$$R_H \approx A \frac{L}{\omega} \Rightarrow \frac{L_t}{w_t} < \frac{L_0}{w_0} \Rightarrow \frac{L_t}{L_0} < \frac{\omega_t}{w_0} \quad (\text{eq 2.14})$$

When using N traps within the same large channel, and without taking into account the distance between the traps, in favour of the trapping process we obtain :

$$\frac{1}{R_{Htraps}} = \sum \frac{1}{R_{Ht}} = \frac{N}{R_{Ht}} \Rightarrow R_{Htraps} = \frac{R_{Ht}}{N} \Rightarrow R_{Htraps} = \frac{R_{Ht}}{N} < R_{H_0} \Rightarrow L_0 > \frac{L_t}{N} \frac{\omega_0}{\omega_t} \quad (\text{eq 2.15})$$

Equation 2.15 shows that with a fixed width for the channels of the traps, and for a length of the principal larger channel bigger than L_0 , the fluid will entirely pass through the traps. Once crystals will be trapped, N will drop, implying that L_0 should be chosen accordingly for an ideal system with multiple trapping possible. The equation also shows that the viscosity of the fluid does not impact the equation. Therefore, only the geometrical properties will influence the path of the liquid.

3.4. Crystals

Often used as a reference system in macromolecular crystallography, Lysozyme and Insulin are proteins that can easily provide uniform and reproducible crystals of quality good enough for diffraction studies. Thus, Lysozyme and Insulin crystals (Fig. 5.1 & 5.4) were grown to realise the proof of principle experiments and confirm the quality of the chips for diffraction experiments. Because of the common use of both proteins as test systems, comparison with other mounting systems is facilitated, including cryo-conditions or diffraction at room temperature using different handling systems. To maximise the signal over noise ratio in X-ray diffraction experiments, crystals should ideally be as large as the measured beam size at the X-ray interaction area ($20 \times 40 \mu\text{m}^2$ at PROXIMA-1, Table 2.1). Moreover, growing crystals encounters numerous issues in the process, notably with difficulties in producing the protein or in growing diffraction quality crystals properly packed and of reasonable size. In the present studies, the good proportion for the dimensions of crystals employed in the tests of the chips would be approximately $40 \mu\text{m}$ for the longest dimension.

4. Chip creation

The microfluidics approach is rich in methods and techniques to engineer a plethora of chips specialised for various applications. In the current project, we will focus on classical methods based on positive resins to make the mold, filled with polydimethylsiloxane (PDMS) polymer and then plasma bonded on a thin sheet of glass, kapton or spin-coated PDMS on kapton layer.

4.1. Instrumentation

4.1.1. Laserwriter

The *KLOE-Dilase 250* (hereafter named Dilase) is a high resolution direct laser (375 nm) lithography system for versatile prototyping and maskless wafer insulation. The technology can insulate a surface as large as a 4-inch wafer with a repeatability of 100 nm, substrate thickness of up to 5 mm with an aspect ratio of 20. A video-based realigning system facilitates the alignment of multiple layers. The Dilase uses a vectorial mode of writing through its *KloéDesign* software that can read previously prepared *DXF* format files from which it can operate the laserwriter. The resolution limit of the laser is 4 microns.

The motorised laser writes the lines at a user-defined speed. The surfaces are made of parallel lines. The insulation time is directly linked to the total length of the design and the speed of the laser. Because the laser speed is limited by the properties of the motors, the time of a full insulation relies directly on the area to be covered by the laser. The laser is mounted on a vertical Z motor, with the sample on an X/Y horizontal plate. All the motors have sub-micron precision. The focussing of the laser on the sample is realised by fixed lenses. As the thickness of the wafer and the resin can vary, the focal point has to be placed at the center of the layer in order to minimise the area insulated by the UV laser. At every

maintenance of the laserwriter, the zero of the Z motor is reset, leading to the requirement to find the focal point for each resin thickness.

In order to find this optimised position, two methods were approached and applied in the course of this work : the optical method, fast but imprecise ; and the insulation method that requires insulating wafers. The optical method is simple to exercise, with the laser that is set at a minimal intensity for illuminating a location in the pattern where a short overexposure is not problematic. In practice, completely empty areas are targeted for this operation. The laser is then modulated in Z until the light spot created by the laser appears as the most focused. Two factors bring imprecisions to this measurement : the lens focusing the light in the UV laser focusses differently depending on the wavelength of the light, leading to a different focal point for visible and UV lights. Consequently, the focal point of the active light will not be exactly at the same Z position. Furthermore, the focal point is confirmed only at the upper surface of the insulated layer, and not at its center ; this leads to less defined focus towards the bottom of the layer.

The insulation method consists in exposing at different Z positions and confirming which height gives the best insulation. The tests are done in simple lines. The values of Z are relative values in this particular example, with the laser beam intensity that is relative to the maximum intensity reachable by the laser. The best Z positions are represented by the last positions that appear after resin development when the beam intensity is reduced to its minimum set value.

4.1.2. KloéDesign software

The *KloéDesign* software is a vectorial 2D writing software developed to create or adapt laser designs into laser path for the laserwriter. It reads *DXF* files, and exports the designs in a format compatible for the laserwriter (*LWO*). For complicated designs, the interpretation of the imported *DXF* format may appear difficult, forcing for a manual optimisation work directly within the *KloéDesign* software to generate a better refined *DXF* output and to reinterpret the drawing.

The *DXF* format registers lines and dots in a text file. In order to generate surfaces, the lines (series of lines delimited by pairs of points) have to be converted into polygons (closed line passing through a series of points). The software can recognise the surface inside the polygon and fill it with a series of vectors in a specific direction, spaced by $d/2$, with d representing the diameter of the focused laser beam. To ensure the homogeneity of the filling at the borders of the surfaces, the filled vectors overwrite outside the polygons. The motorisations of the laser are set to use this border extension trajectory to reduce its speed and change direction. It ensures homogeneity while filling the areas. Optimisations in the software interpretation of the pattern can lead to the reduction of the laser path and therefore of the insulation time (Fig. [2.7](#)). With proper optimisations, the insulation time can be reduced by 2 000% on certain designs.

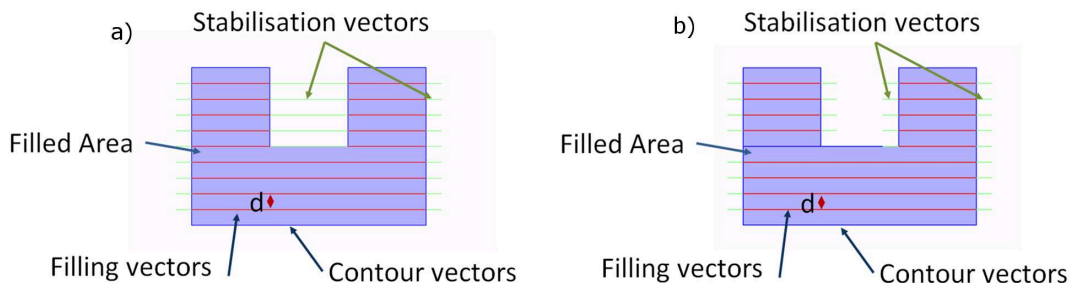


Figure 2.7 : Illustration of filling strategy of KloéDesign.

Here is an example of a design (*blue contour*) filled with horizontal lines using the *KloéDesign* software. The filling lines (*red*) are calculated from the shape to fill (*blue*) and the distance d between two paths. The stabilisation vectors (*green*) are continuations of the filling lines 0.1 mm before and after the shape surface. The laser will follow the *blue*, *red* and *green* lines while being powered ON. Optimisation in the design can lead to different path length when compared with the time set for insulation. (a) The software created stabilisation vectors in the window at the top. (b) A small optimisation of the design leads to the diminution of the stabilisation vectors in the window, and therefore a reduction of time for insulation.

4.1.3. Plasma chamber

The difficulty linked with the use of the plasma chamber [Henniker] while manufacturing the chip is related to the mass of the sample to be ionised. The thin $10 \times 20 \times 0.05 \mu\text{m}^3$ PDMS on the kapton sheet can be lifted by the air flow entering the chamber after ionisation until reaching atmospheric pressure. To limit the occurrences of these events, the PDMS sheets are fixed to the metallic plate supporting the samples in the plasma chamber.

4.1.4. Corona ioniser

A *Corona ionizer* applies high alternating voltage to the tip of the instrument. The potential difference between the ground and the tip creates a strong electric field that expulses electrons from atoms on the exposed surface creating a corona discharge [Zhu]. Molecules present in the air can be ionised, leading to only a small portion of the generated plasma composed of oxygen atoms, of lower quality than pure oxygen plasma instruments. Furthermore, the plasma intensity in the *Corona ionizer* can only be controlled by the distance between the *Corona ionizer* and the sample, and the shape of the nozzle. The bigger the nozzle, the bigger the ionised area will be. The electric field, thus the ionisation strength will be inversely proportional to the area covered. Although the quality of the plasma is difficult to estimate, in practice the ionisation quality appeared sufficient for all of the applications developed in the course of this work.

4.2. *Pattern designs*

All of the designs for the various patterns were drawn using the *SolidWorks* software suite, and exported in *DXF* file format for compatibility with the *KloéDesign* software. The file is then exported in *LWO* format for use by the laserwriter. All of the different patterns and designs with their evolutions are available in Annexe [4](#).

4.3. *Materials*

PDMS. Historically, the approach of microfluidics began in the 1990s with heavy glass chips, which were expensive, hard to manufacture and fragile. In the 2000s, PDMS chips appeared, bringing to the field a battery of advantages, among which a high degree of precision in the manufacturing of the chips, the obtention of optically clear objects, biocompatible, having a good aspect ratio and mechanical properties making this material easy to handle and work with. The PDMS is stored in a highly viscous liquid state, mixed with a reticulant in a 10:1 ratio. It is then flowed into a mold and heated to accelerate the reticulation process. *In fine*, the PDMS is transparent, biocompatible, slightly elastic, can support temperatures between -40°C to 200°C without losing its properties. These properties lead the PDMS to be the most popular material in microfluidics. In its liquid state, it can fill molds up to the nanometer scale, leading to high precision molding. PDMS is by default hydrophobic but can be hydrophilic when activated by plasma. The reticulation process is accelerated with the temperature, taking 24 hours to reticulate at 20°C and 15 min at 70°C . Of interest for our experiments, the PDMS is partially made of Silicon (14 electrons *per atom*), which is more X-ray absorbing when compared with carbon-based components (6 electrons *per atom*). As a direct consequence, when designing X-ray compatible chips, the PDMS section will have to be minimised in order to reduce the potential impact on the experiments.

SU-8. It is a photosensitive positive epoxy resin made by *MicroChem* [[MicroChem](#)]. When exposed to UV-light, the SU-8 solidifies. It is used for mold creation when spin coated on a wafer, followed by an exposition of the wafer using a mask and a uniform UV-light or a laserwriter. A solvent will then dissolve all of the non-exposed resin. SU-8 resins have different viscosities optimised for ranges of thickness after spin-coating and different versions with updated chemicals constitution to optimise the properties, like maximum aspect ratio, thermal and chemical resistance, compatibility, etc. The two resins used during the current work were SU-8 2015 and SU-8 2050, in order to prepare 40 and 80 μm thick layers, respectively.

4.4. *Manufacturing steps*

The manufacturing of the chip results from a stepwise process that follows a well-defined protocol and that uses standard methods applied in microfluidics, such as *spin-coating* and *plasma bonding*.

4.4.1. Spin-coating

A *spin-coater* is used to fix the thickness of a viscous liquid on a plane surface ; in the present work, this technique was applied to fix the thickness of the PDMS and SU-8 epoxy resins, respectively [Hall]. In order to fix the height of the channels, the SU-8 epoxy resin is first deposited on the wafer, and then the wafer is rotated at a fixed speed during a predefined time. The height of the resin depends directly on the rotation speed, the rotation time and the viscosity of the resin. Figure 2.8 shows the thickness of different spin-coated SU-8 epoxy resins after rotating at different rotation speeds during 30 seconds. The same strategy is applied to the PDMS [Zhang WY] in order to apply a known chip thickness.

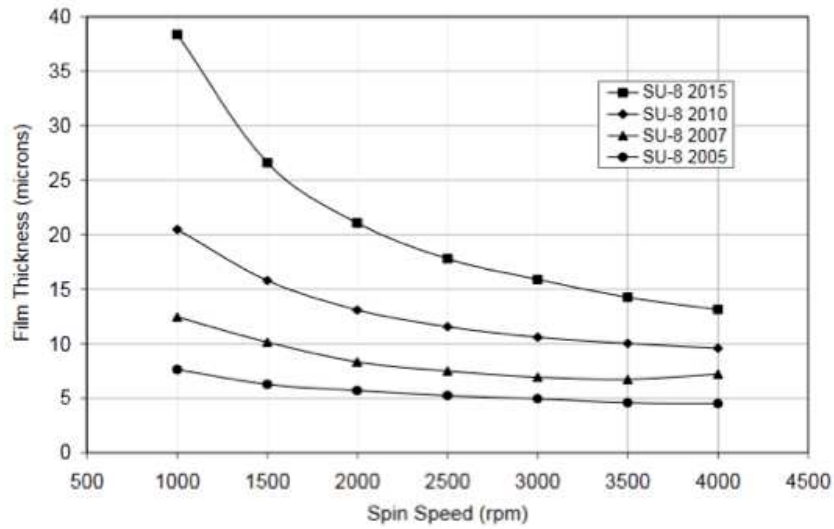
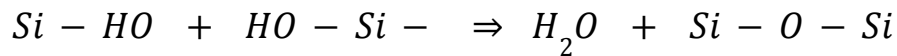


Figure 2.8 : Film thickness over spin-coating speed.

The graphic shows the thickness of different spin-coated SU-8 epoxy resins during 30 seconds [Hall].

4.4.2. Plasma bonding

As indicated by its name, plasma bonding is a method employed to covalently bind two elements, mostly silicon-based materials. The advantage of plasma bonding when compared to more classical resin-based bonding methods lies in the accessibility to working on specific micro/nano-sized areas, where resins may fill partially or fully the channels. In order to bind two surfaces of PDMS, both surfaces are treated by an oxygen plasma that induces the generation of high densities Si-OH. The treated surfaces are then brought in close contacts, pushing towards polymerisation (equation 2.16).



(eq 2.16)

The bond created is mechanically strong enough that external stresses will eventually break other parts of the microfluidic device before affecting the bonding itself. During this work, plasma bonding was approached by two different techniques made available in the laboratory of microfluidics at Synchrotron SOLEIL. Both techniques were randomly used, depending on the disponibilities of the instruments.

Plasma chamber. The low pressure plasma system *Atto* (Diener Henniker HPT-100 [[Henniker](#)]) creates a low pressure O₂ environment. All of the parameters of the plasma chamber can be precisely tuned. The control of the plasma quality and timer precision is not needed to have the system working, however it remains a luxury well appreciated, especially as it provides with the possibilities to confidently reproduce the methods. In contrast, during the plasma bonding, the depressurisation step creates air turbulence that flip the light membranes. The thin PDMS / kapton membranes have to be temporarily attached on the plasma chamber support using small cubes cut in PDMS in order to prevent them from flying during the re-pressurization of the chamber.

Corona discharger. A *Corona discharger* ionises the air and the O₂ to generate the plasma. It is made of a head with an alternating high tension. It generates plasma and an electric arc between the head and a support linked with mass. For safety issues it has to be manually manipulated under a hood. Because handling this equipment is performed manually, the discharging time and the quality of the resulting plasma cannot be guaranteed and will vary for each experiment.

4.4.3. Detailed procedure

Here is a short description of the various steps in order of execution and in reference to figure [2.9](#).

1. The spin-coating of the resin on the silicon wafer. The thickness of the layer will depend on the viscosity of the resin and the momentum applied during spin-coating, directly linked to the speed of rotation.
2. The insolation will selectively activate the resin. The selection of the resin to be activated may be done through a mask or making use of a laser writing device. In this specific chip realisation, the minimal writing precision will depend on the quality of this particular step.
3. The detergent at the basis of the development step will react with all the non activated resin to dilute it, allowing to keep only the activated resin.

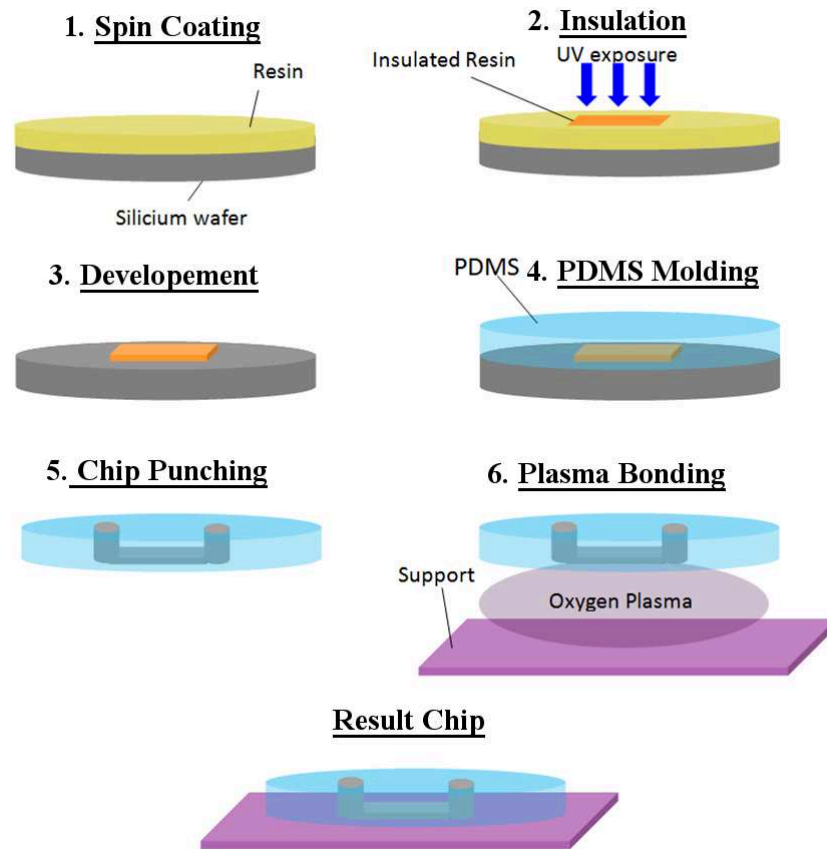


Figure 2.9 : Illustration of the different steps of chip making.

4. The step of PDMS molding consists in melting the PDMS with a curing agent, followed by depressuring it to clear out any bubble resulting from the process, before depositing it on the wafer.
5. An additional step of mechanical work on the PDMS chip is necessary to favour the contacts of the inside channels with the exterior of the chip, ended by one last cut of the chip to its final shape.
6. Plasma-bonding will ensure pasting the PDMS part to the supporting material (glass or kapton) and hermetically close the chips.

4.4.4. Mold preparation

The SU-8 Molds of 80 μm thick layers are prepared by spin coating (Laurell WS-650-23NPP spin-coater) SU-8 2050 resin at 2000 rpm for 30 sec on a silicon wafer following the protocol described by the manufacturer [[MicroChem](#)]. The spin-coated wafer is then heated at 95°C for 7 minutes in an initial soft-baking step, and then placed in the laser writer (KLOE UV-KUB).

The centering of the wafer in the laserwriter is an important step for a precise writing of the chip pattern. By placing the observation camera on three points at the edges of the wafer, the center C of the wafer disk was calculated and determined following equations [2.17](#).

$$x_c = \frac{\frac{x_3^2 - x_2^2 + y_3^2 - y_2^2}{2(y_3 - y_2)} - \frac{x_2^2 - x_1^2 + y_2^2 - y_1^2}{2(y_2 - y_1)}}{\frac{x_2 - x_1}{y_2 - y_1} - \frac{x_3 - x_2}{y_3 - y_2}} \text{ and } y_c = \frac{x_2 - x_1}{y_2 - y_1} x_c + \frac{x_2^2 - x_1^2 + y_2^2 - y_1^2}{2(y_2 - y_1)} \quad (\text{eq 2.17})$$

The coordinates (x_c, y_c) of the point C will be the point of calibration for the laser writer. When writing on the wafer, the energy deposition is set at 40% and the laser speed at 5 mm/s. Once the insulation is finished, the wafer is heated at 95°C for 5 min. The SU-8 is then developed using specific SU-8 developers.

4.5. Chip characteristics

For the current designs and chips, the ratio of PDMS and reticulant was similar and consisted in a ratio of 10:1 of PDMS over curing agent. The PDMS kapton chip was made in two layers. The first layer of the PDMS/kapton chip is deposited using a Spin-coater (Laurell WS-650-23NPP Spin-coater) set at 1,000 rpm for 30 sec to deposit 100 μm of PDMS on a 3-inch silicon wafer crafted with the appropriate design. The wafer was then heated at 70°C for 30 min. The mask was then disposed of in the window, with the external mold surrounding the chip. The mold was then filled by 3 mm PDMS. After heating the wafer at 70°C for 30 min, the mold was removed, and the chips were cut following the marks delimiting its exterior. Holes for the connectics were punched using a dedicated 1.5 mm diameter puncher.

The second PDMS layer of the chip was spin-coated at 3,000 rpm for 5 min on a 25 μm kapton sheet. The PDMS was then heated at 70°C for 30 min, and the sheet cut using scissors to fit the external counter of the chip (rectangles of approximately 15 mm by 30 mm). The two layers were bonded together by exposing the two PDMS faces to plasma at a power of 50% on a Diener Henniker HPT-100 for 3 min. The last step consists of heating the chip at 70° for 30 min.

To prepare the connecting parts, a 3 mm PDMS sheet is poured onto a flat silicon wafer and heated at 70°C for 1 hour. After polymerisation, the PDMS is removed from the wafer and cut in multiple rectangles of 4 mm by 6 mm dimensions. A hole is then punched at the center of each rectangle using a

1.5 mm diameter puncher. If the chip is aimed to contain several connectics in proximity, several holes have to be punched in a unique rectangle at the relative positions for the connectics. The side of the chip with PDMS and the rectangles are then exposed to plasma (50% power on a Diener Henniker HPT-100 [Henniker]) for 3 min before bonding those with precision in order to align the rectangle holes on the chip holes. The final chip is then heated at 70° for 30 min.

The PDMS chip measured 20 mm in width and 30 mm in height, respectively. It was accommodated inside an adapted 3D-printed frame for further mounting on the goniometer head at PROXIMA-1. The selected method of manufacturing was optimised to trap 20 to 50 µm (longest direction) crystals. The trap channel width is 10 µm, leading to the difficulty to trap samples smaller than 15 µm.

5. Sample injection

5.1. Constraints during injection

Low pressure : during an injection, the size of the channels, its length and the viscosity of the liquid lead to pressure drop. For a certain liquid, the pressure is proportional to the speed of the flow. The pressure needs to be kept within certain limits depending on the fragility of each crystal type while preventing reduction of the symmetries within the chip that would result in a decrease of resolution.

Injection success rate : access to synchrotron beamtime is strongly dependent on the availability of the end-station for experiments. Typically, at PROXIMA-1 multiple shifts of 8 hrs are being allocated to users. Ideally, microfluidic chips would be prepared before the actual experiments, and stored ready for diffraction experiments. The thin PDMS layer composing the chip however let the air pass through, leading to the evaporation of the mother liquor inside the loaded chip. The evaporation changes the ratio of the chemicals within the composition of the mother liquor, impacting to some degree the quality of the crystals. Therefore, depending on the crystals, the time between the end of an injection and the start of data collection has to be under 10 hours. For high viscosity mother liquors, previous injection tests have to ensure the timing for injection.

5.2. Injection techniques

5.2.1. Pressure controller

For easier handling of the crystal sample solution, the tubing exterior to the chip and used for injecting the crystals are of large diameter in comparison with the chip channels; as a consequence, the ratio of the volumes between the chip and the connectors is superior to 10^3 , thus affecting the injection time that has to be adapted. The use of a classical injector implies a pattern filling time at least 10^4 faster than the time required to inject in the exterior tubing, forcing the flow rate of the fluid to go 10^4 faster for a fixed speed of injected volume. In opposite, running at constant speed in such a way that the whole

volume of sample contained within the connectors goes through the microfluidic chip would take several days of handling (*e.g.* at constant throughput, while it takes 1 sec for the liquid to run through the pattern, it will take $4 \cdot 10^7$ sec or 1.2 year to fill a 300 mm pipe of 0.4 mm diameter). To bypass this problem of overpressure, a pressure controller may be added to the injector adapted to the microfluidic chip. Using such a controller, the speed of injection will be tuned via the pressure in the system rather than the injected volume. This workaround allows a differential flow rate between the fluid within the large diameter tube of the connectors and the tubes inside the microfluidic pattern, where the flow will drop to safe speeds. Additionally, the ratio between the velocity of the fluid inside the chip and the pressure depends on the geometry of the tube assembly, as dictated by the $\rho g \vec{z}$ factor induced by the mass of the liquid.

5.2.2. Depressurised and capillary injection

To avoid generating issues when working with large volumes while connecting injection tubings, all the external and bulky injection system may be replaced by a somewhat simpler internal injection system. In this approach, the pattern of the chip presents a deep and wide empty volume hereafter referred as “reservoir”, located at the entrance of the channels. To inject the sample, a drop of liquid is first deposited in front of the entry area, and the reservoir has to be mechanically ‘pressed and released’. Through this manipulation of the chip, the air trapped in the reservoir will flow out of the chip first, leaving the place for the depressurised chip to drag the liquid in. With a reservoir volume several times larger than the volume confined in the chip, the liquid will be naturally dragged into the channels, bringing crystals together with the liquid. To gain better control, the chip may be punched in the reservoir, and the use of a pipette could help to depressurise. This manual operation allows making multiple trials when the liquid does not fill the entire chip or if too few crystals are trapped.

Although this approach allows testing efficiently the chips without damaging its inner patterns, the large quantity of crystalline sample lost at the reservoir when not entering the chip stands as a real drawback. Indeed, the majority of the liquid and the crystals within stays in the initial drop, and reinjection becomes hardly difficult. Furthermore, the technique has a low reproducibility.

5.2.3. Peristaltic pump

A peristaltic pump is a simple solution to sample injection that allows to automatically and constantly re-inject the solution and the crystals within. Some improvements are still required for properly handling the sample and the chip. Each pumping cycle may cause extensive liquid movement in the chip that may untrap crystals. To bypass this issue, a first ‘back-and-forth’ injection with round trips permits removing the air bubbles. Nevertheless, the pressure is not controlled during the injection and hard to calculate because of the non-constant flow. This technique may only be considered to handle crystals strongly resistant, and shall be avoided for fragiles macromolecular crystals.

5.3. *Injection protocol*

The injection protocol has been optimised using a pressure controller (Fluigent) with a minimum of two entries and with an adaptable pressure ranging from 0 to 200 mbar. Plastic tubings (0.5 mm inner diameter) are adapted to the chip and to the pressure controller in entry. The loading is observed through a microscope. Tubings are handled with a pincette, and eventually sealed with a gas heater to warm the pincette. For an efficient loading, 1 mL of the mother liquor (crystallisation condition) may be necessary. The following protocol is applied to the microfluidic chip design V22 (Supp. Fig. 8) , adapted in a 3D-printed support frame adapted to the beamline goniometer. The microfluidic chip is glued to the 3D-printed support frame to assure that the pattern is centered at the middle of the X-ray entering window within the support frame. The glue joints are classically disposed under the two heavy PDMS layers.

6. **Chemical tests**

6.1. *Injection of coloured chemicals*

The initial experiments consist of injecting in the chip the chemical compounds by a pressure controller and observing the behaviour of the chip through a x10 bench microscope. For easier visualisation, the contrast of the injected liquid was increased by mixing the chemicals with neutral food coloring, followed by a continuous injection at 50 mBar for 10 hours. Images are recorded every 3 min.

6.2. *Injection of glass beads*

In order to verify that the chip trapping properties were not altered by the tested chemicals, the adopted strategy consisted in adding solid objects with an approximate size mimicking the crystals in order to test the trapping with the chemicals. Glass was chosen as it remains inert with most chemicals ; 50 μm diameter glass beads were preferred over 80 μm diameter beads because of accumulation and clogging of the bigger beads at the entrance to the chips (Annex 6). For systematic studies, a 3 mm PDMS 1 mm PDMS chip (V19, Supp. Fig. 7) was designed, allowing for a better visualisation under a dedicated microscopy setup. Although the dimensions of this chip design for test experiments is slightly different than the actual chip used for ‘real’ experiment, it does not affect the relevance of the results obtained because the test environment stays the same, *i.e.* one PDMS structure and a PDMS / PDMS bonding.

In the course of the injection experiments, some chemicals such as Ammonium Sulfate (Ammonium Sulfate) reacted with the food coloring, leading to the trapping of dusty objects in place of the glass beads (Annex 6). To avoid hampering the experiments, the food coloring was removed entirely from the injection mixture where necessary.

6.3. *Injection protocols*

A final testing setup needs to confirm whereas the chip satisfies the three parameters described previously : no destruction of the chip, no leaks and efficient trapping of the crystalline samples. The two

first conditions need to be fulfilled for long injection times, however, the third condition hardly fits with large volumes (~3 mL) needed for long injections. Consequently, two types of injections have been investigated :

- One first long injection, over 24 hours and for a sample volume of 3 mL with beads displayed in a pressure controller reservoir. This setup will answer the stability of the injection over time, and check for leaks appearance or complete destruction of the chip, for each chemical.
- The second injection was described in the previous paragraph ; it consists in injecting 300 μ L during 10 to 40 min, to keep a homogeneous repartition of the beads in the liquid in order to test the trapping quality.

7. Permeability towards oxygen

7.1. *Chemical tests*

When working with dioxygen sensitive molecules, and prior to loading the chip with the crystals, it is important to ensure the impermeability of the chip towards oxygen. For the purpose of identifying the level of permeability of the microfluidic chip, some reactants highly reactive with dioxygen, could be injected in the chip, and the reaction followed over time. The chemical methyl viologen diluted in ethanol and reduced with dithionite in a 5:1 ratio presents a strong blue color, and becomes transparent when oxidized by dioxygen. As such, it is considered a very sensitive dioxygen probe, and represents the chemical of choice for the current qualitative experiments. To prepare the experiments, one windowed chip model V9 (Supp. Fig. [3](#)) was first cleared of traces of oxygen by being placed in an anaerobic chamber for 40 hours. Methyl viologen was then injected, the chip using a specific UV activated glue, and the reaction within the chip was followed after removing it from the anaerobic chamber.

7.2. *Control experiments with ChipX3*

Various microfluidic chips are available for macromolecular crystallography, each design having specificities that favour crystal growth, diffraction screenings or others. Among these chips, the ChipX3 [[Wijn](#)] was designed to combine protein crystallisation screening on a chip, with X-ray diffraction experiments on the newly grown protein crystals (Fig. [2.10](#)). The original design of the ChipX3 was engineered to favour crystallisation screenings, and therefore lacks the crystal trapping option. However, its composite being different than PDMS, it was considered here for a potential alternative device for oxygen free in situ diffraction experiments.

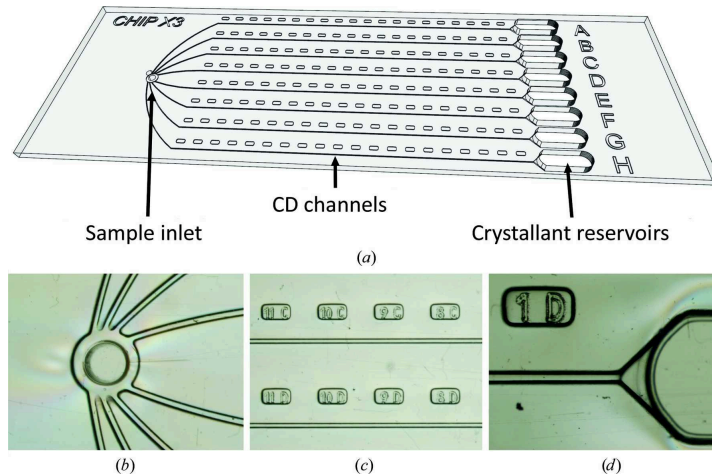


Figure 2.10 : Design of the ChipX3 [Wijn].

The ChipX3 combines two sets of entries : the protein solution is injected through the entry located on the left side of the chip, and different crystallisation solutions are deposited in the entries A to H on the right side of the chip. Channels connect both entrances and regular marking on the channel paths have been added to properly locate the crystals and deduce the information on the crystallisation conditions. (a) Schematic view of the chip, which has the dimensions of a microscope slide ($75 \times 25 \text{ mm}^2$) and eight channels with a straight segment of 40 mm and a cross-section of $80 \times 80 \mu\text{m}^2$. Zoomed views are shown of (b) the inlet for the biomacromolecule solution, (c) the channels and labels, and (d) the end of the channel and the crystallant reservoir [Wijn, Fig.1] .

8. Optional design for ligand injection

8.1. Specific microfluidic requirements

The approach of crystal soaking can only be successful if the small molecule can access the active site of the protein of interest, which will depend on the crystal packing and the interactions among the proteins inside the crystal. The complex formation between the protein and the ligand strongly relies on the affinity of the ligand for the active site of the protein ; the soaking time can thus vary and may need to be adapted.

As introduced earlier, the liquid flow can be guided through different paths depending on the needs. By adjusting the pressures at different entries, liquids containing the ligands could be directed in specific locations where the crystals would be trapped (Fig. 2.11a). The soaking time may be controlled by adjusting the pressure of the liquid flow. Additionally, as the flow passing through the crystals remains directional, they will not get out of the traps.

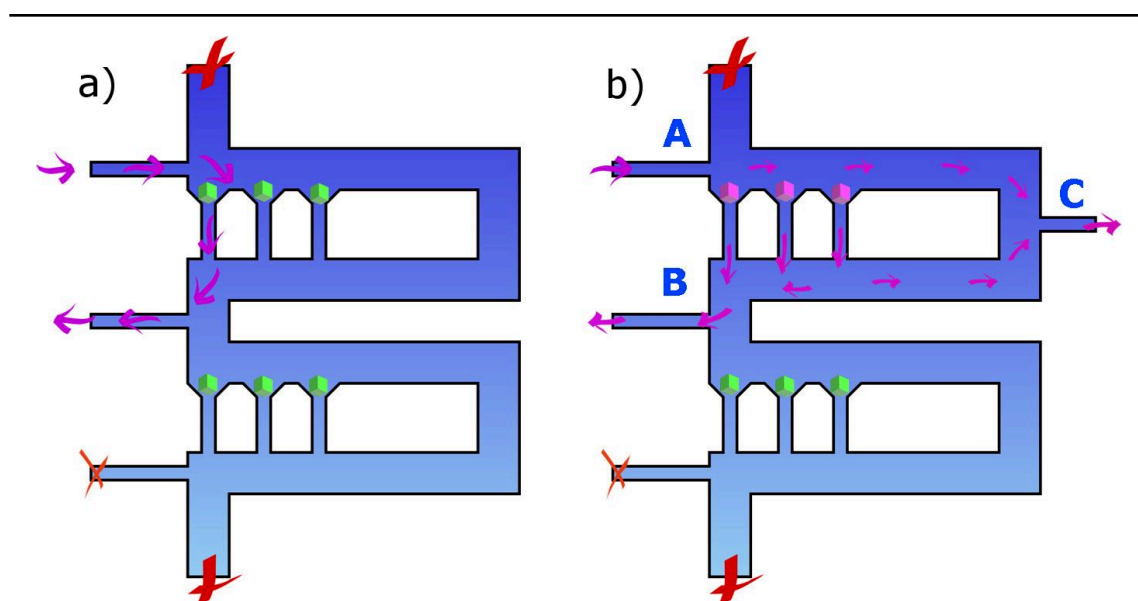


Figure 2.11 : Mechanism behind *in-chip* ligand soaking.

The schemes represent a microfluidic chip filled with protein crystals trapped in green, soaked with ligands represented by the violet arrows. (a) the flow of ligand is directed in the first trap(s) of a row. (b) the flow of ligand goes through the entire first row.

In order to precisely manipulate the liquid within the chip independently for each trapping row, three entries are needed per set of row : one before the row (A), one in parallel to the traps (B) and one after the row (C). In order to inject in the complete row (Fig. 2.11b), a relative positive pressure has to be set in (A) together with a negative pressure at (B) and (C) (Fig. 2.11b). The liquid will then split

depending on the relative pressures applied in (B) and (C). Only by playing with the (B)/(C) pressure ratio, all the crystals may get soaked with the ligand. At the end of the soaking experiments, the chip can be washed by injecting mother liquor through the same path.

8.2. Chip modifications

In order to soak the crystals with ligands, six channels were added to the design version 13 (Fig. 2.12). The design brings the three entries needed to soak the crystals of one single row without affecting the other lanes of the chip.

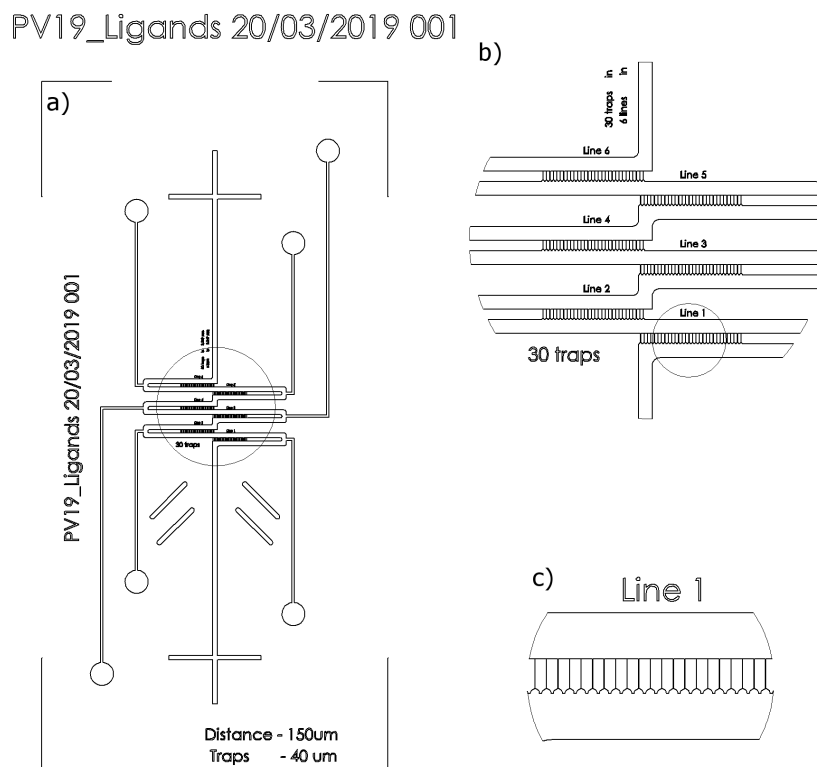


Figure 2.12 : Design version 13 for Ligand soaking.

(a) SolidWorks design of the first layer of the ostromer chip. (b) and (c) are zoomed views focusing on the traps. The chip is composed of 6 supplementary channels linked to independant inlets.

9. Optional designs for cell trapping

9.1. Grid cell trapping

9.1.1. Adapted strategy for trapping

In order to arrange a large number of cells in a geometrically defined array, a design inspired from the literature [Lim] was considered. The principle is based on building an array distribution of wells surrounded by protruding domes. Under low flow rates, the objects will settle by sedimentation inside the wells. Once trapped these objects experience a much lower flow rate due to the protection of the enclosing domes. The principle of the chip has been reproduced at Synchrotron SOLEIL with the goal to replicate the trapping mechanism with sample cells. Two designs have been created : one made of wells only (the two layers pattern) to validate the production of the multilayer mold, and one made of wells and pillars (the three layers pattern).

9.1.2. Chip preparation

The protocol to prepare the two layers as well as the three layers patterns was inspired from [Lim]. The figure 2.13a shows the overall model of the mold, with in particular the chamber (in blue) and the pattern (in red). The first pattern (Fig. 2.13b-2.13c - two layers) consists of a series of $20 \times 20 \times 50 \mu\text{m}^3$ pillars spaced by $100 \mu\text{m}$. These pillars will produce the wells in the PDMS chips. The second pattern (Fig. 2.13d-2.13e - three layers) has the same core as the first one with an additional intermediate layer made of $20 \times 20 \times 50 \mu\text{m}^3$ holes (that will be domes in the final PDMS chip) placed between the pillars. For both patterns, large rectangular structures (white in Fig. 2.13a) are included to support the chamber during the bonding and avoid collapsing. An $80 \mu\text{m}$ empty space of $80 \mu\text{m}$ above the patterns will allow the injected solution containing the cells to flow above the wells and let the cells sediment in the traps.

Of primary concern during the printing of the molds, two manufacturing artefacts need further consideration for their impact on the chip function:

- 1 to 5% of the pillars randomly distributed broke during the development of the SU-8 resin (Fig. 2.13b). These rare and isolated events would likely not interfere with the trapping quality of the remaining pillars.
- The pillars and the holes of the three layers chip mold are misaligned (Fig. 2.13d) due to the lack of alignment precision of the laserwriter ; the holes are not centered on the pillars hexagonal arrangement. The function of the holes (domes in the PDMS chip) is to slow down the flow near the pillars (wells in the PDMS chip). As long as the density and the uniformity of the distribution of both wells and domes are conserved, the combination of their respective roles is expected to remain unchanged.

Taken together, these two artefacts are not expected to interfere with the foreseen trapping efficiency.

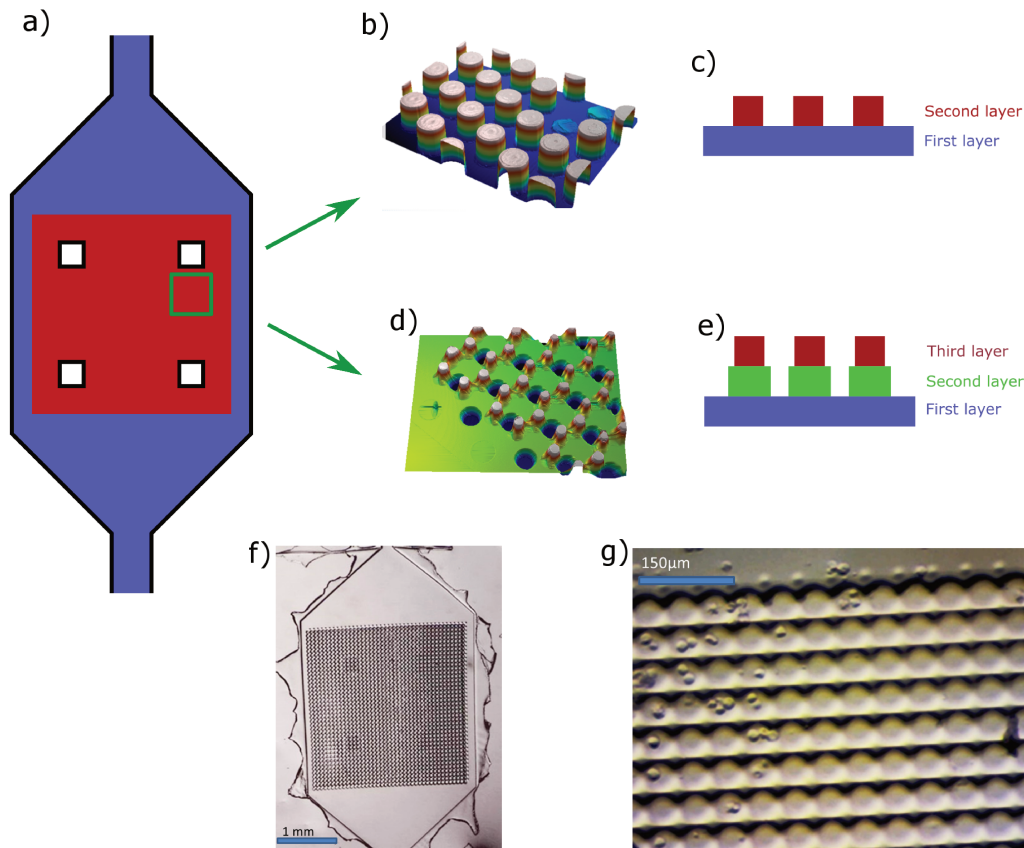


Figure 2.13 : Two and three layers trapping designs and printed results.

Images (a) to (e) represent the silicon mold. The mold represented is a negative of the final PDMS chip. (a) the overall chip design with in blue the channel of the chip chamber and in red the patterned area. A two layer pattern and a three layer pattern were printed. (b) A zoom in the 3d view of a 2 layer pattern with a sectional view of the pattern in (c). The pillars are organised in a square pattern. (d) A zoom in the 3D view of the 3 layer pattern with a sectional view of the pattern in (c). The pillars and holes are organised in a hexagonal pattern. Figure (d) highlights a small misalignment of the holes and the pillars. (f) The printed chip with a 3 layer pattern printed. (g) A zoom in a 2 layers loaded chip with cells placed. Only a small portion of the traps are filled with the cells.

9.2. Line cell placing

9.2.1. Design presentation

The third approach designed for in-cellulo automated serial diffraction chip was inspired from the X-rays centering techniques [Hilgart]. A ‘raster’ feature enables sample centering via diffraction scanning over two-dimensional grids. The feature is used to locate crystals that are optically invisible due to their small size or are visually obfuscated due to the properties of the sample mount.

A sample centering via diffraction scanning over a one-dimensional grid could be made possible by placing the crystals in a beam sized capillary. The usage of such a scan would optimise the collection time ensuring to collect only the crystal containing cells. In contrast, the intensity of the scanning beam the crystals is a compromise between the signal over noise, and the crystal deterioration. The removal dimension reduction from 2D to 1D prevents the sedimentation of the cells contained in the liquid, leading and ensures collecting the whole sample volume.

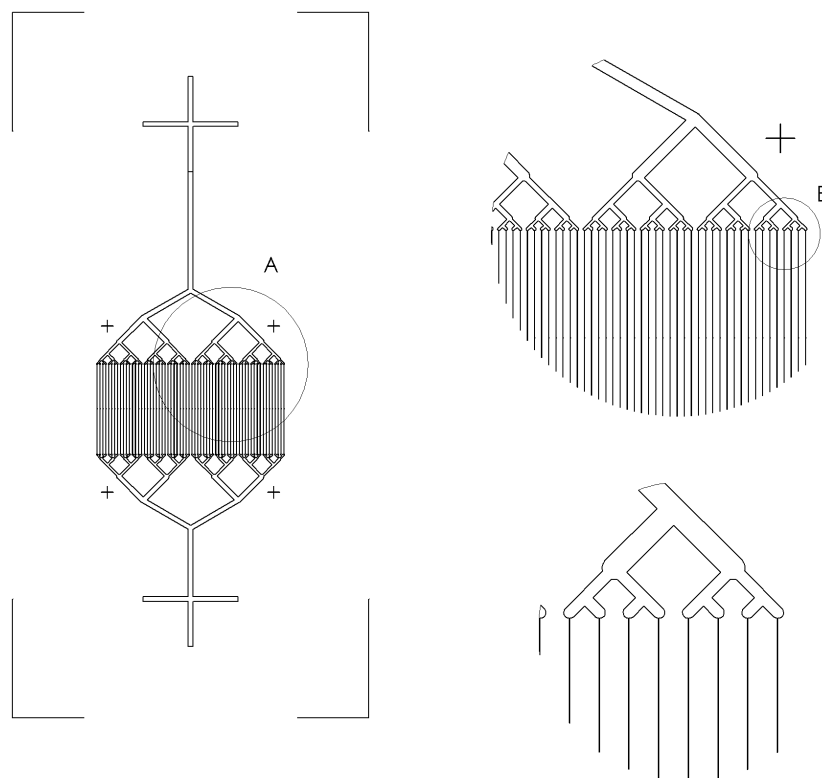


Figure 2.14 : Design of the one lane cell placing chip.

The solidworks model of the design (64 lanes) of chip with details.

The chip, called line cell placing chip, is designed to distribute the cells in one dimension channels . The chip is made of 64 $40 \times 40 \times 2,000 \mu\text{m}^3$ channels with equal pressure drop for each of them (Fig. 2.14) leading to a total volume of $0.2 \mu\text{L}$. The multiplication of channels aims to reduce the obstruction percentage by a cell clumping or any debris. Each channel similarly divides in two successively 6 times ensuring equivalent paths for all the lines, thus homogeneous injection.

10. CATS chip manipulation

The CATS sample exchange robot is adapted to manipulate cryoprotected pins and crystallisation screening plates. Similarly, a specific gripper was developed and adapted for handling the microfluidic chips (Fig. 2.15). Although these implementations push towards a better automation for systematic screening of microfluidic chips on the beamline, the robotic arm option for mounting chips on the goniometer head has not been fully investigated in the course of this work.

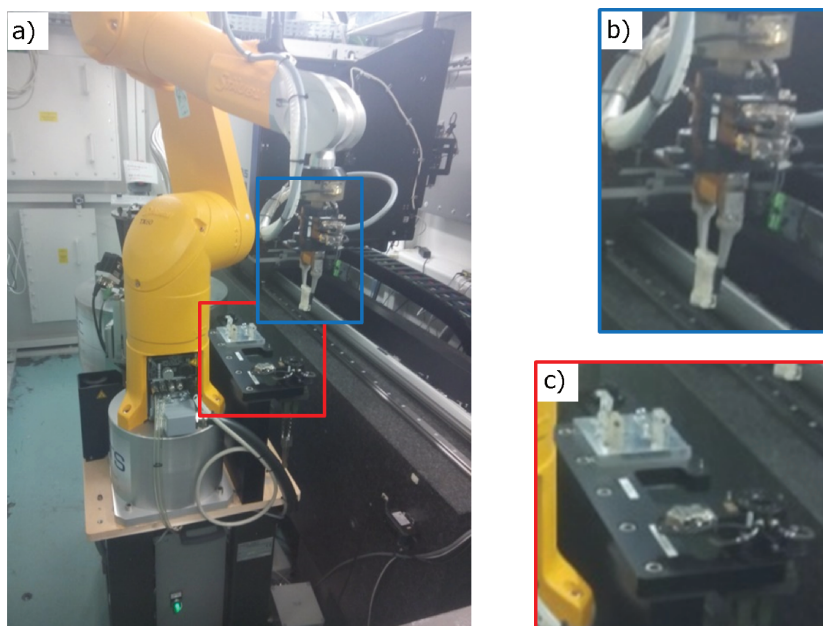


Figure 2.15 : Chip handling by the CATS robot.

The picture shows the CATS sample exchange robot arm with a gripper adapted to the chip support frame and grabbing such a frame (a). The gripper with the chip (b) and the chip stack (c) are highlighted in the insets. The size of the 3D printed chip-support handled by the gripper is $18 \times 40 \times 5 \text{ mm}^3$.

11. X-ray data collection

11.1. *Chip mounting on the goniometer*

While commissioning the technique, the chip is placed by hand on the goniometer head of the beamline. Eventually, this operation can be handled using an automated loading procedure through the CATS sample handling robot installed on PROXIMA-1.

The chip is vertically placed on the goniometer head set at an Omega angle of 0°, with the upper side pointing towards the detector. To make sure that no hardware collision of the chip could happen with the other instrumentation of the sample environment, the beamstop and the capillary are inserted close to the chip, and rotations of 40° in Omega around the mounted position are confirmed collision free. Similarly, prior to perform automated chip-mounting with the CATS robot, all the chip holder frames need to adopt a standard design, that will be confirmed beforehand collision free.

11.2. *In-situ Geometrically Optimised Raster scanning*

11.2.1. Goal of the I.G.O.R. scanning¹

The approach of using a microfluidic chip on an MX beamline consisted in designing some devices that could be used for automated data collection. The traps have been designed to place the crystals at known spatial positions in order to perform an optimised data collection at each position without spending time to re-center. For this purpose, computational developments in complement to the design of the chips had to be toned to properly handle and set the chip on the beamline. The MXCuBE software [[Gabadinho](#)] stands at the interface between the use of the beamline and its instruments ; it was therefore naturally extended to support the handling options. At the final state, the software MXCuBE should be able to :

- obtain through user actions the type of chip mounted on the goniometer, the data collection strategy, and any other useful information on the geometry and nature of the chip
- send commands to the sample exchange robot for the robot to pick up chips from their storage location

¹ Disclaimer : the name “In-situ Geometrically Optimised Raster scanning” leading to ‘I.G.O.R. scanning’ is clearly (not) linked with my name. I want to ensure that I was not an active actor of this name. During the work on automated, I named the scripts we made ‘grid scan’, because it allowed us to make a scanning of a grid. But the concept was already implemented elsewhere to center samples. P. Gourhant, working with me on the script named it ‘Igor Scan’ in order to find it easily on the large amount of PROXIMA-1 scripts. One morning, L. Chavas, the beamline manager, entered the beamline yelling : ‘I found it, I found it’... and he found the explanation to make this name official.

- make use of special marks within the chip to calculate all of the crystal coordinates within the mounted microfluidic chip
- move the chip to each position and optically identify whereas the trap is filled with an object or remains empty, take a snapshot of the traps, and eventually optically realign the crystals
- move the chip to each position and perform a data collection based on user predefined settings
- properly order and arrange collected data in a self-explanatory arborescence
- provide external software with necessary information for data treatment and merging of all the collected data.

In the course of the current work, only parts of the above automation has been implemented. Notably, the optical automated alignment of marks and crystals was not addressed ; similarly, the automated data treatment, quality scoring and merging remains a work in progress.

11.2.2. Scripted procedure

In order to satisfy the goals behind the I.G.O.R. scanning approach, an initial implementation was developed where a Python script (PROXIMA-1-SC-Scan) gathered the data collection information in addition to some vectorial values for a movement in X and Z axis to automatically shift the chip at all possible positions covered by the script. The calculated vector corresponds to the distance necessary to move the chip between two traps within a grid pattern. Rotation of the goniometer at PROXIMA-1 is performed around the omega axis.

In order to place the samples trapped inside the chip at the X-ray beam position, two sets of motors could be used. The first set of motors is part of the goniometer, which has micrometer precision. By construction, these motors have a travelling course of 10 mm. The second set of motors is located underneath the goniometer and are used for its general alignment in the diffractometer environment. These motors have a precision of 10 microns with a travelling course of 100 mm. In the first development phase of the approach, the goniometer table motors were preferred to reach the full length of the chip, especially in the X direction. In practice, some misalignments of the traps were noticed (Fig [2.16](#)), leading to reconsider the goniometer axis for the Z translation, and the table motors for the X translation.

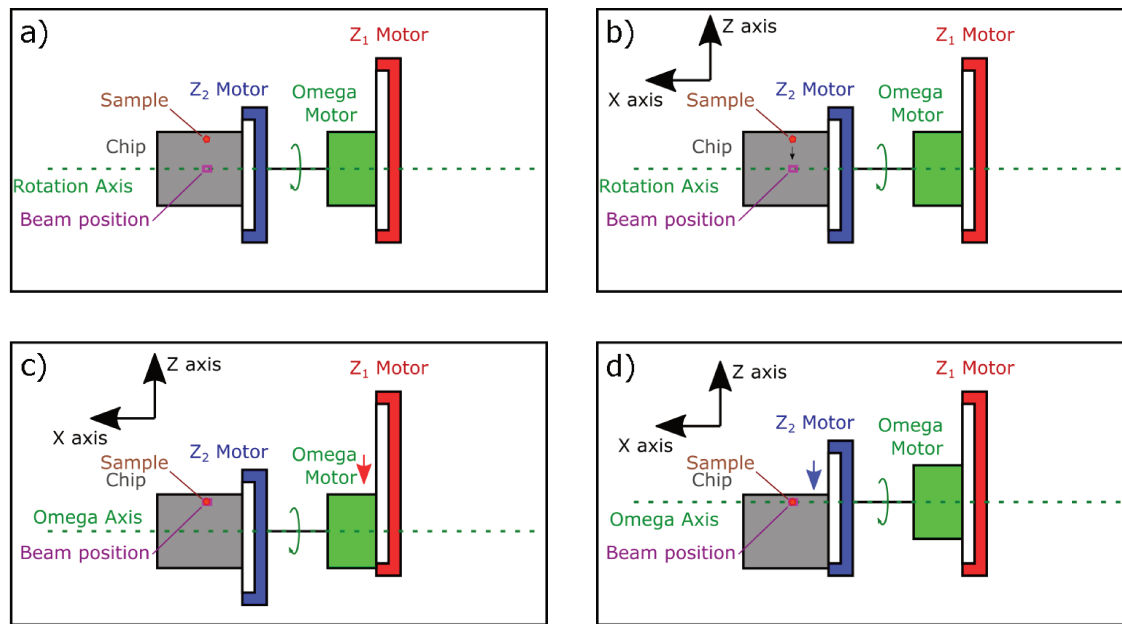


Figure 2.16 : Alignment challenges using motorisation located before the rotation axis.

(a) and (b) show the sample placed on the goniometer yet not aligned on the beam position. The Z₁ and Z₂ motors stand for the goniometer and the table motors, respectively. (c) shows the alignment performed by the Z₁ motor, moving the chip together with the omega axis and placing the sample at the beam position. In this centering scheme, however, the omega rotation axis is not on the beam position anymore. (d) shows the alignment performed by the Z₂ motor, moving the chip independently to the omega axis and placing the sample at the beam position.

To assure collision-free experiments, the Python script was completed with motor state sanity checks. Additionally, the script was implemented to save the position of each motor in order to replace the beamline at its previous state. Further human precautions were taken for redundant hardware security.

11.2.3. Coding details

Change of referential : In order to improve the precision of the placement of the crystals loaded in the chip on the beamline, the positions passed from being defined by X and Z shift to coordinates individual coordinates for each point. It allows handling any kind of chip design without the requirement to precisely orient the chip vertically and orthogonally to the X-ray beam. Using X and Z coordinates to place the samples in the focal position of the beam requires to obtain the coordinates of each trap and to calculate the operation to change the coordinates referential from the chip to the goniometer one.

From the theoretical coordinates of the traps and their real coordinates on the chip, several transformations can occur :

- translation : because the referential used by the beamline is linked to the instrumentation and the precision of the placement of the chip on its support

- rotation : when the chip is cut and placed on the chip support, a small tilt appears. Furthermore, the placement of the chip on the goniometer is not perfectly vertical and orthogonal to the X-ray beam
- homothety : stretch can be applied during the plasma bonding of the chip leading to scales modifications between
- non isotropic linear stretching : the stretch induced during the plasma bonding step can apply a linear stretch or shear stretch
- non linear stretching : during the assembling and bonding of the chip, the thin PDMS sheet is manipulated manually and therefore easily stretchable. Some deformations can be non linear, as stretching depending on the position on the chip of similar rotation on one part relative to another.

All the linear stretching or transformations of the chip can be registered in two three-dimensional vectors, hereafter referred as V and V' , for the translation and a 3x3 matrix M for the transformations. The non linear transformations will be discussed later. When the vectors V , V' and the matrix M are known, the conversion of the coordinates of a point A from the theoretical space $A(x,y,z)$ to the real space in the coordinates of the beamlines $A(X,Y,Z)$ follow the equation :

$$A(x, y, z) \times M - V = A(X, Y, Z) \times M - V' \quad (\text{eq 2.15})$$

In order to calculate the vector V and the matrix M for the change of basis, three non-aligned coordinates need to be determined in both referentials. The coordinates of the first point are subtracted from each other point and saved as the vectors V and V' , respectively. The following linear equations can then be solved :

$$\begin{aligned} (A_1(x_1, y_1, z_1) - V) \times M &= A_1(X_1, Y_1, Z_1) - V' \\ (A_2(x_2, y_2, z_2) - V) \times M &= A_2(X_2, Y_2, Z_2) - V' \\ (A_3(x_3, y_3, z_3) - V) \times M &= A_3(X_3, Y_3, Z_3) - V' \end{aligned} \quad (\text{eq 2.16})$$

Scanning range : The reference points used to make a change of referential are represented by the positions of the extremities of the traps within the chip. For the first tests, only three reference points were used in the hole chip leading to two flaws. First, when the chip size is of dimensions larger than what the goniometer alignment motors can reach, aligning on all the extremities became difficult. The chip may then for some parts stand outside of the goniometer range. An additional development in the operation of the chip on the beamline consisted in combining goniometer and goniometer table motorisations for the X direction. Second, the nature of the chip may cause issues. During the fabrication, in the bonding step, the thin PDMS layer can be slightly non uniformly stretched, leading to global angular distortions within the chip and precision loss in terms of trap positioning. The actual design of the chip is made of several rows

of traps each separated by 0.5 mm. Stretching may affect the relative positions of the traps in one single row. One solution for this stretching flaw lies in centering the each row of the chip.

Acquisition of the coordinates of the traps : In order to get the real coordinates of the traps, the theoretical positions of the traps have to be defined relative to the reference points defining the change of referential. At first, the coordinates of the traps and the reference points were manually registered with the known trap positions. In order to generalise the coordinates acquisition, a script was developed to extract a series of coordinates from the SolidWorks chip design as seen in Annex 5. The points have first to be placed in the precise trap positions in the 3D design. The script then registers each of the positions. The three first coordinates are registered as reference for the change of basis. Two different formats of the extracted coordinates were designed ; a simple table registered in an MS-Excel format ; a text record in .xml format with individual information for each trap coordinate, leading to more freedom when extracting this information to apply specific strategies.

Centering strategy Depending on the shape and the size of both the crystals and the traps, the crystals can tram in the trap at different positions. A 70 μm diameter crystal and a 10 μm crystal will be trapped differently. The larger diameter one will be blocked at the center of the trap, while the smaller diameter crystal at its tip. The 40 x 20 μm^2 X-ray beam available at PROXIMA-1 is not adapted for these different positions. One solution for this issue lies in the designed pattern shown in Fig. 2.18c, where the points A and C correspond to the positions of crystal traps ; both positions can then be centered depending on the most common crystal placement. The position of point B in this pattern does not need modification. Furthermore, if the crystals get trapped at two different positions within the traps, two series of collects may eventually be defined, one on each of the positions. For example thinner crystals may enter the smaller channels, and bigger crystals fix with the expected place. One series of data collection could here be defined only on the crystals at the entrance of the trap ; the second data collection could be set at the middle of the smaller channels.

11.3. MXCuBE implementations

The implementation of the I.G.O.R. scanning procedure within the MXCuBE software permits to register in a library the chip trap positions, using the coordinates acquisition script from the SolidWorks model by default. The implementation was scripted in such a way that other types of coordinates could still be considered without loss of functionality for eventual future developments. Using MXCuBE, the type of chip used for the experiments is chosen, three points are centered to the X-ray beam position virtualized in the MXCuBE centring interface (Fig. 2.17). The traps are then selected using the adapted widgets (Fig. 2.18d). The correspondence between the numbered coordinates (1-3 : 1-10 on the example in figure 2.18b) and the real coordinates of the chip is indicated in the description of the chip.



Figure 2.17 : MXCuBE interface as of March 2019.

The image shows the MXCuBE interface with a chip loaded with protein crystals. The various functional areas are highlighted in *red* for the Collection queue, *purple* for the image of the chip, and *green* for the data collection parameters.

11.4. Data collection

Data collection on the samples loaded inside the chip is made using the MXCuBE software and either center manually the crystals or use the I.G.O.R. scanning option. The centering mode is put on the specific 'chip' option, and the beamstop-to-sample distance is set to a minimum of 20 mm. Similarly, the data collection scheme is set to the 'chip' option.

While using the MXCuBE option (Fig. 2.18), centering of the chip is realised on a single row, using three reference points that need to be centered and saved in position. MXCuBE also allows selecting the type of the chip. The three previously centered positions can then be correlated with the selected chip reference points, which will open the full geometry of the chip to MXCuBE. The settings for the data collection are set with a starting angle of -10° , an oscillation angle of 0.05° per image over 20° in total (400 images). The name of the diffraction images is deduced from the position inside the chip. The locations of the crystals can then be selected, either in full or manually after performing a quick visual check at the traps to remove non-loaded traps. Fully automated data collection can finally be launched for all the selected trapping positions.

The beamline parameters of most of the experiment were set to the following : The energy was set to 12.67 keV just above the selenium peak, the detector to sample distance was set to satisfy a 2 \AA maximum recordable resolution, the oscillation angle per image was set to 0.05° and the beam intensity

was set to 10% of the maximum intensity, leading to $5 \cdot 10^{11}$ photons on the interaction surface of $20 \times 40 \mu\text{m}^2$.

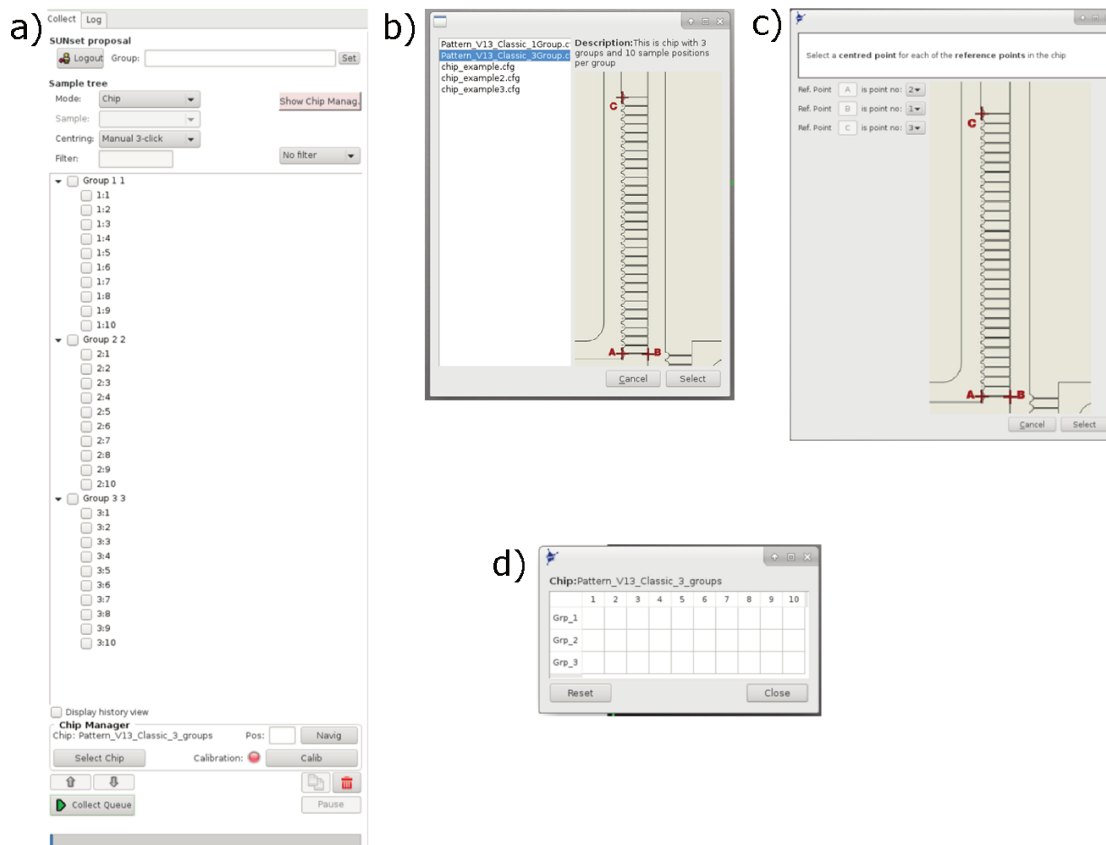


Figure 2.18 : MXCuBE I.G.O.R. scanning selection windows.

(a) The chip type selection screen developed in the MXCuBE software. (b) The centered point selection. (c) The trap selection window. It is a part of the MXCuBE interface that acts as a selection panel where the traps can be selected to be automatically centered to the X-ray beam position. The traps are grouped into sections and the traps can be selected by groups. (d) A widget tool made for an easier selection of the traps.

CHIP DESIGN, TESTS AND RESULTS

1. Introduction

In the course of this work, the microfluidic chips developed at PROXIMA-1 have been in constant improvement. Among the numerous versions, the thickness of the chip was decreased, improving its response to X-ray exposition. Additionally, the channel design inside the chip evolves dramatically, in order to optimise the trapping chances and pulling down the risks of clogging. Moreover, intensive work on the injection method has been provided to increase the number of crystals effectively injected into the chip, lying to better trapping results. The PROXIMA-1 beamline could be adapted to the chips by improving the approach for automation and adapting the sample environment. The automation is now accessible within MXCuBE through the I.G.O.R. scanning. Hardware equipment of the sample environment was modified to optimise the chip handling. Implementations have been made added to the CATS robot, with the installation of a new handling tool for robot-assisted chip mounting on the goniometer head. Besides, careful work on the fabrication methods helped to improve the fabrication success rate of the chips and its manufacturing time. Furthermore, in order to qualify the impact of the chip on the signal over noise ratio, the interaction between the chip and the X-ray beam has been studied. As the chip is supposed to obtain data acquisition from most macromolecular crystals possible, a protocol of chemical testing has been implemented and tested with the most common chemicals used in crystallography.

2. Design of the chip pattern

The patterns and channel design were improved in order to work around the different difficulties encountered through manufacturing and responses to sample-loading pressures. As a concrete example, optimising the injection, trapping or adapting the chip to different methods took great efforts, the main goal being to develop some generic reproducible tools. The complete list of the chip designs is available in Annex [5](#). The accepted and validated design of the chip (Fig. [3.1](#)) contains four entries: two main inlets for sample injection ; and two additional entries for ligand soaking. If the ligand entries are sealed or not punched, the chip acts as if no optional entries existed. The chip contains 180 traps ramified in three double rows. It is optimised to trap 20 μm to 50 μm crystals.

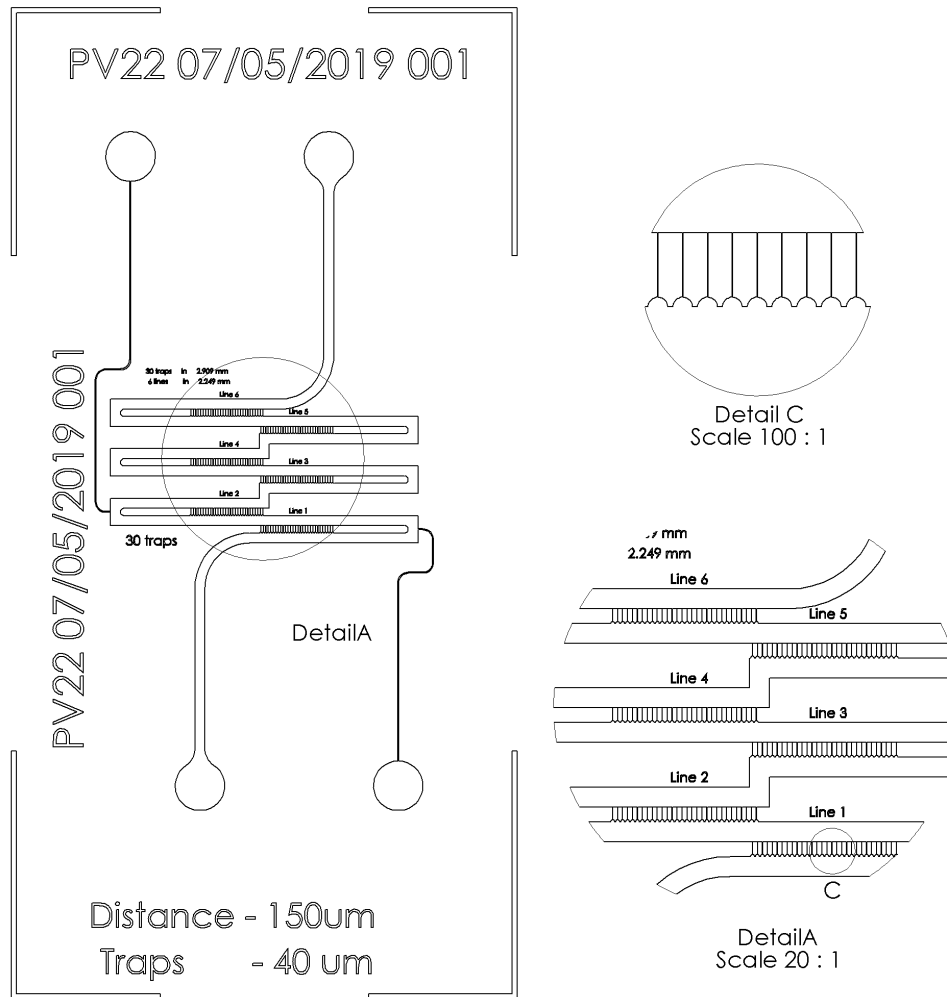


Figure 3.1 : Chip design V22.

Highlighted sections *DetailA* and *DetailC* are shown for illustration purpose. Three double-rows of 30 traps each provide the chip with 180 possible trapping positions. Optional ligand injection inlets are present for the first row. The injection direction goes from bottom to top.

3. Improvement of the chip molding

Along the steps towards the creation of the chip and during the molding of the PDMS, the shape and thickness of the chip were optimised, with improvements in order to artificially reduce its absorption towards X-rays, to reduce the PDMS consumption during the molding process, and to improve the chip fitting in its support frame.

3.1. Window creation

The chip is composed of two different layers with individual thicknesses. The first layer is 3 to 5 mm thick at the inlet locations in order to ensure the hermeticity of the connection between the chip and

the injection tubes. The second layer has to be the thinnest possible in order to reduce the impact of the noise induced by the chip on the experiment when absorbing the incoming X-rays. A compromise between the absorption and the mechanical resistance leads to 100 μm thickness. In order to achieve these goals, during the PDMS molding step of the chip creation, a 100 μm layer is first deposited in the mold using a spin coater, reticulated in an oven, the interaction zone is covered by an home-made cover and the rest of the PDMS is poured to reach the 3 to 5 mm thickness.

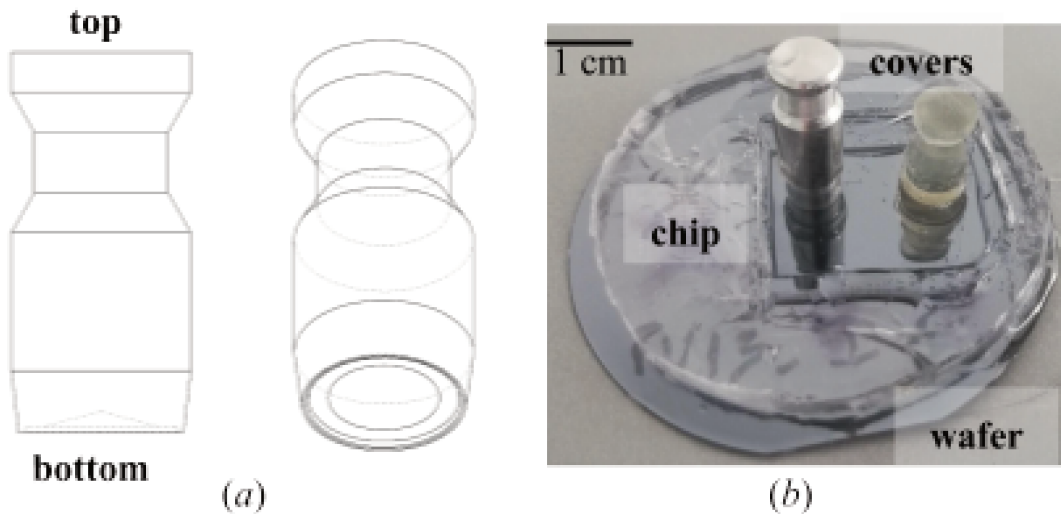


Figure 3.2 : Covers for creating a window on the chip.

(a) Designs of the cylinders viewed from the side (left) and with a small angle (right) to highlight the indented part at the bottom to prevent the cylinder surface from interacting with the PDMS zone. (b) Picture of a wafer at the end of the PDMS molding step, before removing the cover cylinders and the mold. Both aluminium (left) and 3D-printed resin (right) cylinders have been placed on the chip.

The cover needed to prevent the PDMS to leak inside the chip window or the interaction zone is formed of a metallic and heavy cylinder with a diameter of 8 mm (Fig. 3.2). Its exact shape has to be adapted for easy handling while removing it from the chip after the PDMS reticulation. The surface quality of the interaction zone needed to be completely smooth. In order to prevent the surface of the metallic cylinder to touch the PDMS and eventually affect the trapping pattern, a 1 mm indentation on the bottom surface was added to the metallic tool itself. This indentation also prevents leaking of PDMS towards the chip window. The initial cylinder was made of aluminium. Attempts were also made with a cylinder manufactured out of a 3D-printed resin. The aluminium cylinders are not thermally insulated, leading to heating in the oven, and a follow-up good PDMS reticulation on the surfaces directly in contact with the metal. The cylinders made of resin do not propagate the heat of the oven when insulated, leading to a reduced reticulated surface and thus to a harder unmolding. In fine, the chip performances were not affected when using either of the cylinder types.

3.2. External mold

During the PDMS molding step, 3-inch diameter wafers were used to mold at once three chips of 15 x 30 mm² dimensions. The initial protocol consisted in pouring the PDMS on top of the wafer placed inside a petri dish to prevent the PDMS from overflowing, with the drawback that it partially went under the wafer and stuck to the petri dish. Unmolding the PDMS became a difficult task that often led to breaking the wafer (success rate of ~20%). Variants of this design and approach were designed in order to reduce the PDMS consumption and increase the wafers life expectancy. In most of the new designs. However, the bottom of the mold was sticking on the thin PDMS layer during the unmolding step, forcing high tensions on the wafers, and resulting with high risks of breakage.

The best solution for this approach consisted in preparing first a PDMS mold using some aluminium sheet underneath to prevent the PDMS to leak off, followed by cutting off the chips based on marks available on the wafer, as reference. The rest of the PDMS can then be kept as mold for the next iteration. This process favoured operations with less breakage of the wafers, leading to an improvement and better efficiency in the manufacturing of the chips.

3.3. Thinner chips

The motivations behind this new manufacturing approach consisted in working with less PDMS material, to reduce as much as possible X-ray absorption by the microfluidic chip. The approach relied on a careful handling of very thin PDMS sheets using pincettes that lead to a drastic reduction of the chip dimensions, and a clear improvement in the chip production, going from 3 to 12 chips mold per wafer. Another generous advantage in this chip design lies in the fact that the fully assembled device will occupy smaller volumes in the sample environment, ensuring to reach rotation angles up to 80° at minima. Moreover, this new kind of chip (Fig. 3.3) permits to circumvent the molding difficulties previously encountered.

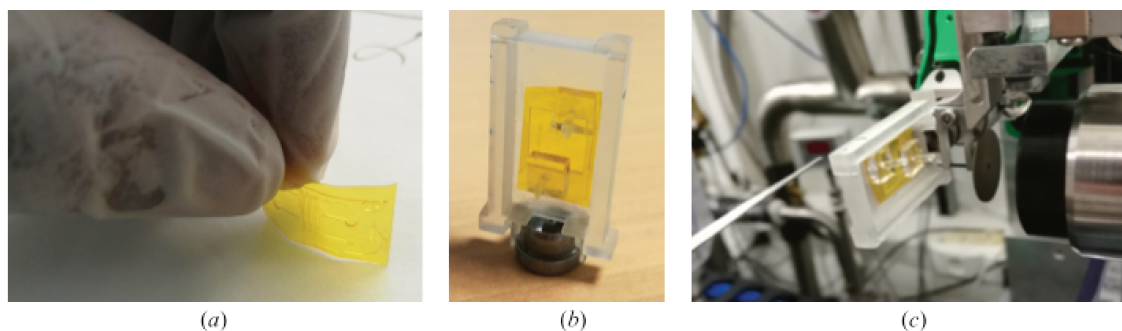


Figure 3.3 : Handling thinner chips.

(a) Manual handling of the the PDMS thinner chip after the bonding process. (b) Thinner chip mounted on the 3D-printed support, loaded with sample, sealed and ready for diffraction experiments. The chip is glued to the support, with the external tubings sealed. (c) Thinner chip mounted on the goniometer head at PROXIMA-1. The size of the 3D printed support is 18 x 40 x 5 mm³.

4. Improvement of the chip environment

4.1. *Chip handling*

In order to acquire high quality data collection from the samples trapped inside the chip, the latter has to be centered to the X-ray interaction point with micrometer precision using the goniometer available at PROXIMA-1. It is therefore necessary to prepare an interface between the chip and the goniometer that will ensure its proper manipulation by the goniometer, which has been developed to accept standardised sample holders. At first glance, the fastest solution would be to glue the chip on a standard pin, already adapted to the goniometer. The implementation has to be more reliable, motivating the design of a 3D-printed frame that would fulfill two important roles. First, the PDMS chip could be protected against mechanical stress on the beamline, which could interfere with the proper trapping and display of the crystal inside the chip. Second, this frame could be manipulated either by the CATS robotic arm on the beamline, the goniometer or manually by non-expert users.

4.2. *Chip support frame*

The chip support frame was designed to give a rigid support that would protect the chip from mechanical stress and deformation, and permit to manipulate the chip either manually or through the CATS robot. The first designs were made of two parts that would assemble to sandwich the chip (Fig. 3.4b). This initial design was engineered in order to confidently manipulate the chip and to ensure hermetic and simplified injections. To help injection, the frame disposes of two inlets for upchurch connectics. The frame facilitates sealing of the junctions through dents of 1 mm around the chip holes. Overall, six different support frame versions were proposed, two of which are hereafter described.

Removal of the tubing at the end of the crystal injection often caused large liquid movements inside the chip ; the first design idea added a blade to cut the tubes at the entry of the chip and therefore get rid of the tube removal step. Although this approach functioned as expected, the method did not answer the requirements to seal the chip entries to avoid evaporation of the liquid and the remaining liquid movements caused by temperature and humidity gradients.

The second design proposed added a screw perpendicular to each entry of the chip. The role of the screw was to compress the tubes until sealing. However, compression of rigid tubes by these small screws did not permit an efficient sealing, with additional difficulties when considering differential pressures resulting from different compressing properties of both screws, which lead here gain to variable flows inside the chip. This design was therefore not developed further.

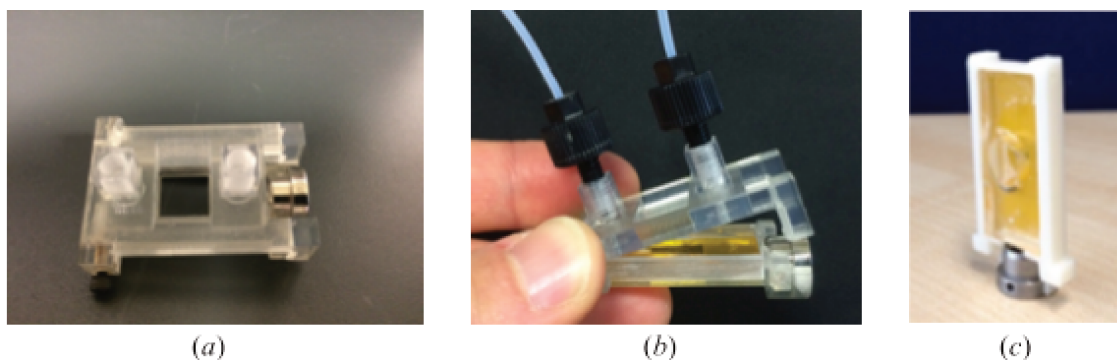


Figure 3.4 : Chip support frame.

(a) The two parts chip support frame closed without chip. (b) The chip in the open support with the inlet and outlet connected to the chip support. (c) The chip in a simplified support, currently used. The dimensions of the chip support frame are $20 \times 40 \times 10 \text{ mm}^3$.

In the above designs, in order to have the connectics of the support frame reaching the chip, the PDMS thickness needs to be $5 \text{ mm} \pm 1 \text{ mm}$, precision difficult to obtain while pouring PDMS in the molding step of the chip. Furthermore, the entries have to be exactly aligned with the entries of the chip, which implies that for all new chip designs with different patterns for inlets and outlets a new chip support frame would have to be developed. Notably, a major issue may appear with the design for the ligand chip (Supp. Fig. 4), where more than two ports are required. Moreover, the bulky shape of the support frame may collide with some equipment of the sample environment when mounted on the goniometer head and during diffraction experiments. For easier handling and safer experiments, the cover of the support frame was removed (Fig. 3.4c).

With the latest developments of the thin chip, a new method to fix the chip on the support frame was established. Since the thin chip is smaller than the 3D-printed support frame, it is glued to the frame and directly under the thick PDMS parts (Fig. 3.3b). The stress induced by the glue is absorbed by the PDMS and then do not interfere with the system.

5. Absorption studies

One of the major motivations behind the current project is to characterise the possibilities of serial crystallography experiments from PROXIMA-1 at Synchrotron SOLEIL using microfluidic chip devices, which implies identifying whereas a proper X-ray diffraction experiment could be recorded. Issues are thus rising on the X-ray absorption effects from PDMS-based materials, and whereas this could be a showstopper for the following implementations and experiments.

5.1. Preliminary absorption studies

For simplicity and in order to obtain comparable results, the transmittance of a chip is defined by the intensity measured on the dome photodiode divided by the intensity reported by the XBPM 04 (Supp. Fig. 10) [Desjardins]. The calculated value has no unit, with an arbitrary scale, for an easier

comparison of the relative intensities. In the current experiments, the transmittance of the different chips is tested depending on :

- The intensity of the incoming X-ray beam. The beam intensity is modulated by vertical and horizontal slits covering partially the photon beam before it is focused by a pair of X-ray mirrors, leading to an overall decrease of the mean intensity. For most of the test experiments, the incoming beam transmission will be set to its operational value : 10% for a ring current of 500 mA, corresponding to a flux of approximately $5 \cdot 10^{11}$ photons/sec.
- The incident angle of the goniometer omega axis between -40° and 10° in steps of 0.1° . The chip (Fig. 3.3) is placed vertically and perpendicular to the X-ray direction, defined as the 0° angle. The limit of -40° is caused by the design and shape of the chip in order to avoid hardware collisions with the surrounding equipment. The 10° limit is also explained by the geometry of the chip, symmetrical. The oscillation range of -10° to 10° is always collected in the current validation experiments, as it will be the favoured oscillation angle in MX experiments. Additional tests will be performed for the incident angle set at 0° , the angle with the smallest chip thickness.
- The energy of the incident photon beam between 6 and 15 keV in steps of 0.1 keV, corresponding to the accessible energies at PROXIMA-1.

5.1.1. Chip thickness

A chip made of 2 mm thick PDMS absorbs approximately 90% (from $5 \cdot 10^{12}$ photons/sec to $5 \cdot 10^{11}$ photons/sec) of the incoming X-rays at 12.7 keV energy ($\sim 0.98 \text{ \AA}$ wavelength) (Fig. 3.5). This strong absorption is coupled with a noticeable noise on the diffraction pictures, originating from the diffusion of the X-rays by the PDMS. Furthermore, because of the refractive index of the PDMS that is different from visible light (~ 1), visual centering of the sample enclosed in the PDMS-chip becomes challenging when the chip is not completely perpendicular to the visualisation camera (Snell-Descartes law).

Calculations of the PDMS X-ray absorption based on its chemical content and at an X-ray energy of 12.7 keV would indicate that a 100 μm thick PDMS chip should be sufficient for X-ray diffraction experiments, the absorption thus decreasing to approximately 70%. With a reported flux delivered at the PROXIMA-1 sample position for 500 mA ring current of $5 \cdot 10^{12}$ photons/sec on the whole surface, more than $1 \cdot 10^{12}$ photons/sec would still pass through a 100 μm thick chip, which would be sufficient for collecting diffraction images from 40 μm thick well-ordered crystalline samples.

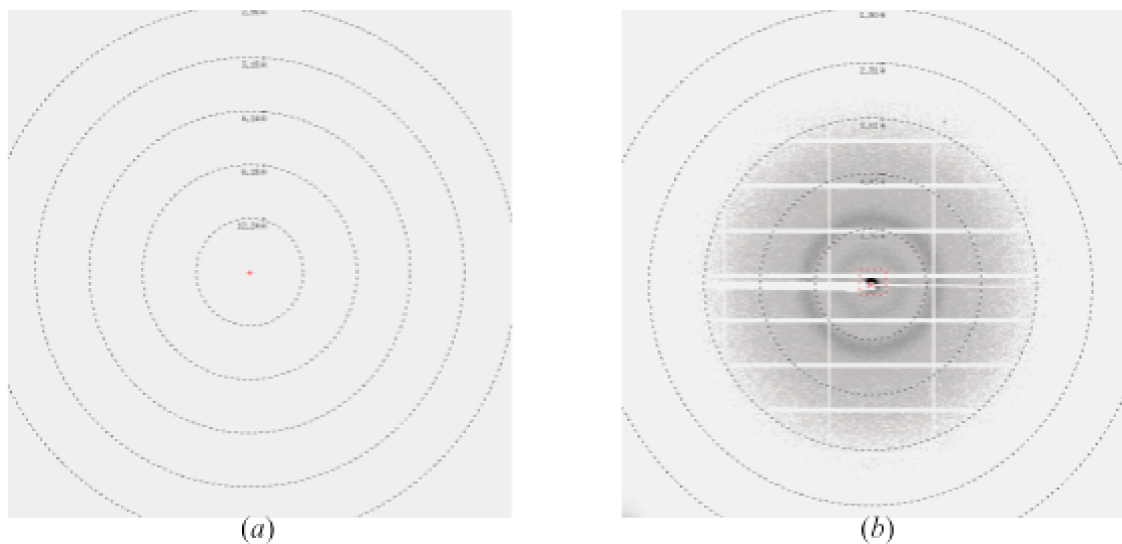


Figure 3.5 : PDMS chip absorption studies at PROXIMA-1.
 X-ray diffraction image without (a) and with (b) the PDMS chip in the beam path. No crystal sample was exposed during these experiments. The PDMS thickness was 2 mm.

5.1.2. PDMS mount

The PDMS is further held by a second material chosen based on four properties. It should be mechanically resistant; easy to handle; transparent to hard X-rays; and reactive to chemical treatment for bonding to PDMS. Taking the above into account, several materials and thicknesses were tested (Table 3.1). Although thin glass plates offer clear advantages for plasma-bonding and mechanical handling, its strong absorption to hard X-rays is a major drawback playing against its efficient use for X-ray diffraction experiments.

Material for PDMS bonding	Thickness (μm)	Measured beam absorption	Bonding quality
Glass	150	70 %	Excellent
Kapton	25	30 %	Bad
PDMS spin-coated kapton	125	35 %	Excellent

Table 3.1 : Absorption and bonding quality of different materials.

5.1.3. Beam impact

When exposed to strong hard X-rays as provided by PROXIMA-1, the resulting energy absorbed by the material composing the chip is majoritarily converted to heat, which could eventually degrade the elements exposed. Indeed, exposing a volume of $40 \times 40 \times 225 \mu\text{m}^3$ with an X-ray energy of 12.7 keV of intensity 5.10^{12} photons/s for 1 sec generates a total heat of $9.6.10^{-6}$ W or $2.6.10^7$ W/m³ on the highly sensitive material. Figure 3.6a shows a channel containing a mixture of Lysozyme crystals and precipitated Lysozyme (brown), together with the impact of the beam (clearer area). The strong X-ray clearly alters the precipitated Lysozyme. As another example of the impact of the X-rays on the chip, figure 3.6b shows the impact of the beam (5.10^{12} photons/s during 0.6 s) on the chip after test experiments with the PROXIMA-1-SC-Scan scripts.

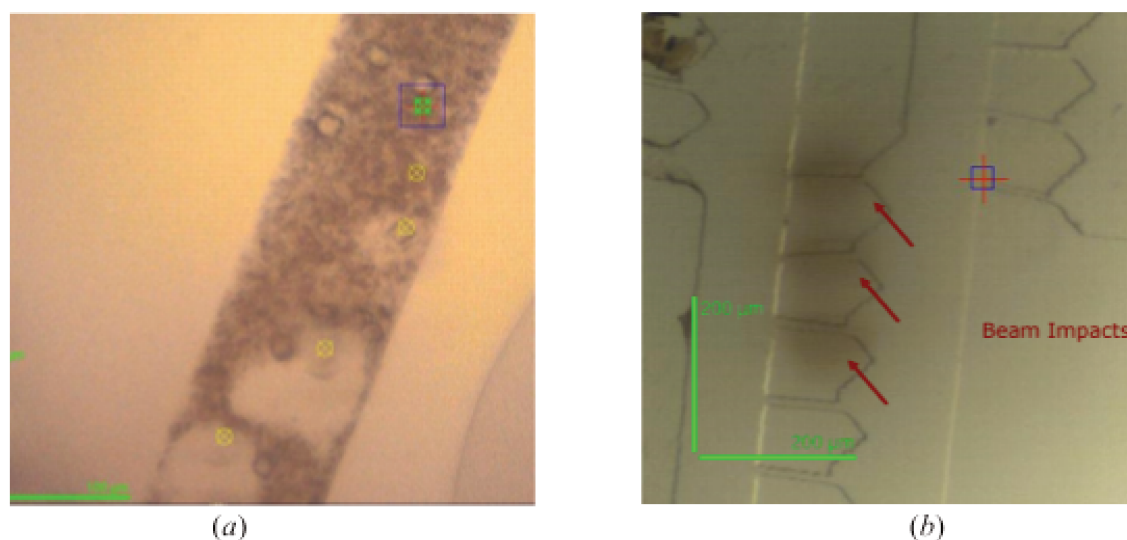


Figure 3.6 : Impact of the beam on the chip.

The yellow targets represent positions of previous beam impact, the blue square is the estimated size of the beam and the red cross is the estimated centered position. (a) A channel containing a mixture of Lysozyme crystals and precipitated Lysozyme (brown), together with the impact of the beam (clearer area) (b) The impact of the beam (darker) is highlighted with the red arrows.

5.2. Chip validation

The different types of chip have first to be compared in order to select the chip with the lowest impact on the beam. While designing the chip, the main parameter to optimise is its transmittance capacity in order to maximise the signal-to-noise ratio. At the X-ray energies used for the diffraction experiments at PROXIMA-1, a thin layer made of lighter atoms such as carbon-based components would fit best for experiments with optimum transmission. Considering the equipment available at Synchrotron SOLEIL and PROXIMA-1, four chips (Table 3.2) differing in composition were selected and compared depending on the nature of the layer the beam will pass through.

5.2.1. Beam transmittance vs incoming beam intensity

Although a notifiable transmittance difference exists among the various chips, their individual transmittance does not depend on the intensity of the incoming beam (Annex 4). Consequently and based on the handling properties of the chip, the chip 4 will be favoured for the rest of the experiments as it shows between 70% and 80% transmittance (Table 3.2).

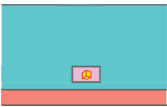
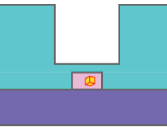
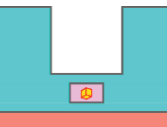
Chip name	Composition	Thickness	Illustration	Transmittance at 12.67 keV (vs 6 keV)	Transmittance decrease ratio for -30° vs 0°
Chip 1 3 mm PDMS chip	PDMS + kapton	3 mm + 25 μ m		10-15% (N/A)	60%
Chip 2 Thin chip on glass	Glass + PDMS	100 μ m + 100 μ m		35-45% (~2%)	60%
Chip 3 Kapton	Kapton (reference)	25 μ m		85-95% (~80%)	N/A
Chip 4 Thin chip on kapton	PDMS + kapton	100 μ m + 25 μ m		70-80% (~10%)	10%

Table 3.2 : Validation process of the chips.

The chips have been tested for reference. The Illustration column is indicative of the chip composition, with PDMS in cyan, kapton in orange, glass in purple, and the channels in pink, respectively.

5.2.2. Beam transmittance vs beam energy

The transmittance of the chip will vary depending on the beam energy, following the principles that the lower the energy, the more the chip will absorb photons ; and the more material the beam will pass through, the more photons will be absorbed, and the lower will be the transmitted beam. Consequently, although chips 2 and 4 are very similar, chip 1 absorbs much more photons and transmits much less. The transmittance measurements confirm that chip 4 remains the chip of choice, with a transmittance showing a linear variation from 10% to 80% for energies ranging from 6 to 15 keV (Table 3.2 and Annex 4).

5.2.3. Chip angle

All the chips show a decreasing transmittance depending on the angle made with the incoming beam direction. Thus, the highest transmittance can be seen at 0° , while the lowest transmittance appears at -40° . When comparing the amount of material the beam has to pass through depending on the angle, at smaller angles the photons interact with less matter, therefore resulting in a lower absorption and higher transmittance (Fig. 3.7 and Table 3.2). More precisely, chips 2 and 4 show a drastic decrease in transmittance starting at angles of 38° and 33° , respectively, most likely due to the shape of the chips (Annex 4). Both chips are made of a combination of a thin layer of PDMS at the center of the chip, surrounded by a thicker level of PDMS. The direct consequence of this geometry lies in the beam that passes through the thicker PDMS layer at higher angles, leading to an even higher absorption.

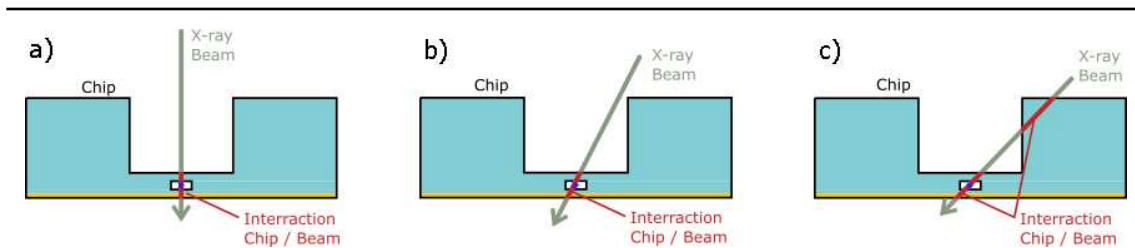


Figure 3.7 : Beam / PDMS interaction depending on the angle in the cross sectional view of the chip.

Layers are coloured cyan for PDMS, and orange for kapton. The beam direction is represented by a green arrow that becomes red at the interaction points with the chip.

In the latest design where the overall thickness of the chip has been minimised, the relative effect of the angle remains, although with a lower impact as the amount of material crossed by the X-ray beam is less. The effects of these differences by angles may affect the quality of the data and the following data processing.

5.2.4. In chip transmittance information

In order to gain information on the impact that may have the injected liquid on the transmitted intensity of the X-ray beam, and based on the previous studies, chip 4 was chosen for tests at four strategic places within the chip, as the transmission will depend on the combined effect of PDMS, CATS and the channel layers. In the following tests, the channel layer composition will depend on the position probed in the chip. The four places tested are:

- The parts surrounding the channel, made of PDMS and kapton. For these tests, the X-ray beam is focused outside a channel yet on the chip.
- The channel layer alone, empty and filled with air.

- The channel layer alone, empty and filled with air, yet with a position shift for every measured data. The shift in position (50 μm) of the exposed spot allows studying the chip unaltered by the previous X-ray exposure.
- The channel layer is filled with distilled water, simulating the condition when crystals will be trapped.

As it could be deduced from chemical composition, 40 μm PDMS absorb more than water or air (Annex [4.2](#)). A drop of the chip transmittance appears between 30% and 70% transmission for the chips loaded with air or water.

5.2.5. Validation of chip design

The above measurements were recorded in order to decide on the best chip design to adopt for optimised diffraction experiments. Among the tested chips, the design 4 made of 100 μm PDMS and 25 μm Kapton appears as the most adapted for the following X-ray diffraction experiments. The impact of the X-ray beam on the quality of the experiments has also been highlighted, emphasizing the impossibility to expose the chips more than once to the X-ray beam. However, as the impact of the radiation damage caused by the X-ray beam on the biological samples is far greater than on the chip itself, this beam impact on the transmission from the chip will be neglected. The transmittance depends on the amount of matter passed through by the X-ray beam, and therefore the design of the chip should take this into account by minimising the interacting distance and making low angle experiment. Because the samples are destroyed after a few degrees of experiment, large angles will not be needed.

6. Chemical tests

The chips have to be able to contain and trap the crystals in their chemical environment. Protein crystals are numerous and diverse in shape, size, chemical composition and response to external stress. Nevertheless, the systematic approaches when attempting to crystallise protein samples bring similar experimental conditions with common buffers and crystallisation medium. Thus, the diversity of the chemicals screened when growing crystals is a lot more restricted than the diversity of the screened molecules. In order to minimise wasting expensive and difficult to produce protein crystals, the chips' efficiency has to be guaranteed using the medium the macromolecular crystals under studies grew in. The method chosen in the current work to acquire this guarantee consists in testing the chip against the crystal environment (buffer and precipitants) with glass beads the size of the crystals, and verify if the beads can be trapped depending on the crystallisation condition injected. As the information on the trapping quality may be linked to the properties of the glass beads and not the medium ones, the trapping statistics presented here may be considered as only informative. Yet it provides a good feeling on the applicability of microfluidic chips.

Because the crystallisation conditions are most of the time composed of the same few components diluted in water, it is possible to test the chips with the highest concentration possible for each of the different chemicals. They have to represent the wider range possible. The possibilities in crystallisation cocktails being numerous, only the most represented components have been selected. The

choice of the different chemicals to test was established based on a broad search of the most used components in crystallisation screens developed at Hampton Research, Jena Bioscience, QIAGEN, and Molecular Dimensions Laboratories (Annexe 1). The full list of chemicals chosen for these experiments consists of the following chemicals : Glycerine, Boric Acid, AmmoSO₄, DMSO, Glycerol, H₂O, Isopropanol, 2-Methyl-2,4-pentanediol (MPD), PEG 8 000, PEG 200, Acetone, Bis Tris.

6.1. Strategy for the tests

In order to verify the functionality of the chip, visible effects of the flaws induced by non adapted buffers have to be characterised. The common defaults identified on the chips can be grouped in three distinct types.

- Visible destruction of the chip or unbonding : the chip is made of PDMS, a biocompatible polymer made of silicon, oxygen and carbon that can alter its structure or bonding properties. As an example, pure acetone can dilute PDMS ; when injected into a functional PDMS chip, it quickly breaks the weaker and smaller parts of the chips, leading to liquid leaks and disassembling of the chip.
- Leaks : leaks on the chips may be caused by low quality bonding or bad quality punching, leading to a non hermetic connection between the tube inlets and the chip.
- Efficiency of trapping : the ratio of liquid passing through the traps does not depend on the viscosity of the liquid. The high percentage of the chemicals used in crystallography, however, may be close to saturation ratio and do not behave as perfect liquids anymore. For example, high concentration MPD creates semi-solid filament-like structures within the liquid and aggregating objects, physically blocking the traps.

Note: for these experiments with glass beads, manual shaking and following handling do not guarantee homogeneous repartition of the glass beads in all the injected liquid. Even so, a perfect uniformity is not needed for the beads experiment as to test the quality of trapping only few beads are needed to be caught on camera and validate the trapping process.

6.2. Effects of the chemicals on trapping

Among the various chemicals tested, the 20% pure Acetone injection rapidly induced leaks in the chip and destroyed the bonding. The rest of the chemicals showed good behaviour, without visual effects on the stability of the chips. Trapping was also efficient and unaffected by the nature of the tested chemicals. The nature and concentration of the chemicals tested are summarised in Table [3.3](#).

Overall, the results of the chemical injections show that the chemical and mechanical properties of the PDMS chips permit to inject an extended range of solutions. Through the described injection and test protocol, any new chemical cocktail can be tested for injection in the chip.

	Maximum concentration	Remarks
H ₂ O	100 %	
Glycerine	1 M	pH 9.0
Boric acid	1 M	pH 4.0
Ammo SO ₄	3.2 M	
DMSO	1 M	
Glycerol	80 %	
Isopropanol	80 %	
MPD	30 %	
PEG 8k	25 %	
PEG 200	80 %	

Table 3.3 : Summary of the chemical validation of the PDMS chips.

7. Permeability towards oxygen

The confined middle of the chip could help expanding crystallography toward sensitive samples. As the chip is sealed before being placed on the beamline, it could be considered to use this confinement to use the chip to protect the sample from the environment, like oxygen sensitive crystals, or to protect the environment from the sample, like toxic molecules or viruses. If the chip is loaded in a controlled environment, it could be used as a protection layer toward the sample. For viruses, the security should be highly enhanced, in order to have at every time a second layer of protection if the chip sealing is compromised, like a decontamination mechanism of the beamline. This layer combined with the workability of the chip should help focusing the experimental choices on the science by removing a layer of constraint. As iron complexed proteins with heavy sensitivity toward dioxygen have been chosen. If the chip can isolate from O_2 , it should isolate most chemical contents and from any living organism.

7.1. Experiment on a kapton-PDMS chip V9

The permeability of the PDMS chip was tested by placing the chip inside an anaerobic chamber and injecting methyl viologen. Once the chip was hermetically closed, it was transported outside of the chamber, and visually inspected for the colour of the injected liquid. While still inside the anaerobic chamber, the liquid appeared dark, highlighting the absence of reaction of methyl viologen with the chip (Fig. 3.8). On the contrary, after taking the chip outside of the anaerobic chamber, the methyl viologen started to react, highlighted by its color changed to translucent.

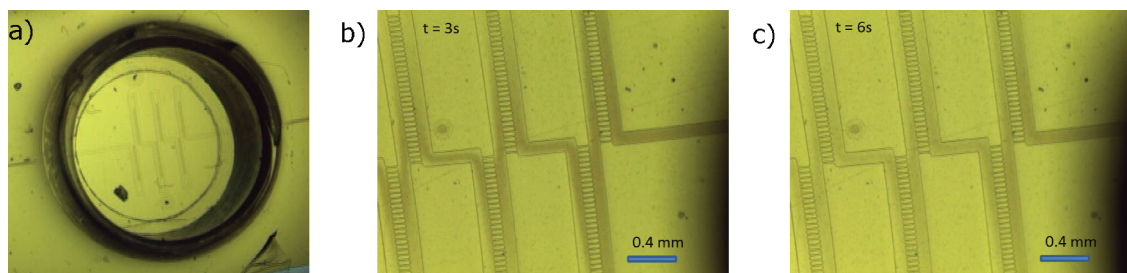


Figure 3.8 : Methyl viologen in a windowed chip model V9.

(a) Picture of a sealed windowed chip model V9 containing reduced methyl viologen. The picture was taken 3 min after exporting the chip outside of the anaerobic chamber. The methyl viologen is translucent inside the window and colored blue / dark outside. The dark color of the methyl viologen is due to the combination of the blue color of the liquid with the yellow background created by the kapton layer.

(b) & (c) Picture of a zoomed area around the window of diffraction, centered on the trapping pattern, while inducing a slight liquid flow running from left to right. The methyl viologen loses its color while entering in the window with a kinetic of the order of seconds.

Most oxygen-sensitive proteins would be affected by getting in contact with dioxygen after a few minutes, while methyl viologen oxidizes in seconds. In the current experiments, the kinetics observed for this reaction on methyl viologen are much faster than the theoretical kinetics. The color change occurred at two distinct speeds depending on the thickness of the PDMS. In the channels located within the diffraction window, the liquid turned translucent in one second. Channels outside of the window change color in two hours, mostly by diffusion effects occurring in the channels. These results are an indication that 50 μm PDMS is not sufficient to block the entrance of oxygen inside the chip. The 3 mm thick layer of PDMS is sufficient for a few hours, but has the clear disadvantage to strongly absorb and diffuse X-rays. Interestingly 50 μm PDMS doubled by 25 μm kapton seems to isolate better the chip from oxygen than PDMS alone. Although various procedures were tested to favour transferring loaded microfluidic chips to the beamline while keeping the direct environment of the chip in an anaerobic state, the beamline is ran in air, and handling of the chip together with all the data collection procedures would not be quick enough to avoid oxygen contamination inside the channels. New materials have then to be considered.

7.2. Control experiments with ChipX3

In order to seal the sample in a chip and also be able to place it on an X-ray beamline for diffraction, the ChipX3 [Wijn] was chosen. The ChipX3 was used as crystallization microfluidic and was made of Cyclic-Olefin Copolymer (COC), transparent to X-rays and hermetic to oxygen.

In the first step, the chip was tested with methyl viologen. After removing the sealed ChipX3 from the anaerobic chamber, the kinetic of color change was followed. After two hours, only a small leak from one of the sealing tape caused a progressive color change (Fig. 3.9a). A second ChipX3 was loaded inside anaerobic environment with iron-containing protein crystals. After sealing the chip with tape, it was brought on the beamline for X-ray diffraction experiments on the injected crystals. Three crystals were located and X-ray diffraction data collected, providing with a maximum resolution of 4 \AA . All

diffraction images contained a strong absorption and intense diffusion rings, most likely caused by the thickness of the chip (1.1 mm). Crystals of the same protein were shown to diffract at 2 Å resolution when fished and cryocooled. Five days after the experiments, the crystals still present inside the ChipX3 kept their brown color, characteristic of the non oxidized state of the iron complex (Fig. 3.9c). The ChipX3 seems therefore to be hermetic to oxygen, yet with a lack of crystal trapping and a strong diffusion background.

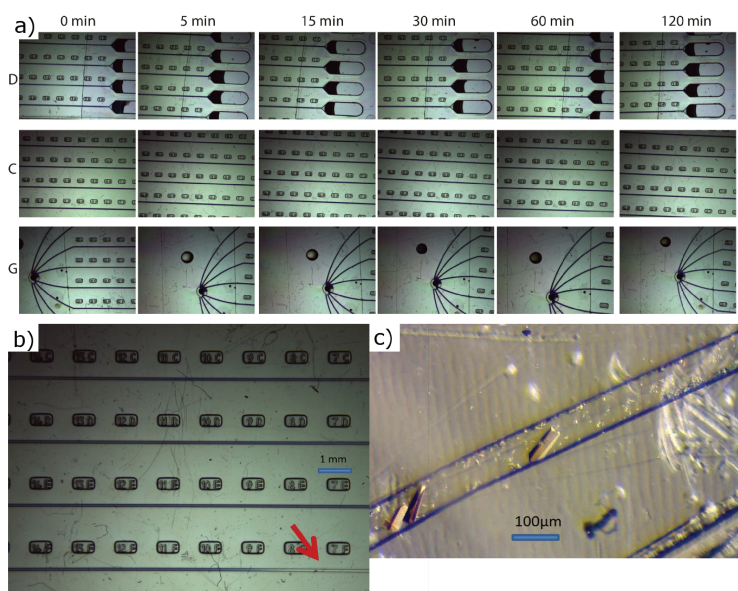


Figure 3.9 : Anaerobic tests on ChipX3.

(a) The pictures are zoomed windows of a ChipX3 loaded with methyl viologen, sealed with tape in an anaerobic chamber, removed from the chamber and finally exposed to air. The pictures are recorded at different time stamps from 0 min to 120 min at the two entrances and in the middle of the channels. A sealing leak can be seen around marks 7F to 10F. The chips have the dimensions of a microscope slide ($75 \times 25 \text{ mm}^2$) and eight channels with a straight segment of 40 mm and a cross-section of $80 \times 80 \mu\text{m}^2$. (b) taken after 240 minutes outside of the anaerobic chamber. The red arrow highlights a small leak coming from the outlet of the bottom channel. (c) Iron-containing protein crystals injected in ChipX3. The brown color of the crystals is characteristic of their non-oxidized state, color caused by the presence of iron complexed to the protein. The picture was taken 30 min after extracting the chip from the anaerobic chamber, and only a few minutes before the X-ray diffraction tests of the crystals.

7.3. Conclusions

The Cyclic-Olefin Copolymer (COC) material was verified as hermetic to oxygen, and the crystals were successfully injected in the ChipX3. The original design of the ChipX3 was engineered to favour crystallisation screenings, and therefore lacks the crystal trapping option. However, its composite being different than PDMS, it was considered here for a potential alternative device for oxygen free in situ diffraction experiments. The next steps of the projects are to create a trapping chip using the COC material and verifying its capacity to obtain diffraction experiment results.

8. Ligand soaking microfluidic preliminary experiment for ligand screening

8.1. Interest of *in-chip* ligand soaking

A microfluidic chip made for trapping crystals and making serial diffraction experiment can be theoretically modified to selectively soak the crystals with ligand after trapping the crystals. This will drastically cut the time and efforts used for ligand screening in the pharmaceutical industry. Experiments are now required to ensure the feasibility of the process by verifying that the precision of the injection could permit a ligand injection. The interest of such a chip is to serialize the ligand injection by injecting several ligand in the same chip and being able to rapidly screen the ligand efficiency with the protein. The information searched is only binary information on the presence or absence of the molecule in the protein. The entire structure is then not required and few degrees with a resolution higher than the ligand size could obtain the information required.

8.2. Ligand soaking injection experiment

In order to control the capacity of the chip and the injection method to precisely soak crystals in a chip without soaking the other crystals, a simplified design was made and colored water was used to represent the mother liquor and the ligand containing liquid. Four pressure controllers were applied on the various inlets (Fig. [3.10](#)), resulting in very precise control of which trap to target. Only the targeted row was soaked, but the control permitted to soak with a precise dynamic each of the traps with a different time with highly repeatable cycles.

8.3. Results

The preliminary experiment highlights the possibility to soak the chips with precision. Furthermore, the precision was even higher than the expected one. The chip permitted to soak independently two different rows, but it could also apply different soaking timing to the crystals of a same row and therefore open the possibility to study the ligand/protein interaction dynamic by comparing the crystals data at different soaking times. The next steps would be to find a well known protein with known ligand interaction (human Quinone Reductase in our case), obtain the structure of the protein as reference and then use the *in-chip* ligand soaking process to soak the crystals and acquire structural informations on the protein to compare it with the reference structure.

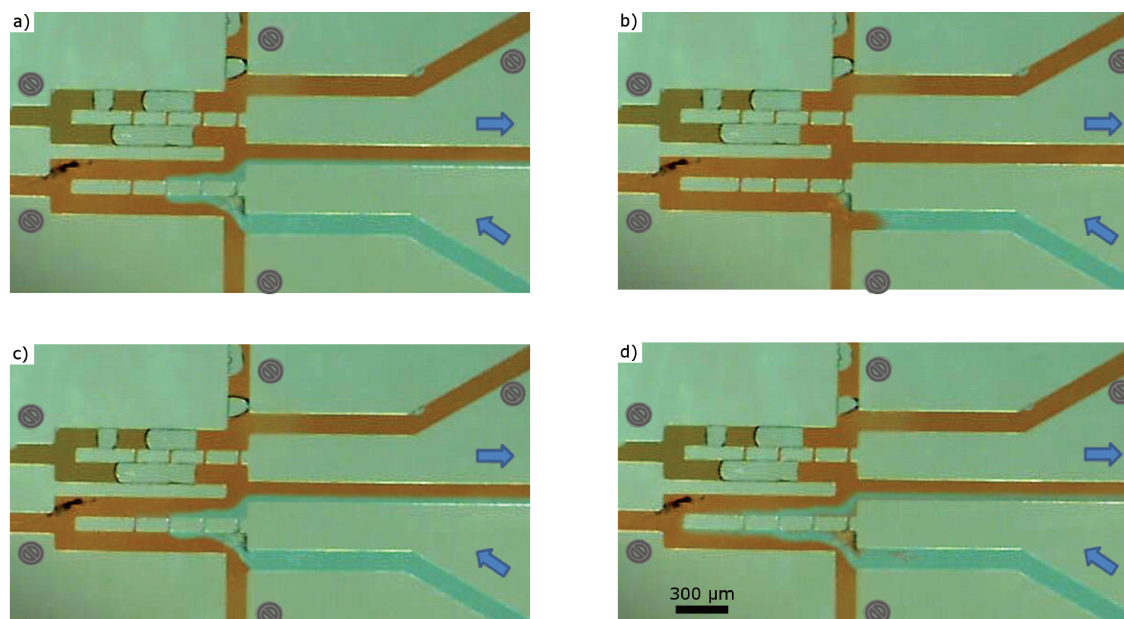


Figure 3.10 : Ligands injection cycle.

(a), (b) and (c) were recorded at various times of the experiments, 20.0 sec, 21.5 sec, 23.0 sec, respectively. Red coloring was used to represent the mother liquor ; the blue coloring represents the ligand containing liquid. Inlets located at the top, bottom, the top-left and top-right were closed ; the inlets at the bottom-left and middle-right were set at 30 and 40 mbar, respectively ; the inlet at the bottom-right had a sinusoidal pressure cycling between 30 and 50 mbar in periods of 3 seconds. The bubbles on the top row underline the immobility of the flow in the rows in which the ligands are not injected. On pictures (a) and (c), the pressure of the bottom-right inlet was set at 50 mbar. In (b), the pressure was changed to 30 mbar. In (d), pressure went up 55 mbar.

9. Conclusions

The pattern design and its environment has been improved in the last three year. The actual design is a fast, easy to make and disposable chips that can contain and diffract most of the macromolecular crystals. The thin layer of the chip has led to a lower beam-chip interaction. The PROXIMA-1 beamline can be handled by the beamline goniometer and the CATS robotic arm thanks to the 3D printed support frame. The absorption studies has led to qualitative information on the interaction between the chip and the X-ray beam, and permitted to validate the design selected. The chemical tests permits to validate the PDMS as compatible with most of the chemicals used in crystallography. In contrast, the thin layer induce a permeability to oxygen, leading to a need to change the composition of the material in the future. Currently, new chips made in COC are investigated as a material sealed material transparent to X-rays and impermeable.

GENERAL ISSUES

1. Injection process

The injection process into the microfluidic chip became a serious challenge. As of today, no general solution and protocol could be developed, although good advances were made to tackle the problem. The tools currently available and used to inject the crystals inside the chip are not fully adapted for volumes of the order of the microliter, classical volume obtained for most of the hanging-drop crystallisation trials. The injection devices consist of pressure controllers, better adapted for volumes of 100 μL minimum ; similar behaviours can be observed for the syringe controllers. As it is a subject of developments common to the different projects, the injections and the sampling difficulties will be discussed here with references to the related chapters.

1.1. *Plunging challenges*

To pump the liquid inside the chip, the injector has to be physically connected to it, guided by an anchoring mark designed in the pattern, allowing to plug the tube and link it to the inner channel network. The mark in the pattern consists of a target 1 to 3 mm wide that indicates where to drill with a puncher through the PDMS. After perforating the holes and bonding the two layers of the chip, inserting the tubes and injecting the liquid may apply some mechanical stress on the connectives, eventually resulting in destructuring and/or unbounding locally the chip, or even crack grooves in the PDMS, causing leaks of sample solution. Additionally, the PDMS will have to be at least 3 mm in thickness within 2 mm of the inlets in order to support structurally the stress linked with the connectives.

The observed leaks are mostly caused by bad operations during the punching step, and the following mechanical stress exercised by the connected injection tubes. The quality of the punching is strongly related to the quality of the puncher tool. It gets worse when the tip of the cylindrical blade is bent or get abraded by punching on hard surfaces like glass. Eventually, the mechanical stress may be reduced by bending the tubes by 90° prior to its end (5 mm before). By adopting this approach, the chip can be placed under a microscope to control the injection and lower the risks of leaking because of stress on the tube connectives.

An additional constraint lies in the complex arrangement of the instrumentation at PROXIMA-1, which cannot easily accept unnecessary tubing around the X-ray interaction area. As a consequence, the tubes have to be pulled out of the chip after the injection and before the X-ray experiments. Simply pulling the tubing out of the chip induces high pressures on the channel network, followed by liquid brassing in volumes larger than what the chip contains, eventually preventing the grasp crystals at all the trapping locations. To bypass this major problem, the tubes have to be inserted into the chip without any

leak nor unnecessary mechanical stress. A supporting tool that favours highly precise contacts between the tool and the chip prior to plugging the tubes has been engineered.

1.2. Sedimentation issues

The biological macromolecular crystals are denser than the solution in which they are stored, resulting in their natural sedimentation, thus reducing the homogeneity in the crystal solution. Depending on the injection strategy, crystal sedimentation may have various effects.

When injecting through syringes disposed in a horizontal state, the crystals settle to the bottom of the syringe. Typically, only the first crystals are still in suspension and can be injected, leading to the injection of only 10 to 100 crystals per chip independently of the number of crystals originally in the solution. For syringes disposed in a vertical position with the tip down, the end results are similar with the crystals that seem to be trapped into the joins between the syringe and the tube.

While injecting through a pressure controller, the reservoirs are vertical and the injection tube inserts down to the bottom of the reservoir. While the mother-liquor is injected, the crystals first run down to the bottom and only follow the liquid up the capillarity at the end of the injection process. As a result, all the crystals co-localise at the end of the liquid trail in the tube. It leads to no crystals during most of the injection and all the crystals packed are injected at the end, resulting in a heavy clogging and leading to crystals clogged in the channels. In order to prevent crystal clogging, a constant and gentle shaking device will be needed to maintain the homogeneity of the crystals in the tube.

For validation of the trapping mechanisms, glass beads are injected in the chips and the effects on the loading and trapping processes are followed on a microscope and recorded on camera. The chemical environment of the crystals is complex and diversified, yet water forms a large part of their composition. As such, their density will be approximated here by the density of water ($1,000 \text{ kg. m}^{-3}$). Glass beads have a density of $2,500 \text{ kg. m}^{-3}$, 2.5 times the density of water, leading to a fast sedimentation. With high viscosity liquids, such as PEG 8,000, the heavy glass beads sediment sufficiently slowly for an efficient injection without major concerns for sedimentation issues. Nevertheless, lower viscosity liquids such as water-based buffers, show faster sedimentation speeds of glass beads, often too fast for a representative injection. A homogeneous mixing of the liquid-containing beads would still end up with a quick sedimentation, faster than the set up time of the injection. Furthermore, the forces applied by the flow of injection remain weaker than the gravitational forces on the bead added to the viscosity of the liquid.

To solve the problem of settling down of the beads, a new injection mechanism has been engineered that consists in using a 1.5 m long tube with an inner diameter of 0.5 mm, representing a volume of approximately 300 μL buffer. The liquid is withdrawn from an open reservoir filled with the beads shaken in 1 mL of the chemical to be studied, using a syringe plugged in the pressurised air inlet of the pressure controller reservoir. The syringe allows for an easier control of the volume withdrawn, to ensure that the liquid stored in the tube and not in the reservoir, as a pressure controller does not have the required precision to precisely handle 300 μL .

1.3. Challenges in crystal sampling

During the course of this work, the crystals samples were obtained from three different methods : crystals in batch, crystals in tubes and crystals in drops. The crystals in batch are usually stored in large volumes. Four proteins types were crystallised in batch, namely Lysozyme, insulin, ZIF-8 and XPA (although this later was particular, being grown in cellulose). The volumes to be sampled approximate 100 μL , with no major sampling issues. Crystallisation in a tube was done on only one protein, Qr2. In this particular case, the major difficulty lay in not losing samples while plugging the tube to the injector (syringe pump or pressure controller). Major difficulties appeared when attempting to sample crystals grown in drops. Two samples were crystallised by vapour diffusion, *hQr2* and *Thermus Aquaticus* Ribosomes, respectively. The volumes of the drops varied between 2 μL and 0.2 μL , depending on the crystallisation method, *i.e.* manually or through a crystallisation robot. In both cases, the volumes were too small for sampling using tubes with a diameter of 500 μm .

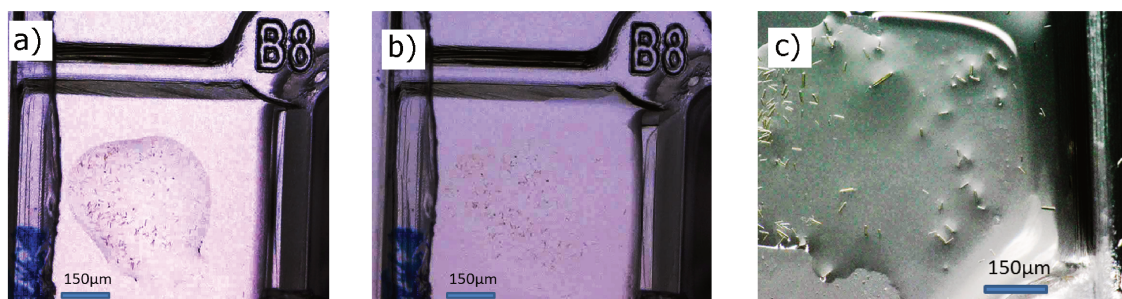


Figure 4.1 : *hQr2* crystals in drops before and after sampling.

(a) and (b) show one *hQr2* crystallisation drop before and after the sampling, respectively. (c) same as (b) with a better contrast. The sampling was performed using the 500 μm diameter injection tube both to add one small drop of crystallisation solution and to suck all the liquid from the drop. A large amount of *hQr2* crystals remains in the crystallisation plate after the sampling, crystals completely lost in the process.

In the particular case of crystals grown in drops, a microliter pipette was used to facilitate the sampling. In the first strategy, the volume of the drops was increased by adding a small amount of mother liquor to the drop and then suck the drop with its content. The micropipette was then used to inject the sample into the chip. Although the technique presents some simplifications in the manipulation when using thin pipette tips, with the possibility to prevent bubble formation, it is strongly dependent on the person manipulating the pipette, and is therefore hardly reproducible.

In a second strategy, the crystallisation drop was topped up by a micropipette. The drop with the crystals within was then sampled using the pressure controller tube. Both strategies proved useful for crystals in suspension in the liquid. In crystallisation drops, however, a complex equilibrium maintains the crystals in a stable state. The viscosity of the mother liquor can vary locally inside the drop, eventually creating some semi solid precipitation from which crystals can start growing. The crystals can also be attached to the crystallisation plate and may need manual breakage prior sampling. A thin membrane can

appear on the surface of the drop, trapping crystals in the flow. All of this heterogeneity in the liquid constituting the drop can prevent an efficient sampling of the crystals in some regions of the drop (Fig. [4.1a](#)). Moreover, drop composition and evolution is fully sample and crystal dependent, which render sampling and crystal handling difficult to predict ; all of these side effects depend heavily on the crystal types and their mother liquor. The inherent fragility of the crystal determines the manoeuvrability to detach the crystals from their support. But if the crystals have to be detached by hand using precise tools with the risk of destroying the crystal symmetries, the microfluidic chips lose their advantage toward the fishing. Meaning that if the advantage of the technique preventing the difficulties of fishing is cancelled with a challenging crystal environment.

1.4. Challenges with the injection

1.4.1. Channel filling

The trapping principle needs to have all the channels filled with liquid. When a channel is not filled with liquid, the pressure stabilisation, together with the raise of the surface tension raise the pressure drop of the non filled channel up to infinity until the channel is filled. During the injection of the crystallisation solution, the larger channels are filled first, with the thinner channels and the traps filled with air, which may prevent an efficient trapping (Fig. [4.2](#)). In order to ensure the proper trapping of the crystals in the first microliters of the injection, a preloading of the chip with the crystallisation solution only fills the channels and ensures better trapping. A minimum pressure is required to balance against the forces maintaining the air bubbles in the channels and traps. The minimum pressure depends on the liquid viscosity, the shape and size of the channels, the properties of the chip against liquid and other properties of the liquid itself. An example evolution of bubble collapsing is highlighted figure [4.3](#). Instinctively, an increase of the pressure will accelerate the collapsing of the bubbles. The kinetic of the bubbles collapsing will not be further investigated here.

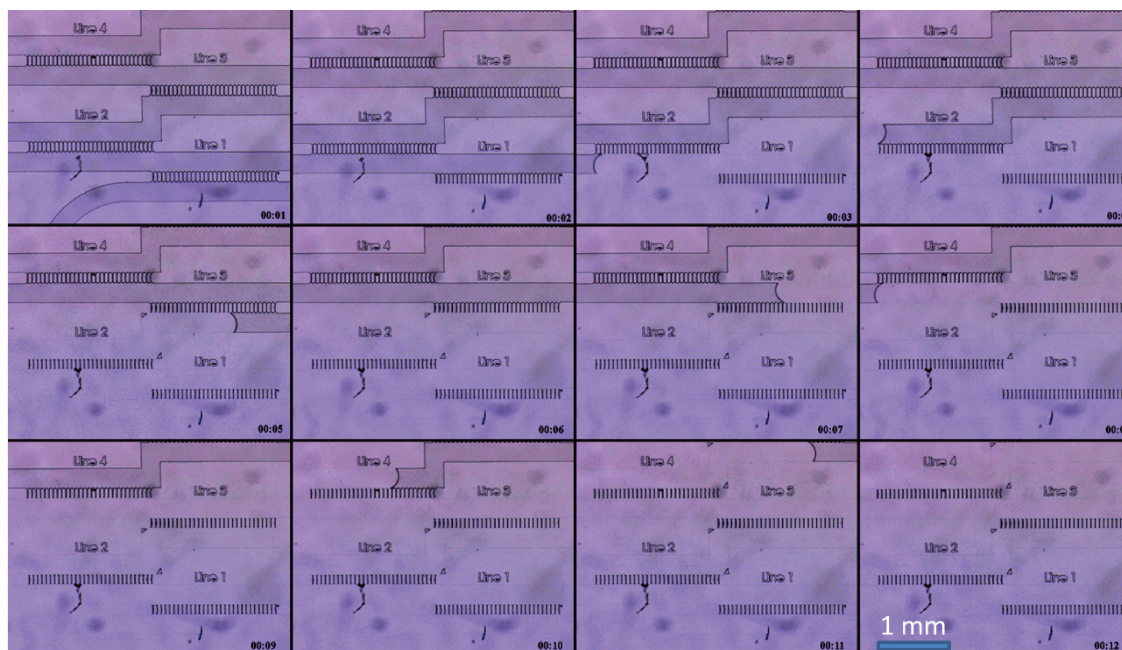


Figure 4.2 : Filling of a chip during injection.

The series of pictures shows the injection of ammonium sulfate at 3.2 M concentration using a pressure controller with a pressure difference of 30 mbar. The liquid is injected from the bottom to the top. The pictures are taken with one second between each picture. It appears that the large channels are filled with liquid but the small vertical channels are not.

1.4.2. Preloading

The solution used for preloading the chip can be injected either prior to crystal loading, while changing the tubes between two injections, or as the crystal solution.

- If the preloading is made with the crystal solution, the solution is tied to the crystal solution in the injection tube. The process needs to sample the solution after the crystal solution without making any air-bubble between the two liquids. During the preloading, the pressure is limited by the crystal ability to sustain the pressure, because the trap filling step requires a minimum pressure (Fig. 4.3).
- If the preloading is realised prior to crystal injection, the traps can be filled with the liquid using high pressures without altering the crystals nor the traps, as both injections are separated. Nevertheless, the method requires exchanging the liquid entry between the two injections, with the risk to inject bubbles in the process.

Choosing the proper injection method depends on the fragility of the crystals. If the crystal fragility is removed from the equation, it is better to simplify the process to first ensure the switch between the preloading solution and the crystal containing solution in order to inject both in one single

injection step. This would secure some continuity in the liquid injection, and therefore prevent the formation of unwanted bubbles inside the chip for a more efficient trapping. In a real case, it is important to measure the pressure the chip can endure when preparing for the experiments. The pressure necessary to fill the chip can be measured, using the crystallisation solution without the crystals as a test. If the pressure required for the filling is too high, the preloading step becomes mandatory ; if the pressure required is low enough, the stress on the crystals is minimum, and the preloading can be realised together with the crystal injection. Furthermore, in order to make sure that all the crystals present in the channels will be trapped, the injection can be followed by an additional postloading injection.

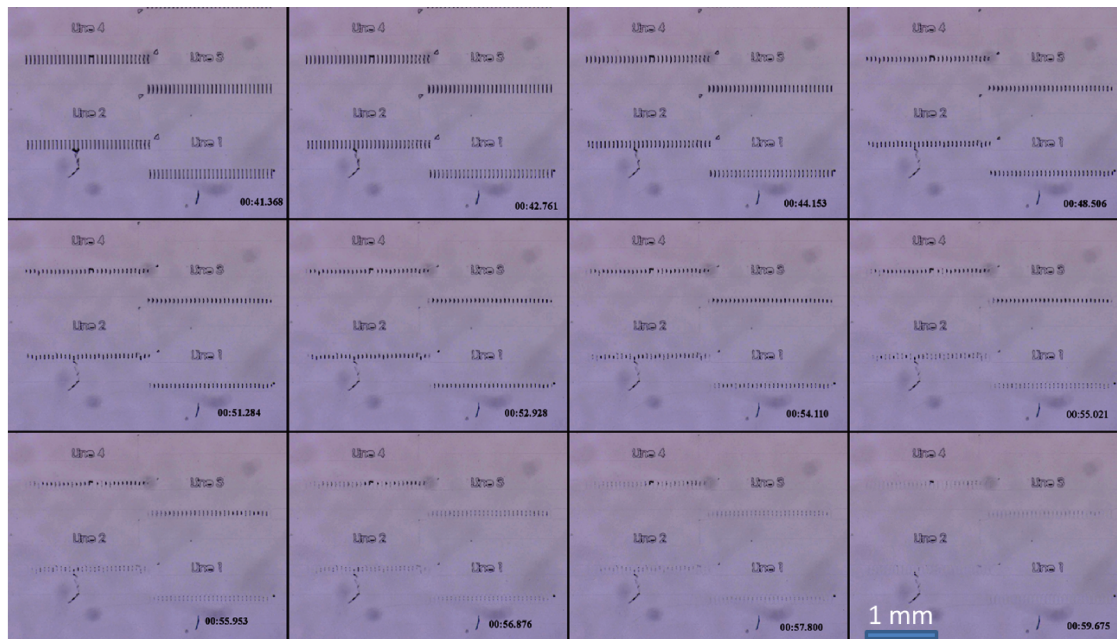


Figure 4.3 : Filling the traps of a chip during the preloading.

The series of pictures shows the injection of ammonium sulfate at 3.2 M concentration using a pressure controller with a pressure difference of 30 mbar and a base pressure of 400 mbar. The bubbles formed in the small channels disappear while the gas dissolves into the PDMS. The bubble dilution speed depends on the pressure of the liquid. With a base pressure of 400 mbar, the bubbles took 20 second to collapse.

1.4.3. Unplugging

Small pressure changes or mechanical deformations on the chip can induce some liquid flow inside the thicker channels. The trapping mechanism is based on the directional flow in one direction to ensure proper trapping. If the liquid flow goes back and forth, the crystals get released from the traps. Unplugging the tubes creates an empty volume of 5 μL that sucks the liquid out of the chip. Compared to the 3.2 nL volume sufficient and necessary to fill the chip, the flow created displays by several times the volume of the chip. Removing the tube after the trapping process, in the direction from the inlet tube toward the outlet creates a large positive flow that shall not cause any harm to the trapping mechanism.

In order to remove the tubes without having the crystals flowing out of their respective traps, several solutions have been considered. First, the tubes were gently removed in order to minimise the pressure difference applied on the chip and let the liquid from the injector fill the empty space created by the tube removal. The solution is non reproducible, the manual handling of the tubes does not guarantee the required precision.

Second, the unplugging was realised on the inlet part first, followed by the outlet. In this approach, all the crystals get untrapped while removing the inlet, and most flow back in position when unplugging the outlet. The control of the forces applied on the removal of both tubes being different and unreliable, the results of the experiments show random behaviours of the crystals. After the second unplugging, a small depression appears at the outlet of the chip using a pipette. A 1 μL pipette was approached near the outlet of the chip and the 1 μL air volume was quickly withdrawn. The process can be repeated several times. It is not sufficient, precise syringe manipulation of the liquid can create the flux necessary to trap the crystals. As the process often requires handmade adjustments, the reproducibility of the technique is not ideal.

Third, the inlet is unplugged in an initial step, with the difference that it will continue injecting the crystallisation solution at a slow rate during the process. This approach permits to keep constant the directional flow towards the injection. The technique appears reliable, however requires manual handling with all the unreliabilities coming with it.

Fourth, the tubes are cut. The technique is reliable and efficient, allowing to safely and precisely unplug the tubes.

Fifth, the use of heated pincettes to cut and seal the tubes at the same time appeared as the best solution. The process creates a small overpressurization with no major influence on the system. The inlet is sealed first, quickly followed by the outlet. The only drawback lies in the fact that the tubes need to be composed of plastic or glass fibers in order to be sealed by heat. Nitrile tubes are resistant against high temperatures and would not seal.

1.5. *Annexe problems*

1.5.1. Injection of air bubbles

Bubbles tend to appear during the injection, either at the preloading step or postloading. It can also come from small leaks during the injection process, located at the junctions between the syringe and the tube if syringes are used, or during the sampling process while small air bubbles are mixed in the liquid. Once in the channels, the bubbles can stay in the rows and interfere with the crystal trapping (Fig. [4.4](#)). The bubbles eventually fully block the liquid to pass through the thicker channel, pushing the liquid to flow through the traps with no possibilities to get around while the traps are being filled, leading to crystal accumulation on the traps and eventually clogging (Fig. [4.5](#)). Because the bubble is cornered, the

liquid passes around it ; to flush the bubble, high pressure is needed (around 500 mbar depending on the solution).

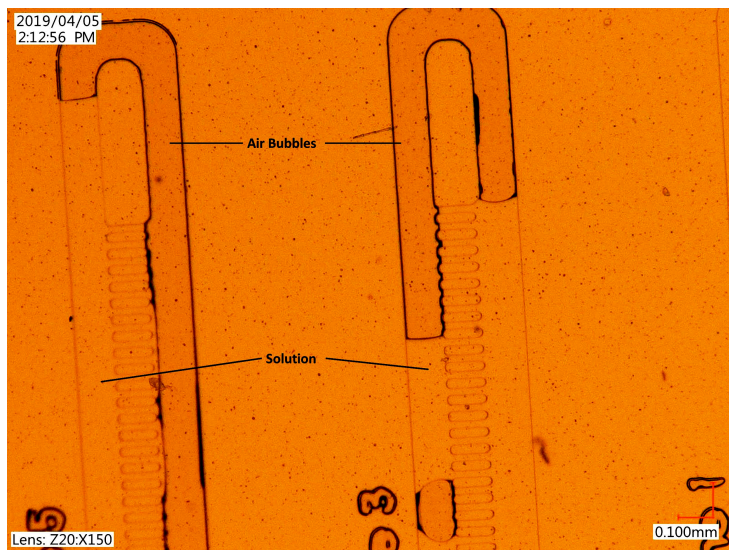


Figure 4.4 : Large bubbles trapped in the largest channels.

The picture was taken while injecting *h*Qr2 crystals together with preloading.

1.5.2. Crystal clogging

The crystals can clog in the channels or in the traps. Most of the time, clogging is caused by large objects stuck in the channel, such as larger crystals, or even unwanted solid or semisolid objects contained in the crystal solution (fibers, dust particles, etc.). While the object is blocked, it reduces the size of the channel and increases the risks that other objects are also blocked, leading to a cascade of events up to a complete clogging of the chip (Fig. 4.5). On the contrary, crystal clogging in the traps are better explained by small sized crystals, often too small to properly block the trap and yet too big to pass through the thinner channels. The blocked crystals favour other crystals to be trapped and eventually accumulate in the one single place while keeping accessible to the liquid the smaller channels. Multiple crystal diffraction cannot be properly processed, which renders the data recording from clogged crystals unreliable.

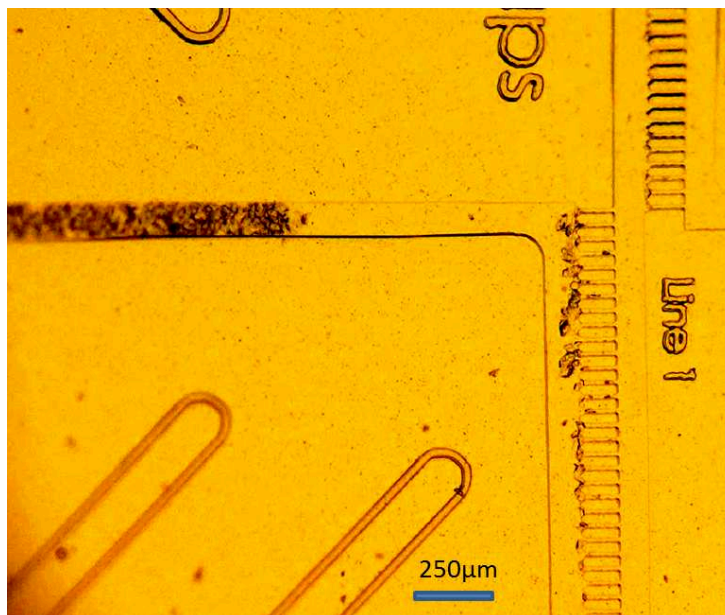


Figure 4.5 : Crystal channel clogging.

The clogging of Insulin crystals in the entrance channel blocks any additional trapping.

2. Beamline adaptations

In order to experiment with microfluidic chips at PROXIMA-1, numerous protocols have been dressed up and automated procedures developed to ensure the safety of the beamline equipment and to reset the beamline in its initial state after the data collections. In the sample environment, three instruments can eventually enter the volume occupied by the chip and thus collide with it : the beamstop, the capillary and the cryostream.

2.1. *Beamstop and capillary*

In the first experimental phase, the capillary was extracted to securise the collect and avoid colliding with the chip. The capillary drastically decreases the noise caused by scattering of the incoming beam with the air and the interaction with upstream equipment. In order to improve the diffraction quality, the insertion of the capillary was added in the procedure. As the experience-based knowledge increased, the capillary was included and the chip systematically tested for the maximum omega angles reachable. These angles, carefully measured before the experiments, fixed the collect angle limits. Moreover, to bring the goniometer to data collection speed, and to stop the rotation at the end of the data collection, additional acceleration and deceleration angles need to be included in the full omega rotation. Typically, for the rotation speeds set by default during the I.G.O.R. scanning ($1^\circ/s$), 7.5° were added prior and after the data collection angles to ensure that the chip does not collide with the capillary. With the pattern evolution of the chips, the overall design became thinner and smaller, pushing towards the possibility to

reach an omega angle of 120° ; collision sanity check thus became optional and not systematic anymore. The safety angles were fixed at -40° and 40° , respectively.

Additionally, PROXIMA-1 is optimised for data collection on macromolecules crystals with large unit cells, providing with a beamstop that can be moved away from the sample position to reduce low angle shadowing and allow for very low resolution data collection. This option benefited the chip handling while moving the beamstop from 10 mm away from the sample position to a new distance of 20 mm (Fig. 4.6).

2.2. Cryostream

The majority of the samples studied at PROXIMA-1 are frozen at cryo temperatures to minimise the impact of X-ray radiation. The experimental setup ensures that at each step of the experience, the sample is kept at cryo conditions. A cryostream sends a nitrogen steam set to 100 K on the sample position and is located 7 to 8 mm away from the X-ray interaction point. In order to mount and operate the chip, the cryostream has to be extracted to prevent possible collisions. The PDMS layers constituting the chip offer small temperature isolation to the sample, preventing good and homogeneous freezing of the samples, would there be needs to freeze them. Moreover, the nitrogen gas flow creates ice crystals and water condensation at the surface of the chip, preventing efficient centering and adding noise to the diffraction patterns. Two solutions appeared to solve this problem : adding some occlusion foil to block the cold flow, or physically remove it entirely.

As the use of cryogenisation remains crucial at PROXIMA-1 for experimenting in cryo conditions, the cryostream has to be precisely repositioned once the data collection on the chips is over. Manual operation was laborious and doubtful ; warming of the cryostream in addition to its full extraction were thus added to the microfluidic chip experimental protocol and to the MXCuBE interface. On this account, experiments can be initiated in approximately 20 min, and more importantly will allow resetting the beamline sample environment in an automated and efficient approach.

2.3. Three-points centering

The MXCuBE software provides the user with a graphical interface for centering samples to the X-ray beam position. The centering options tune the number of points N with the angle W between two consecutive centering points. Practically, for centering a sample , the user clicks on a dedicated button on the interface, that starts the incremented centering procedure. The goniometer then rotates by W degrees in the omega axis and repeats the procedure until the N clicks have been confirmed. By default, the user has preselected a classical three points centering with 120° between two consecutive clicks in order to cover 360° with high precision. This operation is iterative until the user is satisfied with the position of the crystal at the beam interaction point.

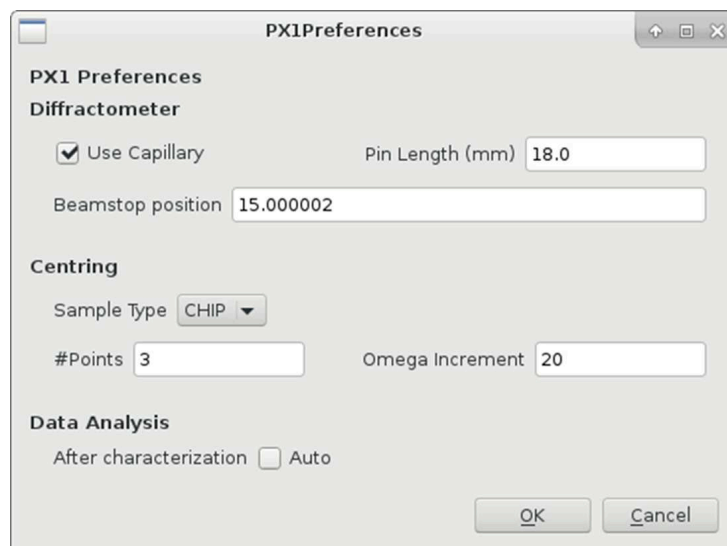


Figure 4.6 : MXCuBE PX1 preferences widget.

The widget has been adapted to monitor the specific parameters of the beamline linked with the chip, such as the optional use of the capillary, the beamstop-to-sample distance, and the centering parameters.

With the 2D geometry of the chip, the information acquired with the centering camera at angles near 90° and -90° becomes irrelevant. The chip only needs to be centered around three points over a total angle wider than the collected oscillation angle to ensure the alignment of the sample on the beam position during the data collection. The addition of new centering methods within the MXCuBE interface properties helped in integrating the chips on the beamline in a comprehensive way (Fig. 4.6).

3. Conclusions

The different difficulties and adaptations have been highlighted in this part. The injection challenges, and the general difficulties to inject that could lead to the loss of a part of the sample during the sampling, during the injection, or just after the injection. The injection of one air bubble during the injection can stop entirely the trapping process of the chip, and a wrong removing of the tubes can untrap the crystals in the chip. These difficulties make room for future improvements of the chip of its biggest actual flaws. The beamline has been well adapted, passing from hours to ensure the chip was properly handled and did not collide with any instrument to a flawless use using the automated I.G.O.R. scanning for fast and efficient collects. The chips have now to be tested on representatives samples to characterise the results of the chip

1. Introduction

In the previous parts, the function and the limits of the chips has been highlighted. The chip can trap up to 180 macromolecular crystals with low and stable absorption of the incident X-ray beam while being adapted to most chemicals commonly used in macromolecular crystallography. The beamline has been adapted to the chip and can handle automatically the samples with a minimal human interaction. Furthermore, the chip can easily be adapted to new challenges by modifying the chip pattern or dimensions in order to fit particular requirements. The chips will be tested on many carefully selected samples.

First, the chips have to be tested on well mastered protein crystals in order to remove the crystallisation hazards from the equation and focus on the chip results Lysozyme [[Jollès, Osserman](#)] has been chosen as reference crystals for technical improvement in crystallography. Then, the chips properties have to be challenged with relevant difficulties in the actual world of crystallography and even permit the access to new fields. In the process of acquiring 3D information on new molecules, the crystallography method lacks the information on the phase of the diffracted beam. This lack of information could be obtained by many methods but more specifically by the anomalous phasing. The Insulin [[Bentley](#)] protein has been chosen as it contains naturally zinc allowing for anomalous data collection on native crystals. A new field of macromolecular crystallisation uses in-cellulo crystallography to grow the crystals in the cells and passing on the crystallisation difficulties to the cells. The HEK293 cells and the XPA protein [[Tsutsui](#)] have been chosen as this combinaison is well documented and the fluorescent properties of the XPA permit to be easily localised. A great part of the current challenges in crystallography are linked to difficult to crystallise proteins and very sensitives crystals with mechanical and chemical weakness. The Ribosomes crystal [[Pellegrino](#)] have been chosen as fragile sample, as many cannot sustain cryoprotectant. In order to be able to compare the results of the technique, the *Thermus Aquaticus* Ribosomes has been chosen. Some crystallography samples could need confinement. It could be due to the sensitivity of the molecule to the exterior or the dangerousness of the sample. The chip will then be tested in its faculty to confine the crystals to the exterior middle. A non published iron containing and oxygen sensitive protein has been chosen as the O_2 molecules are one of the smallest molecules and therefore induce a high confinement test. In the process of acquiring new medicine, the pharmaceutical industries do ligand screening, consisting in testing the interaction of a protein with numerous ligands in order to check their possible interaction. As a yes or no signal is required, the small wedging and the high automation of the chip process linked with adaptations of the chips could accelerate the process and thus pulling up the research process in drug design. *hQr2* [[Boutin](#)] has been chosen as well mastered with known interacting ligands.

2. Wedge serial crystallography on test sample

2.1. Lysozyme

Lysozyme, a well known and characterised protein, is the molecule of choice for proof of principle studies in macromolecular crystallography ; as such, it was used in the early stage of the current work to test the quality of the technique.

2.1.1. Crystallisation

The current crystallisation protocol refers to previous work [[Chaussavoine](#)], with several optimisations made to increase the size of the crystals from 10 μm to approximately 20 μm . The protocol employed to grow Lysozyme crystals having the particularity to allow fast crystal growth from batch methods, the distribution of the crystal size and shapes is rather random (Fig. [5.1](#)), with a tendency to generate crystals of 30 μm in the longest direction.

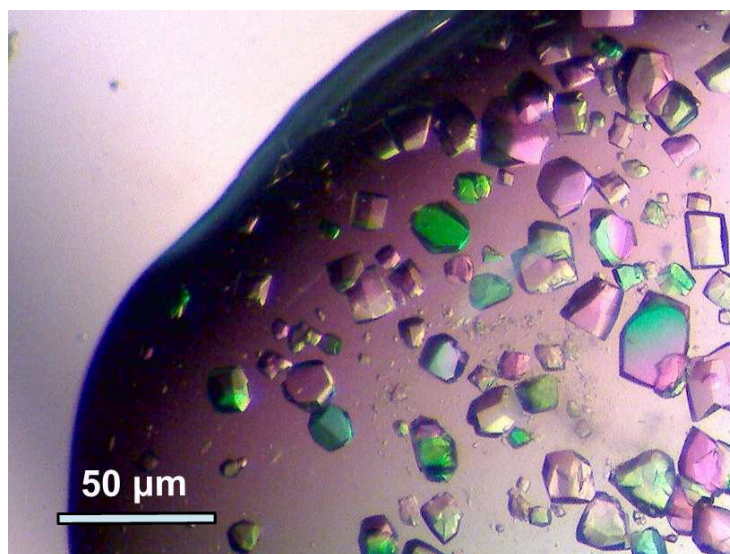


Figure 5.1 : Lysozyme crystals grown in batch.

2.1.2. Crystal loading

In the following experiments, Lysozyme crystals were loaded on a microfluidic chip with a V9 pattern (Supp. Fig. [3](#)) using syringes. The mother liquor of the crystallisation condition was clear of

visible aggregates, leading to smooth sample loading and crystal trapping without major congestion difficulties (Fig. [5.2](#)).

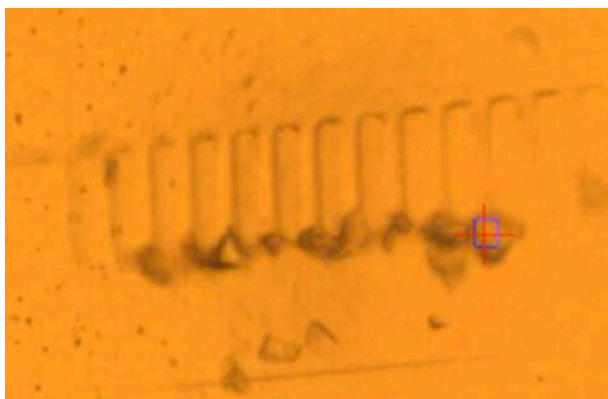


Figure 5.2 : Lysozyme crystal trapping.

Lysozyme crystals trapped in a V9 pattern viewed from the MXCuBE interface (the blue and red target represent the beam shape and position, respectively).

2.1.3. Data collection

Data on Lysozyme crystals were collected using the automated through the first set of chip handling scripts. A single row of 30 crystals was aligned using the MXCuBE three points centering, followed by data collection on each trapped crystal via a 50 μm vertical shift along the goniometer Z motor (distance between each trap). A small angle existed between the orientation of the chip and the direction of the goniometer Z motor ; at the early stage of the experiments, this was not taken into account in the calculations of the crystal positions, leading to possible misalignments of the samples. Nevertheless, diffraction data were recorded automatically for all the potential trap positions, collecting total wedges of 30° with 0.1° oscillation per image, with 10% of the PROXIMA-1 flux ($\sim 5.10^{11}$ photons/sec at 12.67 keV) and 10 images per second, on a Pilatus-6M (Dectris, Ltd.).

2.1.4. Data processing and structure determination

Out of the 30 collected data, 9 were preselected based on their identical crystal lattice parameters that could eventually merge in a constructive way. The best data were obtained by merging data sets coming from 3 crystals. The structure of Lysozyme was solved by molecular replacement using the protein data bank coordinates entry 4dt3 as the search model. The phasing was only performed to confirm that no major problems occur with the protein structure ; thus, a single run of restrained refinement using the *Refmac5* software suite [[Murshudov](#)] followed the molecular replacement step, with no addition of water molecules. The structure folds as the expected Lysozyme structure (Fig. [5.3](#)). Interestingly, the electron density is very well defined, with radiation damages clearly not visible, as confirmed by the undamaged disulfide bridges identified (Fig. [5.3b](#)), classically more fragile to radiation. Data analysis and refinement statistics are shown in Table [5.1](#).

METHOD	<i>In-situ</i> Lysozyme for molecular replacement				<i>Cryogenized</i> Lysozyme for molecular replacement
MERGED CRYSTALS	3	1	1	1	/
RESOLUTION	1.6 Å	1.6 Å	1.6 Å	1.6 Å	1.4 Å
R-MERGE	0.064 (0.89)	0.059 (0.825)	0.063 (0.567)	0.058 (0.218)	0.268 (1.247)
I/SIG(I)	15.5 (1.4)	12.3 (1.2)	9.1 (1.5)	16.6 (7.1)	10.9 (1.5)
COMPLETE (%)	99.3 (99.3)	95.5 (94.8)	86.8 (79.1)	76.6 (79.4)	99.3 (90.7)
MULTI	7.1 (4.7)	3.5 (3.3)	2.2 (2.4)	4.2 (3.9)	24.3 (13.9)
CC1/2	0.997 (0.65)	0.997 (0.66)	99.5 (77.0)	99.7 (97.1)	0.992 (0.727)

Table 5.1 : Lysozyme data processing and refinement statistics.

Values in parentheses are for the highest resolution shell.

$$R_{merge} = \frac{\sum_h \sum_j |I_j(h) - \langle I(h) \rangle|}{\sum_h \sum_j I_j(h)}$$

where $I_j(h)$ is the j th measurement of reflection indices h , and $\langle I(h) \rangle$ is the beam intensity [Karpplus]

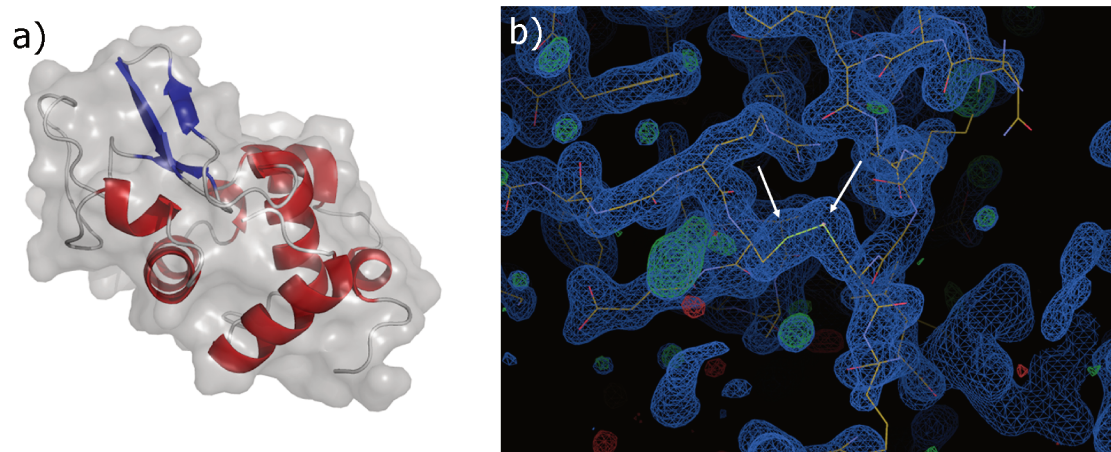


Figure 5.3 : In situ Lysozyme crystal structure.

(a) Overall fold of Lysozyme structure. The figure shows the structure of Lysozyme solved by the molecular replacement method using data collected from three crystals and merged (Table 3.2). Helices and beta-strands are colored in red and blue, respectively. The surface of the protein is represented in grey. (b) Electron density map of the Lysozyme structure, centered on one disulfide bridge (white arrows). The blue electron density is a $2Fo-Fc$ map contoured at 1.4σ . Green and red stand for positive and negative $Fo-Fc$ maps contoured at 2.0σ , respectively. The structure is modeled in sticks, colored by atom type. No water molecule was added during the unique refinement run, explaining the presence of the green blobs around the protein backbone.

2.1.5. Conclusions

Data acquisition on Lysozyme was performed at an early stage of the current work in order to confirm the feasibility of the approach and to understand the possible caveats of the technique. The experiments showed excellent results as of the acquisition of a complete data set leading to the structure determination at high resolution, in situ and yet with a very limited number of crystals.

The data collected from 30 crystals had lead to the obtention of a structure with a comparable quality with the reference crystal, with a similar resolution (1.6 Å compared to 1.4 Å), similar I/sigma (15.5 compared to 10.9), a lower multiplicity, linked with the small amount of data collected (only 3 crystals merged with 30° oscillation each ; 7.1 compared to 24.3 with a 360° oscillation angle collected). The CC½ is quite similar too (0.997 compared to 0.992). The experiments validate the chip trapping, the approach of automated data acquisition, and the quality of the collected data.

2.2. Insulin

As Lysozyme, the Insulin is a well known protein. Acquiring the structure of Insulin permits to validate the method on a second protein. More importantly, validating the chip with the Insulin protein opens the possibility to experiment the chip with Single-wavelength Anomalous Diffraction (SAD).

2.2.1. Crystallisation

The crystallisation protocol of the Insulin was inspired from an unpublished protocol established for SFX experiments at XFELs. The protocol was refined to fit the requirements of the experiments with the microfluidic chips in terms of crystal size and homogeneity. The Insulin crystals grew in six hours in bi-pyramidal shapes with the longest dimension between 10 and 40 µm (Fig. [5.4](#)), while the original protocol provided crystals with dimensions up to 70 µm, which could create chip clogging. The protocol could not be better refined in terms of concentration of crystalline objects, which stands very high and therefore causes potential issues when loading the chip.

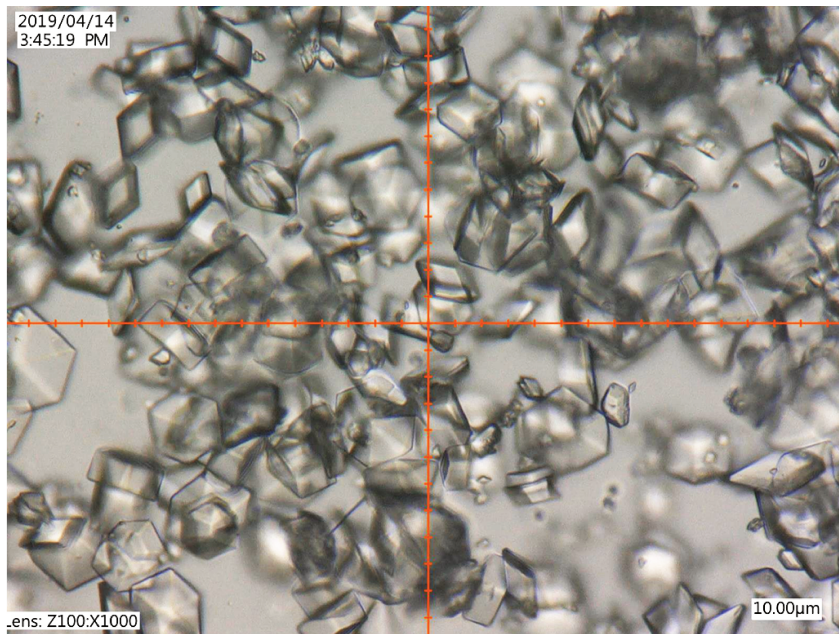


Figure 5.4 : Insulin crystals grown in batch.

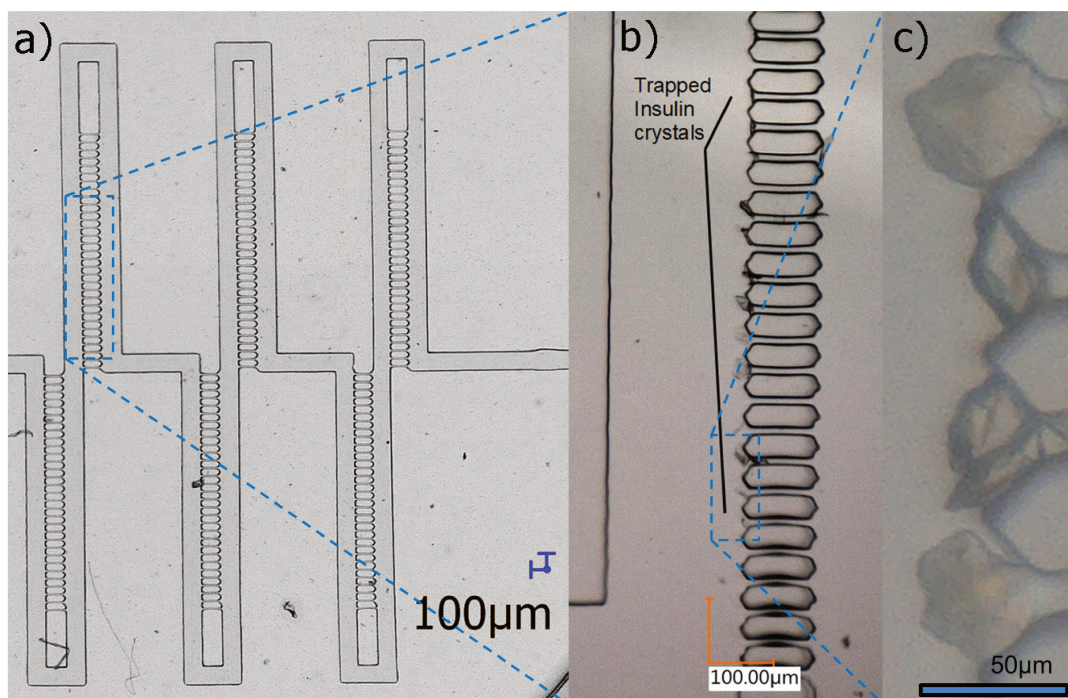


Figure 5.5 : Insulin crystal trapping.

(a) Insulin crystal blocked in traps on a V20 chip. The flow of injection goes from left to right. Crystals and other objects can be observed on the left part of the traps. (b) Zoomed views of trapped Insulin crystal properly blocked.

2.2.2. Crystal loading

The injection procedure has been improved after rounds of refinement because of repetitive failures in loading properly the crystals, mostly caused by clogging. A great gain in efficiency could be observed with the final injection procedure that led to obtaining positive trapping in most of the traps (Fig. [5.5](#)). The crystals were loaded in a V22 chip (Supp. Fig. [8](#)) using a pressure controller with a 50 mbar pressure difference.

2.2.3. Data collection

Data were collected using the I.G.O.R. scanning. Diffraction data were recorded automatically for all the potential trap positions, collecting total wedges of 10° with 0.05° oscillation per image, with 10% of the PROXIMA-1 flux ($\sim 5 \cdot 10^{11}$ photons/sec at 12.67 keV) and 20 images per second, on a EigerX-16M (Dectris, Ltd.).

2.2.4. Data processing and structure determination

Out of the 180 collected data, 13 were selected and merged using an *in-house* script (Chavas. L) and preselected based on their identical crystal lattice parameters that could eventually merge in a constructive way. A single run of restrained refinement using the *Refmac5* software suite [[Murshudov](#)] followed the molecular replacement step, with no addition of water molecules. Data analysis and refinement statistics are shown in Table [5.2](#).

2.2.5. Conclusions

Data acquisition on Insulin was performed as a first step before using the single Single Anomalous Diffraction in order to confirm that the structure of the insulin could be acquired with the method. The data qualities are comparable between the cryogenized and the in-situ Insulin (resolution 2.33 Å compared 2.56 Å and a CC½ of 0.996 compared to 0.890). Therefore, the data acquisition on Insulin permits to have a structure and validate the first step before using the Single-wavelength Anomalous Diffraction (SAD). The anomalous phasing can then be experimented on Insulin.

METHOD	<i>In-situ</i> insulin For molecular replacement	Cryogenized insulin For molecular replacement
MOSAICITY	0	0.18
MERGED CRYSTALS	13	1
SPACE GROUP	146 (H 3)	146 (H 3)
CELL PARAMETERS (Å)	83.08 83.08 34.39 90.000 90.000 120.000	82.14 82.14 34.00 90.000 90.000 120.000
(°)		
RESOLUTION	41.54 (2.33Å)	41.07 (2.56Å)
R-MERGE	0.295 (0.554)	0.080 (0.249)
I/SIG(I)	5.7 (0.9)	10.8 (3.9)
COMPLETE	65.1 (37.0)	99.1 (91.9)
MULTI	3.9 (1.6)	3.5 (3.5)
CC ½	0.890 (0.560)	0.996 (0.936)

Table 5.2 Insulin data processing and refinement statistics using data replacement.

Both of the techniques used the PDB model 3w7z.pdb in order to make phasing by molecular replacement. Values in parentheses are for the highest resolution shell.

3. Anomalous phasing using Insulin as an example

3.1.1. Contextual setting

The Insulin protein has the particularity to fix one zinc atom at the interface between three molecules constituting the crystal lattice. The 30 electrons of the zinc atoms have a high impact on the diffraction signal as the intensity scales with the square of the electron number, thus allowing for acquiring anomalous data for experimental structure determination using the Single-wavelength Anomalous Diffraction (SAD) approach. The following section will detail the experimental diffraction studies performed on Insulin crystals, at the energy of 9.67 keV, just above the Zinc absorption energy in order to perform SAD data collection. Information on crystallisation and crystal loading into the chips are similar to the conditions described above for the native data.

3.1.2. Data collection

Data were collected using the I.G.O.R. scanning. Diffraction data were recorded automatically for all the potential trap positions, collecting total wedges of 10° with 0.05° oscillation per image, with 10% of the PROXIMA-1 flux ($\sim 5 \cdot 10^{11}$ photons/sec at 9.67 keV) and 20 images per second, on a EigerX-16M (Dectris, Ltd.).

3.1.3. Data processing and structure determination

Out of the 180 collected data, 13 were selected and merged using an *in-house* script (Chavas. L) were preselected based on their identical crystal lattice parameters that could eventually merge in a constructive way. A single run of restrained refinement using the *Refmac5* software suite [Murshudov] followed the molecular replacement step, with no addition of water molecules lead to the structure determination. Data analysis and refinement statistics are shown in Table 5.3. The anomalous data was obtained (Fig. 5.6) but was not enough to solve the structure a contrary to the reference method.

METHOD	<i>In-situ</i> insulin For SAD	Cryogenized insulin For SAD
MOSAICITY	0	0.15
MERGED CRYSTALS	13	1
SPACE GROUP	146 (H 3)	146 (H 3)
CELL PARAMETERS (Å) (°)	83.08 83.08 34.39 90.000 90.000 120.000	82.18 82.18 34.02 90.000 90.000 120.000
RESOLUTION	41.54 (2.33Å)	41.09 (2.56Å)
R-MERGE	0.295 (0.554)	0.105 (0.251)
I/SIG(I)	5.7 (0.9)	16.8 (7.1)
COMPLETE	65.1 (37.0)	99.7 (96.3)
MULTI	3.9 (1.6)	10.5 (9.8)
CC1/2	0.890 (0.560)	0.997 (0.974)
ANOM. COMPLETE	35.1 (9.4)	99.2 (90.4)

Table 5.3 Insulin data processing and refinement statistics using SAD.

Both of the techniques used the Single-wavelength Anomalous Diffraction (SAD) in order to make the phasing. The In-situ data used the data previously collected *in-situ* on insulin (Table 5.2) . Values in parentheses are for the highest resolution shell.

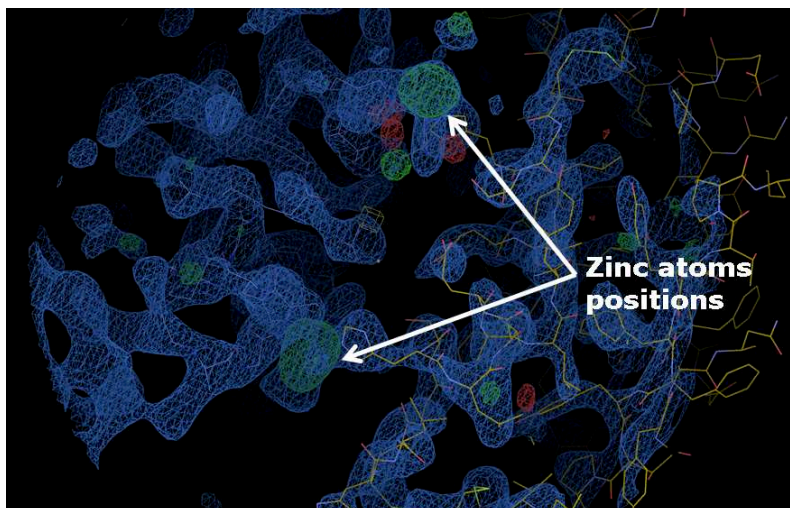


Figure 5.6 : In situ Insulin SAD anomalous information compared to molecular replacement structure obtained.

Electron density map of the Insulin structure, centered on one disulfide bridge (*white arrows*). The *blue* electron density is a $2Fo-Fc$ map contoured at 1.4σ . *Green* and *red* stand for positive and negative $Fo-Fc$ maps contoured at 2.0σ , respectively. The structure is modeled in sticks, colored by atom type. No water molecule was added during the unique refinement run, explaining the presence of the green blobs around the protein backbone. The anomalous signal obtained highlights the Zinc atoms positions (*in Green*).

3.1.4. Conclusions

The current experiments performed on Insulin crystals validated further the operational protocol of the chip, notably with successful repeatability of the experiments. Anomalous data could be acquired, confirming that *in situ* data collection on microfluidic chips are not a showstopper for experimental structure determination.

4. *In vivo* macromolecular crystallography

4.1. General context

The aim of this work is to decipher the principle of the protein crystallisation occurring within living eukaryotic cells and eventually set up an *in vivo* crystallography platform open to the synchrotron users. X-ray diffraction is still nowadays the main method to obtain high resolution structures of biological macromolecules. This very popular and longstanding method still presents two main bottlenecks that are protein purification to homogeneity and crystallogenesis through extensive semi-empirical formulation screens. These two limiting steps are time and effort consuming leading to the development of many alternative approaches over the years to increase the rate of high resolution structure determination [[Moreno](#)]. Recent improvements in the synchrotron radiation light sources such as

microfocus beamlines and the serial crystallography approaches allow considering methods that can produce micron sized protein crystals for structure determination such as *in vivo* crystallography.

In vivo crystallography is a phenomenon in which proteins crystallise spontaneously within the living cell. This process has been observed to occur in the cytoplasm or within specific subcellular compartments. First observed in functionally relevant or in pathological cases [Doye], this phenomenon has been described more recently for heterologously expressed proteins [Schönherr, Hasegawa], thus becoming a new candidate to expand the modern structural biology toolkit. Such crystals are limited in size but, on the contrary to classical *in vitro* crystallography, are produced in a native like environment. In addition to being an alternative way to obtain crystals of proteins for which classical *in vitro* crystal growth revealed unsuccessful, anticipated benefits of *in vivo* crystallography are to minimize the efforts provided in optimizing samples purification as well as crystal production and handling [Boudes]. Additionally this method provides the unique opportunity to study functionally important post-translational modifications. Due to the size of the cells and the need to go for serial X-ray crystallography, the development of a microfluidic device to trap a large number of cultured cells is essential.

In order to reveal the full potential of *in vivo* crystallography and the feasibility of implementing such method within a synchrotron facility, a model system has been chosen via a collaboration between the PROXIMA-1 beamline and Professor Tsutsui's laboratory. Through serendipity, Professor Tsutsui described recently the spontaneous crystallisation of a fluorescent coral protein mutant named XPA in human HEK293 cells and hippocampal neuron [Tsutsui]. *In vivo* nucleation of XPA crystals led to high resolution structure of *in vivo* grown XPA crystals. This protein is an ideal model due to its fluorescent properties facilitating the detection of XPA within the cells, and its ability to form diffraction quality crystals.

At Synchrotron SOLEIL, the HEK293 Freestyle (HEK293FS) expression system was favoured among other cell types for its easier handling properties. These cells are round-shaped with sizes ranging from 10 to 20 μm in diameter. XPA crystals appear after two to six days post transfection, no bigger than the cells and more typically 15 μm in the longest dimension. *In vivo* nucleation of XPA crystals is a stochastic event and only one to 100 transfected cells undergo XPA crystallisation (Fig. 5.7). In classical crystallography experiments, a crystal containing cell has to be isolated in a nylon loop, flash frozen and mounted on the goniometer to perform *in vitro* X-ray diffraction experiments. This tedious operation might be facilitated by the use of a microfluidic device designed primarily to detect rare events and trap them for subsequent semi-automated X-ray diffraction analysis. Noteworthy, in various conditions XPA crystals may be expelled in the extracellular medium. Such crystals should also be considered to be trapped along the crystal containing cells as their X-ray diffraction properties have to be assessed as well.

Due to the intrinsically different properties of crystals and cells, three types of trapping devices were considered for this work :

- the pattern used for classical crystal trapping ;
- a grid-based cell trapping [Lim] ;
- a single dimensional cell trapping approach. Using a one lane cell placing chip.

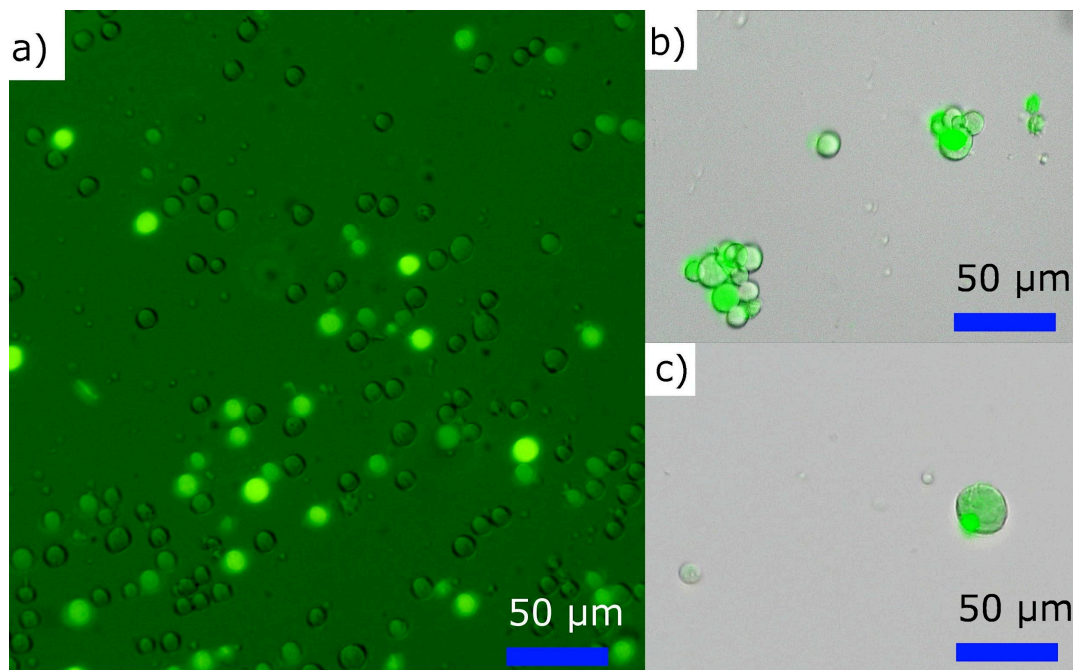


Figure 5.7 : HEK cells with fluorescent crystal (XPA).

HEK293 cells with fluorescent protein (XPA) expressed (in *green*). (a) The expression of the protein before crystallisation. (b) & (c) Zoom in cells containing crystals.

4.2. Classical trapping

4.2.1. Crystal loading

In the following experiments, *in vivo* crystals were loaded on microfluidic chip with a V22 pattern (Supp. Fig. 8) using syringes under a fluorescent microscope [Olympus]. The mother liquor of the crystallisation condition was clear of visible aggregates, leading to smooth sample loading and crystal trapping without major congestion difficulties (Fig. 5.8). During the experiment, 1 to 5 crystals were trapped in each chip. The crystals were localised via markers on the chip. The crystal was not visible without the fluorescence. Therefore the experiments were performed without visual confirmation of the position of the crystal. Only one collection showed diffraction spots and the targeted crystal was outside the traps. In between the injection and the collect, bubbles appearance and sedimentation lead to difficulties to align the invisible crystal with the beam.

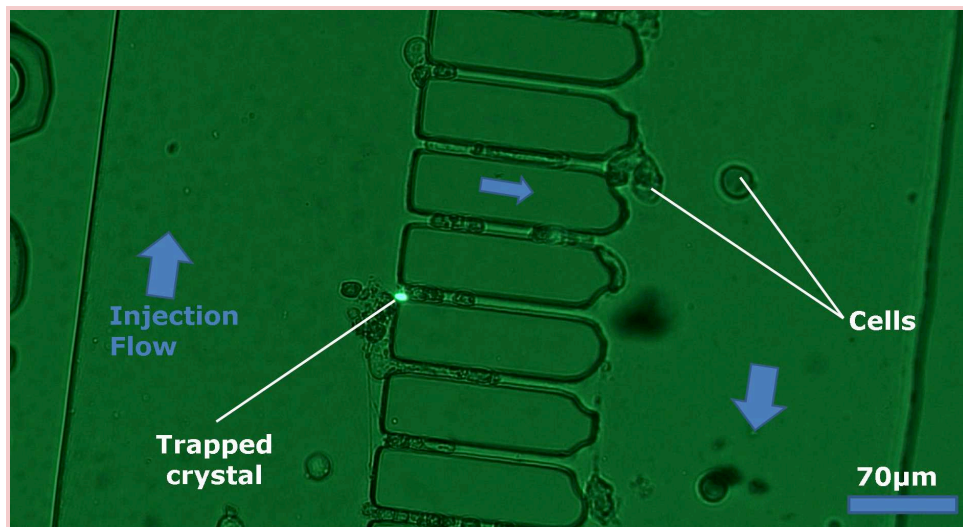


Figure 5.8 : *In-cellulo* grown XPA crystal trapped in a V22 Pattern chip.

In-cellulo grown XPA fluorescent crystal trapped in a V22 pattern viewed from a fluorescent (20x) microscope. The blue arrows show the flow direction during the injection. The fluorescence excitation was between 457 and 487 nm and the emitted fluorescence was between 502 and 538 nm.

4.2.2. Data collection

Data on XPA crystals were centered manually using the MXCuBE three point centering. Collecting total wedges of 5° with 0.05° oscillation per image, with 10% of the PROXIMA-1 flux ($\sim 5 \cdot 10^{11}$ photons/sec at 12.67 keV) and 100 images per second, on a EigerX-16M (Dectris, Ltd. Fig. [5.9](#)).

4.2.3. Data processing and structure determination

The Data processing leads to 40.3% of indexed spots, with a resolution limit of 2.88 Å (space group : 23 (*I*222) ; cell constants $a = 50.0$ Å, $b = 86.2$ Å, $c = 119$ Å, $\alpha = \beta = \gamma = 90^\circ$) (Montaville P. unpublished data).

4.2.4. Conclusions

The technique requires optimisations to properly work. The low crystal over cell ratio may make the V22 chip non optimised for this kind of samples. Furthermore, a preselection of the crystals prior to the chip injection may help highering the crystal over cell ratio and improve the relevance of the chip in the experiment. In order to pull up the relevance of the chip, different trap patterns optimised on placing cells could be evaluated.

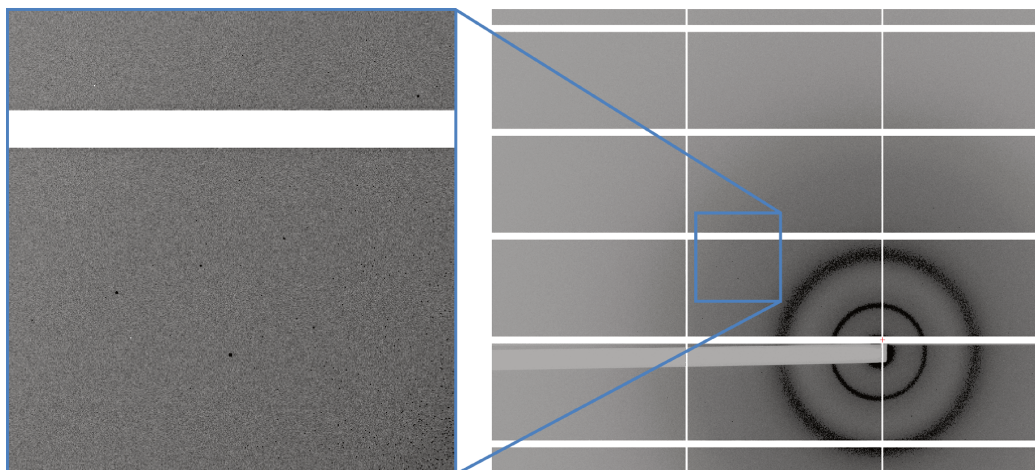


Figure 5.9 : Diffraction Pattern obtained with the *In-cellulo* grown XPA collected *in-situ*. The pattern was obtained by merging images of 3° diffraction patterns summed. It shows the water absorption ring and diffraction pattern visible by eye up to 4.2\AA .

4.3. *Alternative trapping results*

Alternative trapping devices were considered for this work. The first design considered was a grid cell trapping, which already showed results to trap objects [Lim]. The second design considered was optimised to utilize an automatic one dimensional X-ray centering [Madden, Savko M. unpublished data]. The designs were created and tested as trapping devices.

4.3.1. Grid cell trapping

HEK293FS cells were injected into a two-layers chip. During the injection, the flow rate slowed down while entering the pattern area due to the array of pillars (red in Fig. 2.13a). Unfortunately, due to the design, the solution is able to circumvent the patterns between the border of the pillar array and the inner limit of the chamber. Only a small fraction of the cells were eventually trapped on a limited peripheral area of the pattern (Fig. 2.13g). The cell concentration could not be increased due to higher clogging events of the inlet channel. As a conclusion in the next chip with this design, the pattern will have to fill the entire chamber width.

The three layers PDMS chip did not allow an efficient cell trapping. This is due to an unexpected preferred flow path circumventing the patterns area leading the cells to pass by the pattern area instead of flowing above it. Most of the injected cells went through this unexpected path probably a result of a lower hydraulic resistance. The $80\ \mu\text{m}$ high empty space above the traps within the chamber seemed not to be sufficient for the cells getting in a proper location for subsequent trapping. Despite not fulfilling the expectations, the experiment showed that single cells could still be trapped in the patterns in places where cells manage to reach the pattern (Fig. 2.13). As a consequence, it can be anticipated that the trapping

efficiency would certainly be increased by filling the whole chamber with the trapping pattern as suggested above.

Another approach would consist in replacing the cell injection protocol by an opened chip drop deposit. As the flow will be suppressed, the cells present in the drop will probably sediment in the trapping area, resulting in a high trap occupancy rate. However, this operation will promote solution evaporation leading to unwanted chemical modifications (*i.e.* solutes concentrations) potentially damaging the cell content and ultimately altering the crystal integrity. Such protocol would require a rapid sealing of the chamber and the benefits of manipulation in a closed environment will be lost.

Moreover, the cells evenly distributed in the 3D drop will sediment onto the pattern akin to a 2D surface. The amount of cells sedimented in an area of the pattern will therefore depend on the thickness of the drop directly above the area, leading to a high concentration at the center of the drop and a lower concentration on the side. Furthermore, the sedimenting cells in the pattern will deposit on the first horizontal surface whether the surface is a trap or not. As the chip expected advantage is to place the crystals in known places in order to automatically record wedged serial diffraction data, the non uniform repartition of the cells created by this type of deposition is unwelcome. A method that would spatially pre-order the cells above the traps within a single layer prior to their sedimentation could improve the efficiency of such a device.

4.3.2. Line cell placing

The line cell placing chip was designed to prevent cell sedimentation during chip manipulation on the goniometer and get a better control on the cell positioning. The width of the channels have been adjusted with the size of the beam ($\sim 40 \mu\text{m}$). Moreover 64 channels are arranged in a parallel fashion in order to increase the amount of objects in the chip. Furthermore, it allows one dimensional X-ray centering [[Madden](#), Savko M. unpublished data] to find the crystals. HEK293FS cells were injected into a Line cell placing chip 10 days after protein expression plasmid transfection (Fig. [5.10](#)). The chip was collected on the PROXIMA-1 beamline without previous confirmation of the presence of a crystal. Manual centering was made on each of the 80 cells. 1° wedge collections were made on all the 80 cells encountered inside the chip without positive diffraction results.

The concentration of the crystals is a major concern of the experiment. As the total volume contained in the entire area scanned is $0.2 \mu\text{L}$, the cell concentration has to be maximised in order to perform X-ray diffraction experiments on a maximum of crystals to optimise the data quality. But too high cell concentrations lead to cell clumping and therefore channels clogging. Three levers can be used to pull up the concentration of crystals per microliters and keeping low clumping chances :

- Cell quality : The cell concentration can be pulled up by using cells with cell-cell interaction, therefore low clumping chances. The cells chosen are the HEK293, one of the few cells nowadays known to grow *in cellulose* crystals. For now, this cell line (HEK293 free style) seems promising in the context for *in vivo* grown proteins crystals production and the clumping stays at a reasonable level for microfluidic chips.

- Cell concentration : The cell concentration has to be optimised to have the highest concentration possible while keeping low chances of cell clumping and channel clogging.
- Cells transfection & crystallisation chances : The actual ratio of one crystal over 5,000 cells could be raised before injection in order to raise up the mean crystals number in the chip.

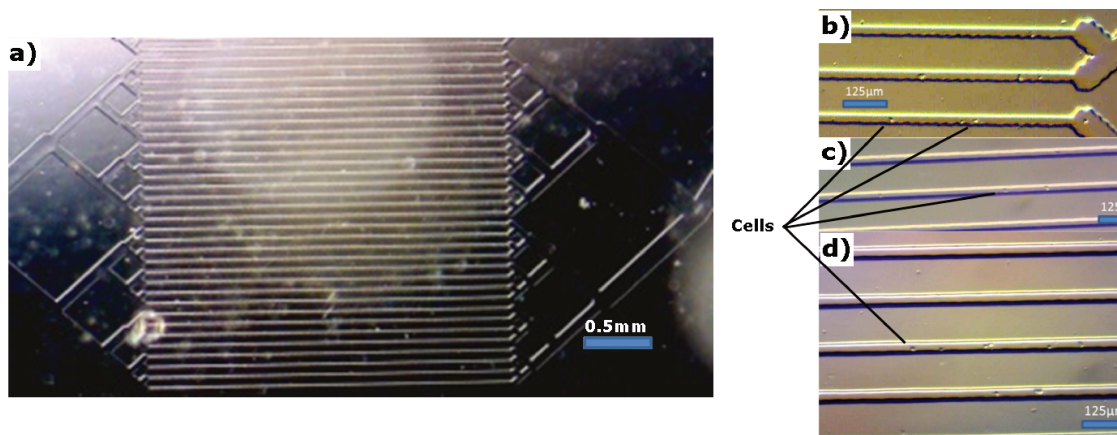


Figure 5.10 : Experimental results of the line cell placing chip injection.

The chip was injected with 1 mL of suspended HEK293FS containing around 100 000 cells and was injected using a Syringe driver. a) An overall view of the chip entirely filled with the cell solution. b), c) and d) Cells in the channels. The concentration of cells in the chip leads to around 80 cells in the collection area.

4.3.3. Conclusions

The alternate cell trapping devices represent interesting potential optimisations for the system. Currently, these devices are in an early stage of development and did not offer any diffraction results but should be considered as potential alternative trapping chips for the cell trapping after optimisation.

4.4. Conclusions

The cell trapping for *in-situ* crystallography of *in-cellulo* grown crystals is at an early stage. It suffers from the difference between crystal size ($\sim 16 \mu\text{m}$) and the chip optimisation range (20 to $70 \mu\text{m}$). Moreover, the crystals are difficult to locate as their cellular environment makes them nearly invisible. Finally, the low number of available crystals, coming from the cells to crystal ratio of the chosen system, pull down the number of crystals per chip. All three of these difficulties can be resolved. The size of the channels can be improved by making chips with a well equipped laboratory. The crystal location challenge can be circumvented by adding a blue light on the beamline OAV and a filter to detect the fluorescence of this specific model protein crystal, because it only works for fluorescent protein. For the crystal over cell ratio, two projects are currently running on site in order to pull the ratio up : The cell transfection is currently in optimisation, and an internal project is addressing the sorting crystal containing cells by using a microfluidic device coupled with a Second Harmonic Generation (SHG) microscope

[Wampler]. With this method, the trapping probability is expected to dramatically rise up. Once the crystal containing cells are trapped, an automated scanning, as the I.G.O.R. scanning could make automated diffraction collection experiments on each of the traps, then automatically select the data collections and finally merge the compatibles diffraction results.

5. Handling sensitive samples, example of Ribosome

5.1.1. Contextual setting

Ribosomes represent a key component of the cells. Considered as protein factories, Ribosomes use coding RNAs to produce proteins by assembling amino acids into the final protein composition. Any faulty operation of Ribosomes goes with high risks of wrong protein coding and cellular deregulation. As one of the biggest molecular complexes of the cells, Ribosomes are composed of multiple independent entities, made of both proteins and RNAs. Ribosomes are greatly difficult to crystallise, often leading to poor quality and badly diffracting crystals. Moreover, these crystals are very sensitive to cryogenic conditions, difficult to optimise, yet necessary for the survival of the molecules for the time of the diffraction experiments. The accumulation of the above mentioned difficulties when working with Ribosomes' crystals pushed to consider making use of microfluidic chips to perform in situ room temperature data collection without prior chemical treatment of the Ribosomes.

The bacteria *Thermus Aquaticus* lives in high temperature waters, at around 50 to 80°C. To live in these extreme conditions is only possible due to the great stability of the molecular components constituting this organism. Ribosomes belonging to this species have been documented to be less fragile than Ribosomes from other more ordinary organisms. The strategy of experimenting on these more stable Ribosomes lead to the structure determination of *Thermus Aquaticus* Ribosomes at higher resolutions [Nierhaus]. As such, *Ta*Ribosomes appeared as a good target to balance the efficiency of the microfluidic-based MX on very large macromolecular complexes.

5.1.2. Crystallisation

If the microfluidic approach can circumvent the requirements in obtaining an efficient and non destructive cryo-condition, room temperature *Ta*Ribosome crystals still have a short life expectancy of one week. The crystals degrade quickly over time, adding to the complexity to schedule experiments with fresh samples loaded in microfluidic chips. Moreover, *Ta*Ribosomes have a tendency to assemble in fragile needle crystals. Furthermore, *Ta*Ribosome crystallisation conditions tend to form membranes of precipitated proteins and/or RNAs (Fig. 5.11), which interferes with the crystal harvesting, being by manual fishing or through liquid-sucking.

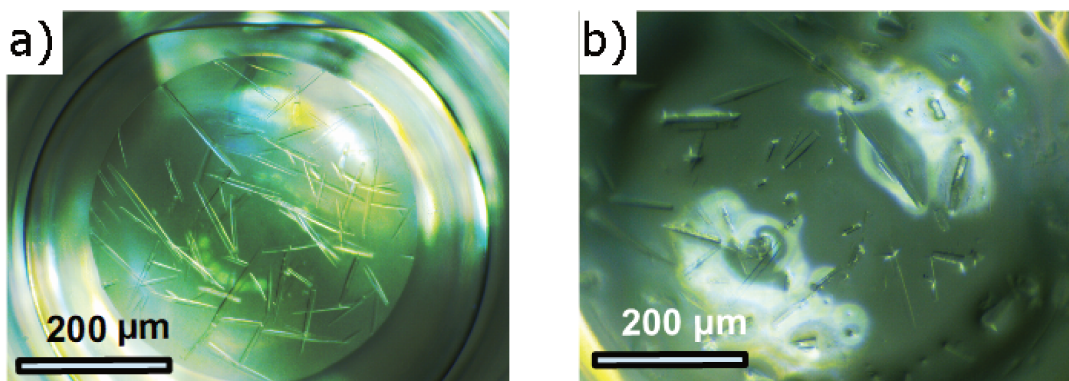


Figure 5.11 : *Ta*Ribosome crystals in the crystallisation plates.

*Ta*Ribosomes crystals before (a) and after (b) the condition sucking for microfluidic injection of chips. The fragility of the crystals can be understood by comparing both pictures, with picture in (b) clearly representing pieces of crystals that were broken in the process of sample sucking.

5.1.3. Crystal loading

Two *Ta*Ribosome crystallisation plates were sent for studies to PROXIMA-1. Prior to the injection process, these Ribosome crystals needed to be extracted from the plate. Their mechanical fragility hampered the fishing experiments, and no Ribosome crystal could be injected inside the chip. A third crystallisation plate was sent, and after solubilisation, the sample crystals were injected into one chip model V19 (Supp. Fig. 7), and later exposed to in situ diffraction tests.

The transport of the crystallisation plates to Synchrotron SOLEIL is a questionable effect that may have affected the quality of the crystals and could therefore explain this poor quality diffraction limits. In an attempt to understand whereas the approach was problematic or if the samples were not adapted to the experiments, the crystal samples were loaded inside the chip at the institute where the crystals grew. The efficiency of the chip transport compared to the transport of the crystallisation plates could therefore be balanced.

In the investigation of the benefits in loading and transporting crystalline samples directly into a microfluidic chip, two chip devices were loaded with Ribosome crystals at the host institute. Prior to the injection process, the samples were mixed in two different solutions, before loading in two different chips. The first condition consisted in the crystallisation mother liquor supplemented by magnesium (hereafter referred to as ribo_chip 1) ; the second condition consisted in a specific crystal treatment solution (Annex 3.1), hereafter referred to as ribo_chip 2. The crystals were grown 11 days prior to the injection into the chips. For both chips, trapping success dropped to 10%, mostly explained by clogging of the channels because of the aggregation of dust and crystals (Fig. 5.12). The injection lasted 30 minutes at crystallisation temperature to remove temperature fluctuations from the equation.

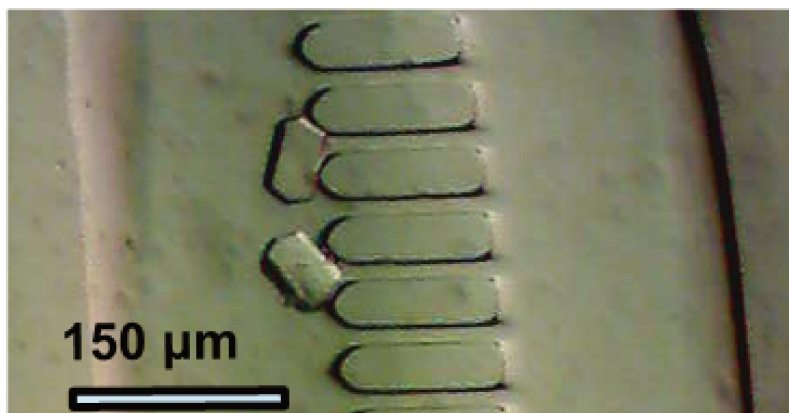


Figure 5.12 : TaRibosome crystals trapped in a V19 chip (Supp. Fig. 7).

To investigate the role played by the chip transport in the crystal diffraction quality, a third chip was loaded with crystal samples collected from the drops, following the application of the dehydration protocol. On the ribo_chip 3 loading experiments, only a few objects were trapped into the chip, as confirmed by visual inspection through a microscope.

5.1.4. Data collection

In order to appreciate the usability of the microfluidic-based *in situ* data collection approach when compared with classical data collection at cryogenic conditions, 4 crystals of each condition (mother liquor with magnesium and special treatment solution, respectively, Annexe 3.1) from the same batch were harvested and frozen in cryoloops. From these crystals, X-ray diffraction tests were performed, leading to 40 Å resolution data (Fig. 5.13a).

Scanning the ribo_chip 1 for X-ray diffraction (Fig. 5.13b) confirmed a higher diffraction resolution limit from *in situ* experiments of up to 37 Å, very similar to the cryocooled crystals. A strong difference in the quality, however, can be appreciated by the well defined diffraction pattern of the *in situ* data when compared to the cryocooled data. Other crystals from the same plate but incubated for a longer time before injection into the chip did not present any diffraction results, confirming the short life expectancy from these Ribosome crystals. No structural or cell parameter information could be acquired from the images collected.

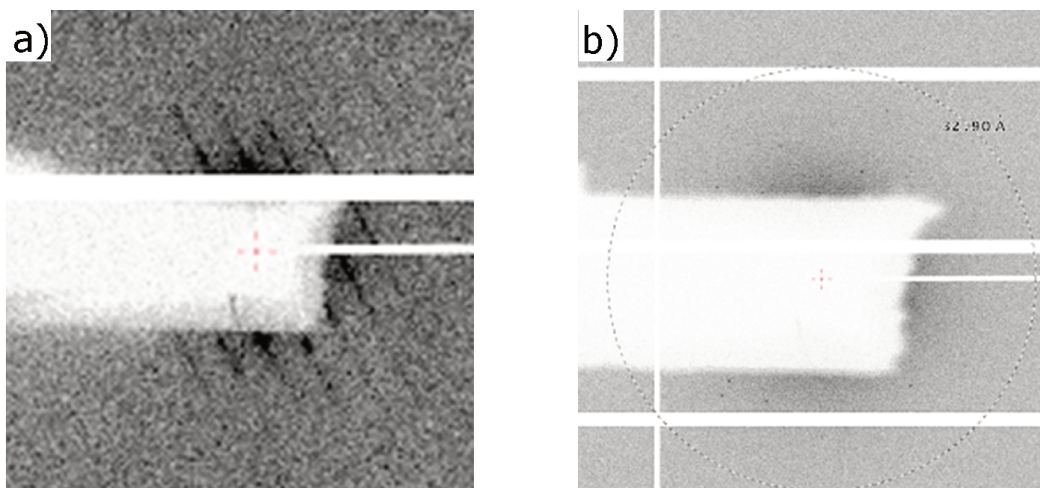


Figure 5.13 : X-ray diffraction from Ribosome crystals.

Comparison of X-ray diffraction from Ribosome crystals (a) cryogenized sample (40 Å diffraction limit) and (b) trapped inside a microfluidic chip (37 Å diffraction limit).

5.1.5. Specific issues with Ribosome crystals

Ribosome samples brought three major issues that rendered the experiments difficult. Here are listed the different situations, together with the solutions that were adopted. These case studies were enlightening as they may represent some extreme situations that could be encountered with other crystalline samples.

Situation 1 : the channels of the traps were too big for the size of the crystals. Three solutions could be investigated for a quick answer to this problematic situation.

- *Solution 1 : lowering the size of the trap channels.* Currently, the size manufactured is the smallest possible when using the laserwriter available at the microfluidic lab of Synchrotron SOLEIL. Other sizes may become available when outsourcing the manufacturing of the chips, however it represents the physical limitations achievable at SOLEIL.
- *Solution 2 : changing the chip pattern.* The pattern used is optimised for cubic or spheric crystals, but not for the rod-shaped ones. In order to answer the present difficulties with special shapes, several needles trapping patterns have been designed (Supp. Fig. 6). Additionally, specific works on the needle-shaped *hQr2* protein crystals highlighted the possibility to use the chip pattern V9 (Supp. Fig. 3) to trap those elongated crystals. This changes the difficulty to the fragility of the crystal and its size.
- *Solution 3 : adapt the size of the crystals to fit with the chip pattern.* In crystallography, controlling the size of the samples has never been an easy task. This solution appears then as

certainly difficult to apply, however, for extreme cases where the size of the crystals can be controlled, it remains a valuable solution.

Situation 2 : the mother liquor contains impurities that could be trapped. In this specific situation, the trapping of the objects may replace the crystals. If the small objects are too numerous or in a negative Ribosome / objects ratio, the trapping of the Ribosome crystals becomes statistically a rare event. Indeed, the microfluidic trapping events are only happening because of the shape of the objects, not their constitutions. Increasing the number of traps available per chip may help getting around the problem, but is not an efficient solution in the long run. The easier solution to be implemented in these cases would be to filter the mother liquor solution prior to injection.

Situation 3 : the volume of the crystallisation drops to load into the chip is very small. This problem exists whatever the injection method, a syringe or a pressure controller. The above mentioned Ribosome crystals experiments were performed before the implementation of the final injection protocols, using only manual injection, which remains limited by the dexterity of the user. After the injection process was improved through the operation of a pressure controller, data collection on the untreated Ribosome crystals still appears as a major challenge as seen by the very low resolution diffraction limits (Fig. [5.13](#)).

5.1.6. Conclusions

The experiments on Ribosome crystals did not bring revolutionary results, however, they could confirm that in situ experiments on samples loaded in microfluidic chips showed competitive results when compared with cryo-protected Ribosome crystals. The low resolution diffraction limits were observed for both diffraction setup, to approximately similar diffraction limits (37 Å and 40 Å diffraction limit respectively for the in-situ and cryogenised samples). This low resolution limits could be due to the crystals, the travel or other factors such as crystal handling.

Furthermore, the current experiments put in light several key points for the future development in the chip use. The shipping of the crystals trapped into the chips showed to be possible, without noticeable effect on the diffraction quality. Obvious improvements and chip preparation protocols have to be implemented for obtaining 100% trapping, chip preparation and delivery. As chips could be adapted to the sizes and shapes of the crystals, an interactivity between the user and the microfluidic lab at Synchrotron SOLEIL is welcome and most likely necessary. Now, aggregates and other dusty objects present in the solution are the biggest challenges yet to be tackled.

6. Protein/Ligand complex formation

6.1. *human Quinone reductase 2*

6.1.1. Contextual settings

Macromolecules regulate their functions by interacting with their environment. Among the diversity of proteins, enzymes are known to interact with specific molecules at their interaction sites. By mimicking the natural ligands of these enzymes, the functions of these proteins can be altered. Depending on the nature of the ligand and its mode of interaction, the macromolecule can be enhanced or inhibited in its functions. In pharmaceuticals, finding the good ligand or inhibitor molecule interacting with the target protein is a crucial step on the way towards drug discovery. The approach of structural-based drug design is common practice for ligand screening to test for possible complex formation between a series of molecules and the protein of interest, with crystallography confirmation for the specificity of the interaction. In practice, protein crystals are mixed with cocktails of small molecules / ligands, and each soaked crystal needs to be manually fished before cryo-protection, freezing and diffraction data recording [[Klebe](#)].

The protein in ligand complex formation can be established in two ways : co-crystallisation or soaking. The co-crystallisation method consists in mixing the protein and the ligands before setting up crystallisation conditions. The soaking method is more commonly used with pharmaceutical targets. It consists in crystallising the protein of interest, and then soaking the crystals in solutions with high concentrations of the ligand(s). The cocktail solutions containing the ligand(s) need to be adapted to the crystallisation condition in order to avoid degradation of the crystal. Moreover, the ligands have to be able to reach the active site of the protein while diffusing through the crystal, which implies that the crystal packing for the protein should be favorable of these soaking experiments.

Between both protein:ligand complex formation methods introduced here, the microfluidic chips developed in the current work are better adapted to the soaking approach. In an attempt to identify the potential issues arising from this approach, the human quinone reductase 2, hereafter referred to as *hQr2*, appears as an ideal target due to its capacity to both crystallise in a known crystallisation condition and bind numerous ligands. By combining microfluidic-based crystallisation of *hQr2* [[ZhangS, Gerard](#)] to in-chip ligand soaking, specific fragment-based drug design could be accelerated and automated, circumventing the tedious step of crystal fishing while allowing to soak for several ligands in single chips.

6.1.2. Crystallisation approach

Before going forward with ligand soaking experiments, it is needed to ensure that the different crystal packings of *hQr2* permit the various ligands accessing the active site without major conformational change of its structure. Among the 62 structures available on the protein data bank (PDB),

60 coordinates share the same lattice parameters, (space group : $P2_12_12_1$; cell constants $a = 60 \text{ \AA}$, $b = 80 \text{ \AA}$, $c = 106 \text{ \AA}$, $\alpha = \beta = \gamma = 90^\circ$). Comparing 10 ligand complex structures lead to the conclusion that the *hQr2* packs as a dimer with the localisation of the ligand in the active site, accessible through solvent channels. The structure coordinates 5LBZ were selected as the model structure for understanding the packing and accessibility to the active site (Fig. 5.14). These *hQr2* crystallisation conditions are thus in favour of soaking experiments, ideal for the foreseen confirmation of the in-chip ligand screening.

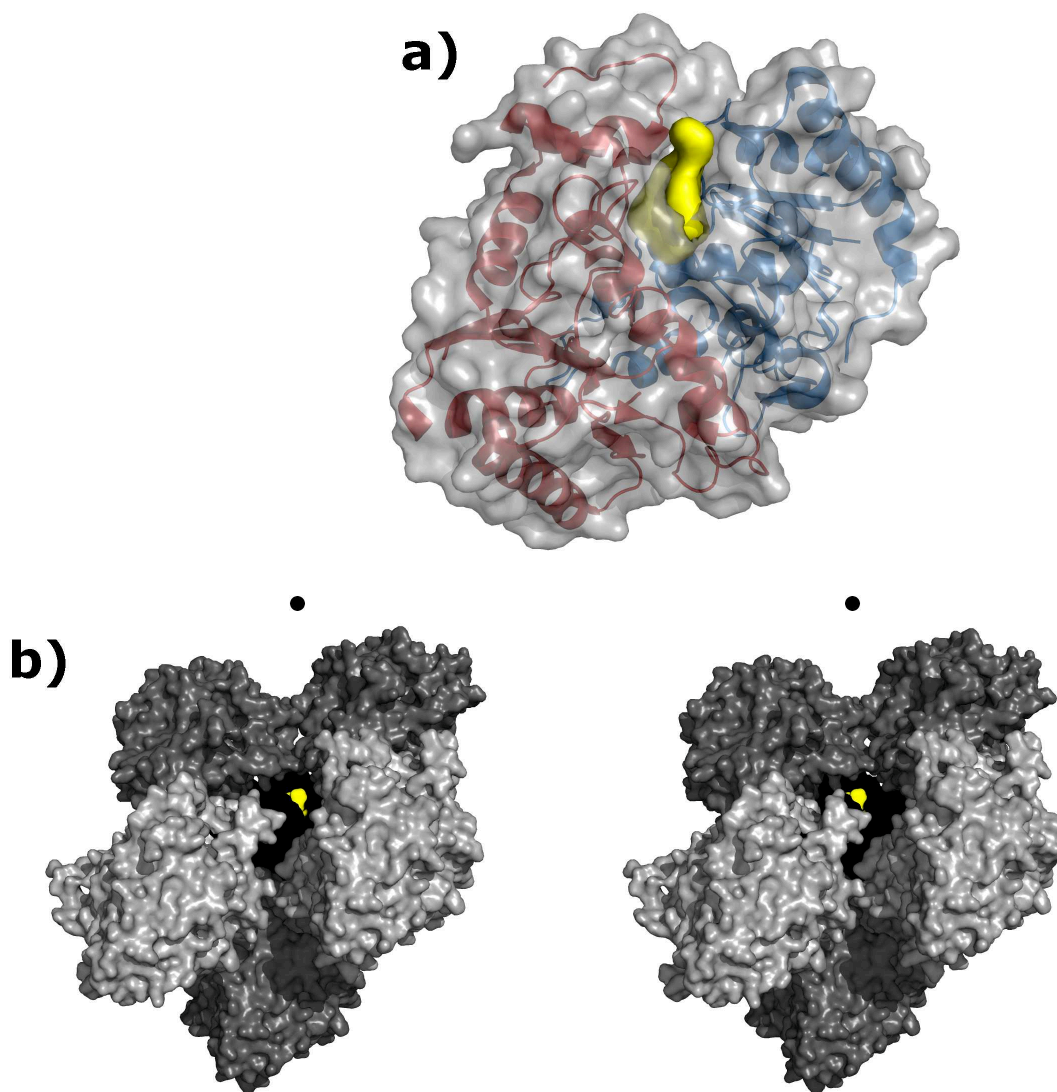


Figure 5.14 : *hQr2*:ligand complex crystal packing.

a) Represent the *hQr2* dimer (red and blue) with the ligand pacrinib (yellow) is in the active site of the *hQr2*. b) and c) represent a stereo view of the *hQr2* dimer (in grey) in a $P2_12_12_1$ packing. The ligand pacrinib (yellow) is in the active site of the *hQr2* and the brightness of the dimer depends on its position toward the viewer (the closest ones in light grey and the protein containing the ligand in black). The view highlights the space between the hQR^{II} molecules permitting the ligand to access the active site. The images are generated by viewing towards the active site inside a solvent channel. The structure was obtained from the PDB database 5lbz.pdb.

hQr2 was first crystallised by vapor diffusion using the 6HIS-*hQr2*/pet28 construct prepared and sent ready for crystallisation by the Servier laboratories. Crystals with dimensions of $50 \times 10 \times 10 \mu\text{m}^3$ grew overnight at 20°C (Fig. 5.15 5.16). Crystals were then used for diffraction experiments within chips on the PROXIMA-1 beamline.

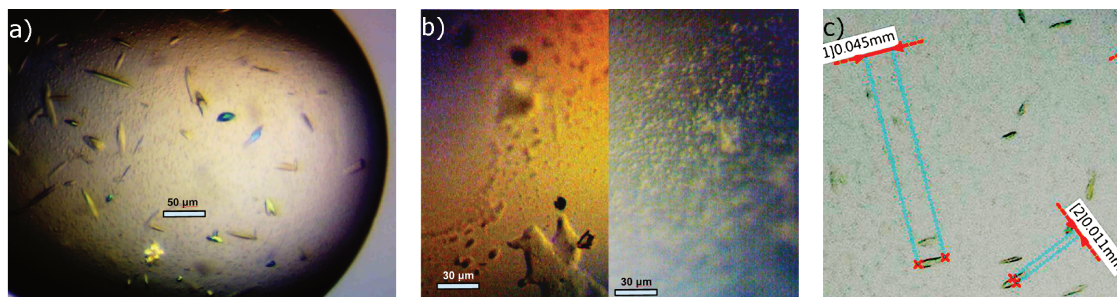


Figure 5.15 : human Quinone reductase II crystallisation.

Various examples of *hQr2* crystallisation depending on the batch used. a) and c) well grown *hQr2* crystals. b) example of precipitations in a crystallisation drop.

6.1.3. Crystal loading

The crystallisation drops of *hQr2* are small and offer difficulties to sampling. A large part of the *hQr2* crystals stays in the crystallisation drops during the sampling process, and the drops dry out within a few minutes, decreasing even further the number of usable crystals.

Sampled *hQr2* crystals were injected into microfluidic chips model V19 (Supp. Fig. 7). Difficulties in sampling together with the crystal shape were problematic for the injection, with only 4 to 12 crystals successfully trapped at known positions. The trapping quality, however, shows novel aspects worth investigating (Fig. 5.16), with the chip that recognises and blocks the needle crystals in two ways. First, crystals were located in the channel; second, they were found with the tip to the trap. Consequently, when applying the I.G.O.R. scanning for diffraction data recording, two typical positions have to be scanned, as represented figure 5.16. Apart from doubling the data recording, this maximises the chances to collect redundant data.

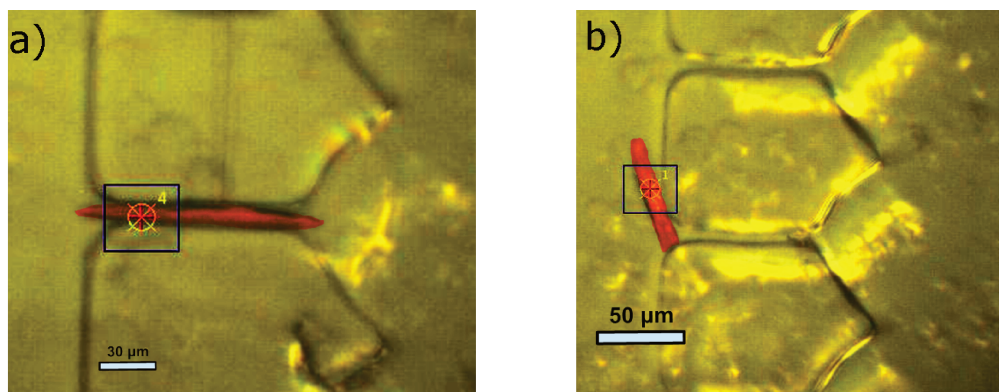


Figure 5.16 : Crystals of human Quinone Reductase II trapped in microfluidic chips.

(a) and (b) show the localisation of the crystals within the chip as seen through the OAV camera on the beamline. The image has been modified to highlight in red the crystal for easier visualization (false color). Yellow targets represent the centered positions after centring the objects as seen through the MXCuBE interface. Blue rectangles represent the measured size of the X-ray beam at the sample position. In the pictures, the liquid flow goes from left to right. (a) The tip of the crystal is stabilised in the trap with the rest of the crystal exposed to the liquid flow. (b) crystal fully trapped within the small channel of the trap.

6.1.4. Data collection

For data collection, the modified I.G.O.R. scanning approach as described above was used, with several centered points collected on each crystal. The crystals diffracted to high resolutions ranging from 1.6 Å to 4 Å. Although issues emerged with crystal sampling, the trapping of *hQr2* needle-shaped crystals provided with promising results, especially with the possibility to double the amount of recordable data *per* elongated crystal.

6.1.5. Data processing and structure determination

Out of the collected data, 5 were selected and merged using an *in-house* script (Chavas. L) were preselected based on their identical crystal lattice parameters that could eventually merge in a constructive way. A single run of restrained refinement using the *Refmac5* software suite [Murshudov] followed the molecular replacement step, with no addition of water molecules. Data analysis and refinement statistics are shown in Table 5.4 (Fig. 5.17).

METHOD	<i>In-situ hQr2</i> For molecular replacement	Cryogenized <i>hQr2</i> From the PDB model 5lbz.pdb
MERGED CRYSTALS	5	-
SPACE GROUP	19 (<i>P</i> 21 21 21)	19 (<i>P</i> 21 21 21)
CELL PARAMETERS (Å) (°)	57.94 82.20 106.72 90 90 90	61.45 79.22 106.23 90 90 90
RESOLUTION	2.72 Å	1.4 Å
R-MERGE	0.237 (0.335)	0.045 (0.329)
I/SIG(I)	2.9 (1.1)	(5.3)
COMPLETE	84.7 (27.7)	95.0 (91.0)
MULTI	2.4 (1.2)	4.5 (4.4)

Table 5.4 human Quinone Reductase II data processing and refinement statistics using data replacement. The cryogenized human quinone reductase 2 used the PDB model 5lbz.pdb in order to make phasing by molecular replacement. Compared to the PDB model 5lbz.pdb.

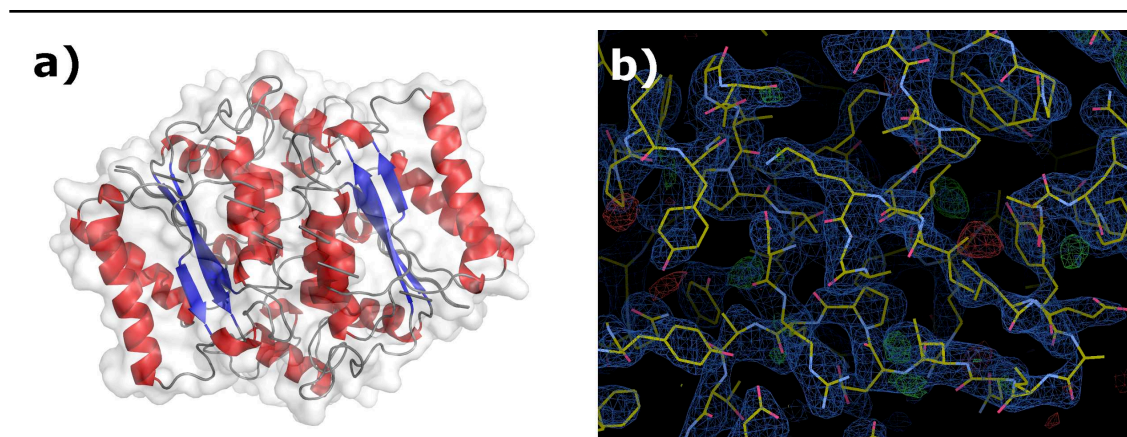


Figure 5.17 : In situ human Quinone Reductase II crystal structure.

(a) Overall fold of *hQr2* structure. The figure shows the structure of *hQr2* solved by the molecular replacement method using data collected from five crystals and merged (Table 5.4). Helices and beta-strands are colored in *red* and *blue*, respectively. The surface of the protein is represented in *grey*. (b) Electron density map of the *hQr2* structure. The *blue* electron density is a $2F_o-F_c$ map contoured at 1.4σ . *Green* and *red* stand for positive and negative F_o-F_c maps contoured at 2.0σ , respectively. The structure is modeled in sticks, colored by atom type. No water molecule was added during the unique refinement run, explaining the presence of the green blobs around the protein backbone.

6.1.6. Conclusions

The *hQr2* protein was chosen as a test sample to experiment on in-chip ligand soaking. The preliminary results for controlled injection into the microfluidic chips have been a success, especially when considering the limited number of trapped *hQr2* crystals. Using colored liquids, it was demonstrated that ligand soaking is feasible, with no flow direction change, and a perfect control of the soaked crystals without affecting its surroundings. The difficulties in sampling *hQr2* hampered the commissioning of the in-chip ligand soaking. The human Quinone Reductase II structure was obtained with the chip at a 2.72 Å resolution which is sufficient to obtain a binary yes or no information on the presence of a particular ligand (3 Å - 3.5 Å resolution needed to obtain such resolution).

7. Conclusions

The different selected samples have been studied, confirming the efficiency of the chip. The chip qualification tests, using Lysozyme and Insulin, lead up to a structure resolution at 1.6 Å and 2.33 Å respectively using the automatic acquisition I.G.O.R. scanning. These results confirmed the chip capacity to acquire high resolution structural information.

The Single-wavelength Anomalous Diffraction (SAD) technique on Insulin lead to the acquisition of anomalous information permitting to confirm the zinc position. These experiments confirm the capacity to acquire anomalous information using the SAD technique. Further experiments are required to acquire a full structure using the single anomalous diffraction to confirm the results obtained. About the *in-vivo* serial crystallography, if the crystal management needs improvements in order to place it easily on the beamline for automatic diffraction, the experiment has shown diffraction results up to 2.88 Å resolution with the proper space group and cell parameters, leading to great expectations. The experiment on sensitives samples, using Ribosome had shown similar resolution results between in-situ and cryogenic experiment. Further experiment should focus on the obtention of a full structure by acquiring data on a wider sample. The Protein/Ligand complex studies, using human Quinone Reductase II, permit to obtain the full protein structure with a resolution (2.72 Å) good enough to detect the presence of ligand. The previous results on ligand injection in the chip showed the efficiency of highly controlled in-chip ligand soaking. The combination of these results lead to high expectations toward the use of the microfluidic chip in the ligand screening technique.

Overall, these experiments highlighted results leading to a great expectation in a wide range of structural crystallography challenges. These experiments pave the way to the expansion of the technique. With the future access to COC chips, the current advances in in-cellulo crystallography and futures collaborations, further structures should be soon solved using the microfluidic chips.

CONCLUSIONS AND PERSPECTIVES

The work reported in this thesis followed some previous investigations on the applicability of microfluidics for macromolecular crystallography at Synchrotron SOLEIL. These early experiments set the working constraints, and confirmed the principles behind microfluidic chip engineering and manufacturing using in house research instrumentations, crystal trapping, and basic diffraction data acquisition on model proteins.

The most laborious part of the work established during the thesis concentrated around the optimisation of the microfluidic chip designs, their manufacturing, and the optimisation of sample injection protocols. As a direct result of these investigations, the principle of crystal trapping has been confirmed to easily adapt to the peculiarities of numerous types of experiments, with the number of traps per microfluidic chip that could be adapted to the needs with no major difficulties. Varying the thickness of the chip and the width of the channels and traps permit to adapt these trapping systems to the different crystal sizes and shapes. The protocol for engineering the PDMS chips can also be exported and shared in any microfluidic laboratory equipped with common instrumentation for microfluidics, *e.g.* a spin-coater, some chip molds and a plasma-bonding instrument.

In some cases, the sampling of the crystals followed by their injection still poses handling difficulties. Crystals contained in crystallisation drops of small volumes are hard and delicate to recover, often leading to the trapping of only a handful of crystals. On the opposite side of the crystal growth methods, crystals grown in batch conditions may pose issues related to their sedimentation along the injection, although advanced techniques may be applied to the crystal solution to circumvent these difficulties [[Yano](#)]. In image to what has already been developed for other applications, some tank rotating instruments are under implementation at the PROXIMA-1 beamline. An alternative for crystallisation is slowly emerging with yet another microfluidic-based mixing approach, consisting in crystallising molecules in drops separated by oil. By plugging the outlet of these crystallisation setups to the trapping chips described in this thesis, one would have a system with the double advantage of storing the crystals in long tubes of isolated conditions, and maximise the chances of crystal injection and trapping without sample loss or clogging caused by crystal congestion.

With minor modifications, the microfluidic chips could be easily implemented on the PROXIMA-1 macromolecular crystallography (MX) beamline. The chips have been designed to be mounted on any classical MX goniometer, adapted to standard sample pin holders. Taken all together, only minor adjustments of the sample environment would be required for a proper integration into standard MX beamlines. Moreover, the I.G.O.R. scanning approach for serial in situ data collection has

been implemented within the MXCuBE project for an easier export of the method to other synchrotrons using this software on their MX beamlines. Implementing the I.G.O.R. scanning at a second MX beamline equipped with MXCuBE remains to be done, and would confirm the potential of the approach for other applications and user communities.

PDMS is an excellent microfluidic fabrication material suitable for biology and design prototyping. Prior to fully validating the design and usefulness of the PDMS chips for MX experiments, their optical properties against X-rays were carefully measured. Additionally, the compatibility of the material with common crystallisation solutions and the relevance of the trapping system in these conditions were deeply investigated, confirming the potential of the chip to accept most of the crystallisation conditions. The diffraction results obtained for Lysozyme, *hQr2* and Insulin confirmed that the chip successfully permits in situ diffraction experiments, yet another alternative to the cryo-loop data acquisition methods more commonly used at MX beamlines. As highlighted for Insulin crystals, anomalous data collection of crystals trapped in the chip is possible, completing the applicability of the chip with experimental phasing methods. Studies on Ribosomes have shown that it is possible to carefully inject fragile crystals into the chips and obtain diffraction data.

When coupled to the I.G.O.R. scanning approach, the chemical composition of the chips made of PDMS is not a showstopper to collecting diffraction data through in situ wedged serial crystallography. Due to its interaction with the beam, and the resulting strong diffuse scattering that adds unnecessary background to the diffraction data, however, the PDMS is not envisioned as the only and final material for manufacturing the chips. Rather, the Cyclic-Olefin Copolymer (COC) alternative material appeared as a potential replacement, being transparent to X-rays and hermetic to slow down evaporation. The PDMS-based chips then qualify better as prototyping optional devices for projects in need of quick developments and tests.

The developments towards automated in-chip ligand soaking highlighted how ligand injection into a microfluidic chip charged with crystals could be mastered. It leads to the possibility to soak different crystals with different ligand solutions or ligand mix solution with highly controlled timings. The advances in the crystallisation and sampling of *hQr2*, used in this work as the ligand-soaking model protein, permit to obtain the *hQr2* structure, but do not allow to perform on-chip ligand soaking experiments. Currently under investigation, different methods are proposed to circumvent these difficulties. As an example, crystallisation in water/oil interface [[Gerard](#)] could solve some of the issues encountered with *hQr2* and therefore accelerate ligand soaking experiments.

The above described technique allows trapping objects and present them to a source of X-ray light in order to acquire diffraction data. In this perspective, any diffracting object could be trapped and studied under X-rays, such as crystal-containing cells. Moreover, the trapping design appears sufficiently generic that the technique could be used in research fields completely different than macromolecular crystallography.

The microfluidic chips designed in this work also offer an in situ alternative to crystals sensitive to cryo-protection or chemical changes. Compared to the other in situ crystallographic approaches, the

I.G.O.R. scanning method presents the advantage of collecting diffraction data in wedges. Although crystals are irradiated with larger doses when compared to other techniques based on raster scanning, the approach drastically reduces the needs in terms of number of images, and by extension in terms of sample consumption.

Considering the plethora of approaches developed for macromolecular crystallography at synchrotrons and other X-ray sources, the microfluidic-based in situ wedged serial crystallography introduced in this work will certainly not replace the more classical and well-advanced techniques. Nevertheless, it makes no doubt that the I.G.O.R. scanning shows strong advantages that will complete the various methods available for serial crystallography. Among the various benefits of the approach, the microfluidics helps in handling the crystalline samples without the necessity to fish them. As an in situ technique, it also helps circumventing possible cryoprotectant issues.

The developments toward confined objects, applicable for oxygen sensitive molecules, or even biologically hazardous samples, highlighted that the current chemical composition of the chip does not ensure a complete sealing. Currently under investigation, the COC should entirely confine the sample inside the chip. The transition of the material constituting the chip will be followed by a series of testing and protocol refinement for the chip creation and the injection. The price is small to be able to work with confined samples.

As the crystallisation techniques evolve, the *in-vivo* crystallisation could use the microfluidic chips. The capacity of the chip to acquire structural information from a diffraction experiment in an *in-vivo* crystallised protein has been established. The next challenges are then toward crystal trapping optimisation. It could be done by using new designs as presented. It could also be done by working on the crystal concentration, increasing the protein expression and the crystallisation occurrences, or preselecting the crystals, by sorting the crystals and the cells coupling SHG detection with microfluidic. Those three optimisation processes are currently under investigation.

Compared to previously published work, the chips studied during this thesis have pros and cons. As the chips are made for wedged crystallography, the time-resolved diffraction, adopted by many techniques adapted for XFEL experiments [[DePonte](#), [Sierra](#), [Weierstall](#), [Grünbein](#)], was traded with crystal consumption optimisation and sample environment mastering. The chip ligand soaking and sample confinement techniques presented previously can be highlighted as examples. In order to adapt the chip to the widest range of macromolecules and not to impose the crystallisation process, the chip was not designed to grow *in-chip* crystals [[Dhouib](#), [Wijn](#)]. The plate screening technique helps making fast crystal screening by removing entirely the shipping process [[Bingel-Erlenmeyer](#), [Le Maire](#)], but do not position the crystals. Moreover, the sample environment is limited to the crystallisation environment contrary to the chip presented in this work. The crystal trapping method introduced during this thesis can be replaced with an X-ray centering [[Ren](#), [Martiel](#)]. This method to locate the sample induces radiation damages due to X-ray exposure prior to data collection.

In summary, although the chips designed during this thesis may benefit from further improvements, they have already shown excellent results and open the field for numerous applications.

The design applied to the chips represents a small part of a wider tendency towards the use of microfluidic approaches for serial crystallography experiments at X-ray sources. Together with the trapping mechanism developed in this work, the concept of in situ microfluidic-based placement of objects at known positions for serial crystallography data acquisition will surely open the door to further revolutionary developments that will assist macromolecular crystallography applications.

ANNEXES

1. Crystallisation solutions

1.1. *hQr2 crystallisation tests*

In this part will be show the different conditions tests made during the PhD:

The crystallisation solution is made of X M Ammonium sulfate, 100 mM Hepes pH Y
Qr2 : QR2 Pool 2 (E.Coli sans Tag) - lot *hQr2Pool2_01/20th/12* at 20mg/mL
with the X and Y varying

20/07/2018 : 1.62 to 1.7 with 0.2 steps M of Ammonium sulfate with steps of 0.02, 100 mM Hepes pH 7 and 7.25 handmade 1 + 1µL sitting drops (leading to crystals)

04/09/2018 : 1.65 and 1.68 M of Ammonium sulfate with steps of 0.02, 100 mM Hepes pH 7 and 7.25 handmade 1 + 1µL sitting drops

06/09/2018 : 1.68 and 1.68 of Ammonium sulfate with steps of 0.02, 100 mM Hepes pH 7 and 7.25 handmade 1 + 1 µL sitting drops with 8 times each conditions

06/09/2018 : 1.58 to 1.75 M of Ammonium sulfate with steps of 0.02, 100 mM Hepes pH 7.2 mosquito made 0.2 + 0.2µL sitting drops

24/10/2018 : 1.61 to 1.71 M of Ammonium sulfate with steps of 0.02, 100 mM Hepes pH 7 handmade 1 + 1µL sitting drops

08/11/2018 : 1.63 to 1.75 M of Ammonium sulfate with steps of 0.02, 100 mM Hepes pH 7 , 7.25,7.5 handmade 1 + 1 µL sitting drops

13/11/2018 : 1.75 M of Ammonium sulfate at 100 mM Hepes pH 7.25 with a Qr2 concentration at 5,10,15,20,25mg/mL handmade 1 + 1 µL sitting drops

20/11/2018: 1.63 to 1.75 M of Ammonium sulfate with steps of 0.02, 100 mM Hepes pH 7 , 7.2,7.25 mosquito made 0.2 + 0.2 µL sitting drops

29/11/2018: 1.54 to 1.76 M of Ammonium sulfate with steps of 0.02, 100 mM Hepes pH 7 , 7.25,7.7 mosquito made 0.2 + 0.2 µL sitting drops.

29/11/2018: 1.54 to 1.76 M of Ammonium sulfate with steps of 0.02, 100 mM Hepes pH 7 , 7.25,7.7 mosquito made 0.2 + 0.2 µL sitting drops. (leading to crystals)

07/02/2019: 1.74 M Ammonium sulfate, 100 mM Hepes pH 7,7.5 mosquito made 0.2 + 0.2 µL sitting drops, using a new Qr2 sample (leading to crystals)

02/04/2019: 1.74 M Ammonium sulfate, 100 mM Hepes pH 7,7.5 mosquito made 0.2 + 0.2 µL sitting drops, using a new Qr2 sample (leading to crystals)

1.2. Commercial screens for chemical tests of chips

The composition of the solutions coming from 14 random crystallisation screening kits commercialised by four companies were inspected for the chemical compositions in order to select major crystallisation compounds. The list of the commercial companies and screens inspected are as follows :

Molecular dimensions

MD1-14 Clear Strategy Screen I

MD1-15 Clear Strategy II

MD1-18 Solubility Tool Kit Box 1

MD1-20 Stura Footprint Screen

MD1-29 PACT premier v2

Hampton research

HR2-086

Jena Bioscience

CS-201L

CS-202L

CS-206L

CS-207L

CS-209L

CS-507L

Qiagen

EasyXtal® and NeXtal® Protein Crystallization Handbook January 2010

2. Protocols for chemical tests

2.1. Long injection protocol

This injection is testing if the liquid affects the PDMS or the bonding of the chip using high concentration of components of solutions commonly used in crystallography.

- tools needed:
 - 3 mL of the buffer in a falcon.
 - ethanol
 - distilled water
 - distilled water with glass beads < 50 μm
 - Microscope with timed auto record and video recording.
 - Pressure controller with 2 outlets and a pressure between 10 mbar to 1000 mbar.
- Preliminary set up
 - inject distilled water water in the chip with a syringe. In order to check for leaks
 - Check the chip with a microscope for defaults. The chip does not have to be entirely full of liquid.
 - Let the chip dry (over night)
- Set in place (for the trash falcon and the buffer falcon):
 - Remove the falcon, wash with distilled water water then with ethanol the tube inside then remove the tube.
 - Place new tubes in the injection devices with the length of the falcon for the buffer one and about 30 mm inside the trash falcon.
 - Bend 90° the end or the tube and insert them into the connectics of the chip, the inlet linked with the buffer side and the outlet at the trash side.
 - Place the chip under the microscope, if needed, use tape to fix it.
 - Place an falcon in the trash side
 - Place a falcon with the Tampon on the Tampon side.
- Injection
 - Take pictures of the pattern
 - Begin a video on the microscope
 - Set the pressure of the Tampon at 300 mbar and the Trash at 200 mbar.
 - If the liquid does not come into the tube, pull up the pressure of the Tampon by 50 mbar until it comes.
 - Watch the liquid entering into the chip.
 - Pull down the pressure of the buffer at 250 mbar and of the Trash at 200 mbar.
 - wait for the liquid to fill all the channels.
 - If the filling does not evolve, pull up the pressure of both the outlet of 50 mbar until the chip continues to fill itself.
 - The chips can handle at least 2 000 mbar of pressure.

- When the bubbles have collapsed and the flow has been stabilised, pull down the pressure to 250 mbar (buffer) and 200 mbar (trash).
- The flow difference can be tuned to have an optically measurable flow speed.
- Stop the video and take pictures of the pattern (every 3 minutes).
- Set both pressure to 0 mbar
- Inject 200 μL of distilled water water with 0 to 50 μm glass beads in the Tampon falcon and a magnetic mixer
- Set the pressure back.
- Wait 10 h to 50 h
- End
 - turn off the pressure off
 - throw the liquids with the falcons, the chip
 - replace the falcons and the tubes

2.2. *Fast injection protocol*

- tools needed:
 - 0.5 mL of the buffer in a falcon.
 - ethanol
 - distilled water water
 - distilled water water with 0.1 mg per mL of beads < 50 μm diameter
 - Microscope with video recording.
 - Pressure controller with 2 outlets and a pressure range of 10 to 2000 mbar.
- Preliminary set up
 - Check visually the chip with a microscope for defaults. The chip does not have to be entirely full of liquid.
 - inject distilled water water in the chip with a syringe. In order to check for leaks
 - Let the chip dry (over night)
- Set in place (for the trash falcon and the buffer falcon):
 - Remove the falcon, wash with distilled water water then with ethanol the tube inside then remove the tube.
 - Place a 1.5 m tube in the buffer falcon, if necessary, roll the middle of it and fix it with tape to reduce the distance. This tube will serve as a container for the liquid.
 - Place a tube in the trash falcon and in the outlet of the chip.
 - bend 90° the end or the tube and insert them into the connectics of the chip.
 - Place the chip under the microscope, then fix it with tape.
 - Place an falcon in the trash side
 - Place an empty falcon in the Tampon side.
 - Remove the air entry
 - Place a fitting 1 mL syringe in the air entry of the falcon
- Injection
 - Take pictures of the pattern
 - Begin a video on the microscope

- Set the pressure of the Tampon at 300 mbar and the Trash at 200 mbar.
- If the liquid does not come into the tube, pull up the pressure of the Tampon by 50 mbar until it comes.
- Watch the liquid entering into the chip.
- Pull down the pressure of the buffer at 250 mbar and of the Trash at 200 mbar.
- wait for the liquid to fill all the channels.
- If the filling does not evolve, pull up the pressure of both the outlet of 50 mbar until the chip continues to fill it self.
- The chips can handle at least 2 000 mbar of pressure.
- When the bubbles have collapsed and the flow has been stabilised, pull down the pressure to 250 mbar (buffer) and 200 mbar (trash).
- The flow difference can be tuned to have a watchable flow speed.
- Stop the video and take pictures of the pattern (every 3 minutes).
- Set both pressure to 0 mbar
- Inject 200 μ L of distilled water water with 0 to 50 μ m glass beads in the buffer falcon and a magnetic mixer
- Set the pressure back.
- Wait 10 h to 50 h
- End
 - turn off the pressure off
 - throw the liquids with the falcons, the chip
 - replace the falcons and the tubes

3. Tests on sample stability

3.1. *Ribosomes injection experiment results*

3.1.1. Tests against dissolution

dilute 3 drops (1 μL each \rightarrow 3 μL) in a volume and wait overnight

- 30 μL [mL+mg] Survive overnight
- 30 μL mL w/o mg Dissolve overnight
- 20 μL 100% treatment solution Survive overnight

3.1.2. Injection protocols

Before injecting the liquid,

H₂O is injected in the chip until the bubbles goes

The mother liquor is injected to replace water (here mL + mg and Treatment solution depending on the chip.

The crystals solution is injected.

Sealing the connectics using glue, beginning with the inlet then the outlet when the first is dry.

Chip 1 (mL + mg)

- Add 10 μL to each of 3 drops merge 3 drops [Mother liquor 5.4% PEG + Mg²⁺ 14 mM]
- Inject the solution

Chip 2 (Treatment solution)

Case where it is necessary to treat Drops with dehydration solutions

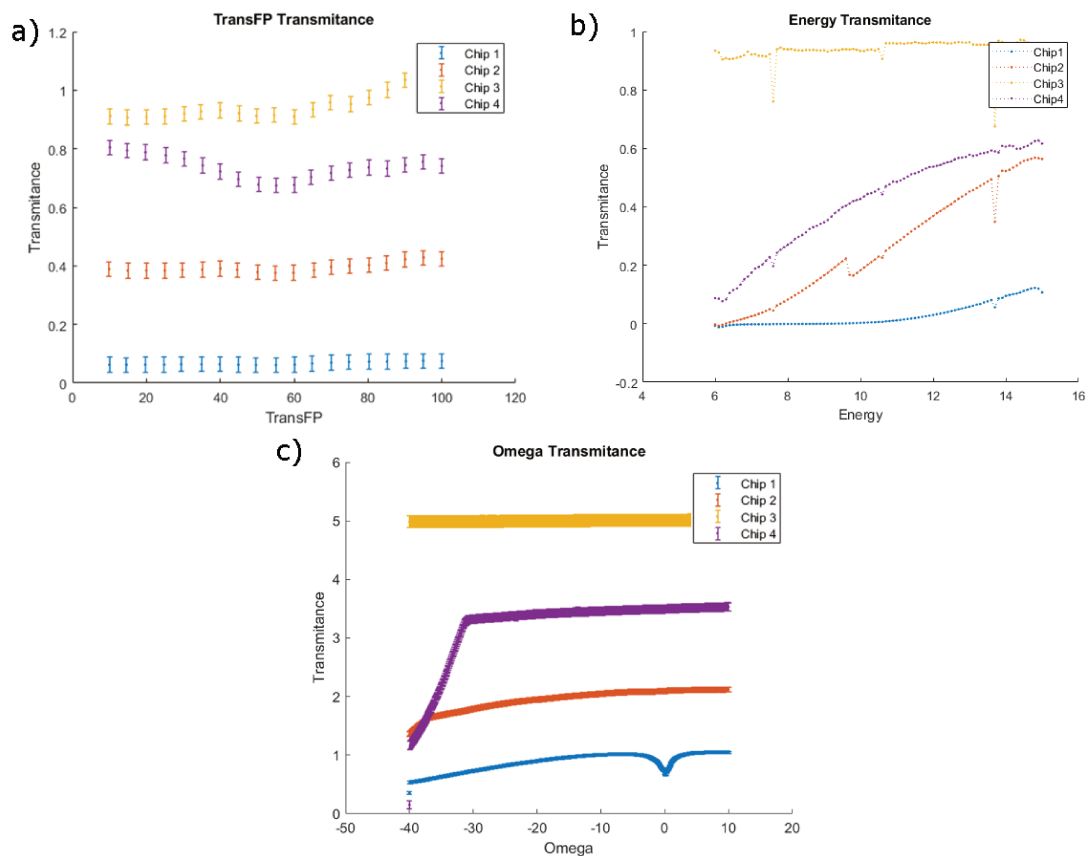
- Solution 1 : 2 Vol of mL : 1 Vol of treatment solution
- Solution 2 : 1 Vol of mL : 2 Vol of treatment solution
- Solution 3 : 100% treatment solution

Standard protocol for dehydration of the crystals

- Put 45 μL of solution 1 into the drop
- Remove 40 μL from the drop
- Put 40 μL of solution 2 into the drop
- Remove 40 μL from the drop
- Put 40 μL of solution 3 into the drop
- Wait 4-8 h before shooting crystals
- Inject the solution

4. Absorptions studies

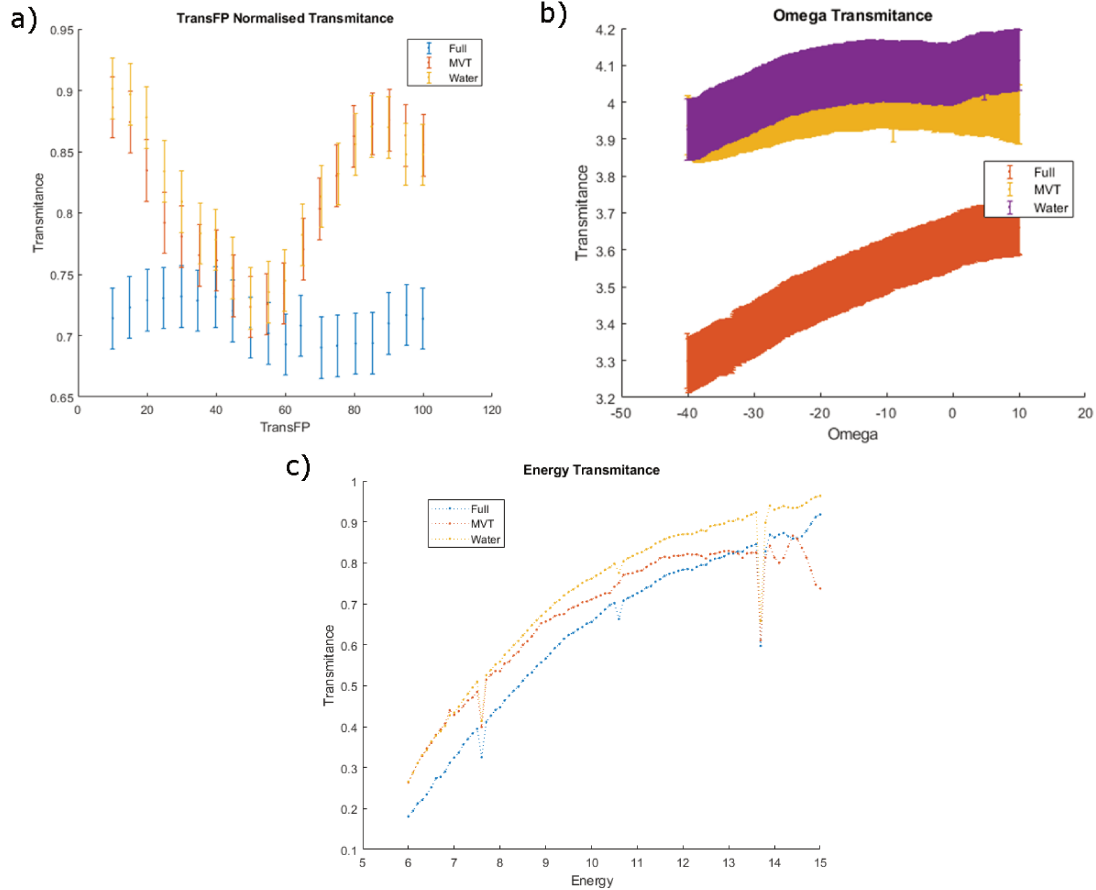
4.1. Chip Transmittance of the different chips



Supplementary Figure 1 : Chip Transmittance of the different chips

Chip transmittance as recorded at the dime photodiode divided by the XBPM 04 and then normalised with the transmittance at similar conditions without chip. Legend : the chip 1,2,3 and 4 are described in the (Table 3.2) a) Beam transmittance : The graphic shows the transmittance depending on the beamline beam attenuation ranging from 10% to 100% in steps of 0.5%. b) Beam energy : The graphic shows the transmittance depending on the energy ranging from 6 keV to 15 keV in steps of 0.1 keV the intensities are normalised by the transmittance of the air. The graph shows an increase of the transmittance with the energy. Furthermore, Absorption peaks can be shown at the energies : 7.6 keV, 10.6 keV, 13.7 keV on the chips 2,3,4 and only at 13.7 keV for the chip1. c) Omega angle : The graphic shows the transmittance depending on the angle of the chip from -40° to 10° with 0° corresponding to the chip perpendicular to the beam.

4.2. Chip transmittance depending on the position in the chip



Supplementary Figure 2 : Chip Transmittance depending on the placement

Chip transmittance as recorded at the dime photodiode divided by the XBPM 04 and then normalised with the transmittance at similar conditions without chip. The chip 3 was used to make the experiment. In the legend, *Full* describes a placement of the beam outside the channels, *Water* describes a placement inside a channel full of water and *MVT* describes a placement inside a channel full of water by changing the placement for each sampling. a) Beam transmittance : The graphic shows the transmittance depending on the beamline beam attenuation ranging from 10% to 100% in steps of 0.5%. b) Beam energy : The graphic shows the transmittance depending on the energy ranging from 6 keV to 15 keV in steps of 0.1 keV the intensities are normalised by the transmittance of the air. The graph shows an increase of the transmittance with the energy. Furthermore, Absorption peaks can be shown at the energies : 7.6 keV, 10.6 keV, 13.7 keV on the chips 2,3,4 and only at 13.7 keV for the chip1. c) Omega angle : The graphic shows the transmittance depending on the angle of the chip from -40° to 10° with 0° corresponding to the chip perpendicular to the beam.

5. List of chip patterns

5.1. Terminology and summary

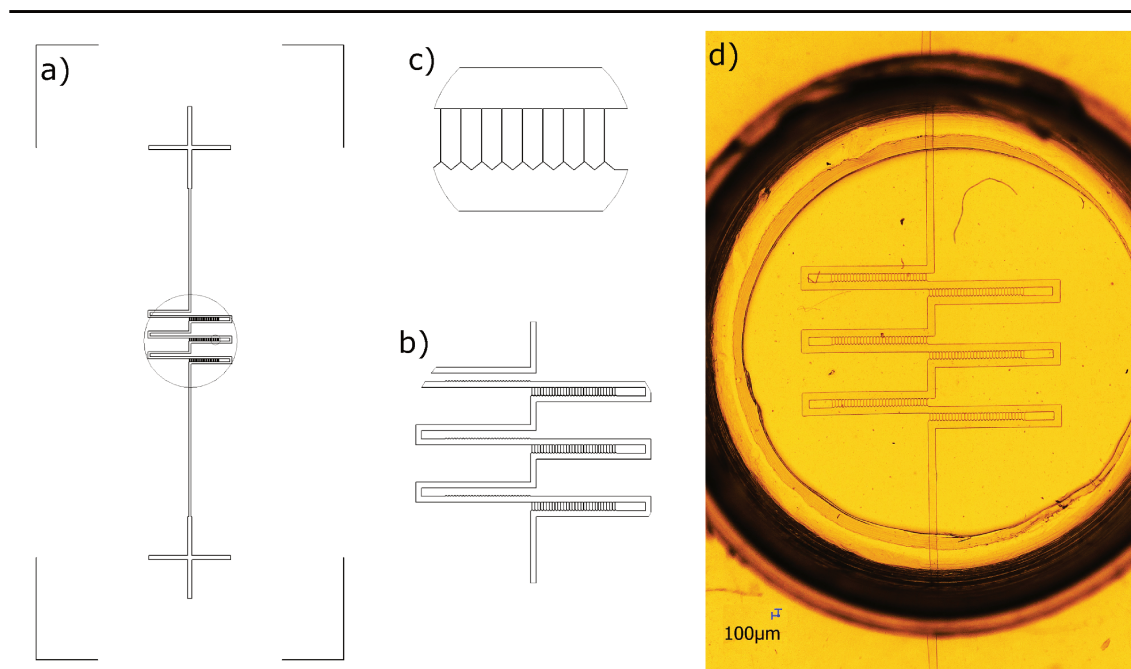
The pattern described by the channels of the chip evolved during the thesis. Depending on the modification, the goal was to adapt the chip to a new sample type, make shape experimentation or just straight chip improvement of the design or optimising the chip creation and production. To ease the organisation, the designs of the patterns were noted with the number of the pattern version completed sometime by notes the chip. They will be noted pattern Version x or pattern Vx or chip V x, with x the number of the version.

Chip version	Chip Function
Version 9	Pattern version of the beginning of the thesis
Version 11	High trap density (240 traps/chip)
Version 12	Injection of big and small crystals (two independent patterns)
Version 13	Ligand injection chips
Version 17	Ostromer-kapton chips for O_2 free chips
Version 18	Traps optimised in trapping needles crystals
Version 19	Standard chip, with designations, ligand compatible
Version 22	Small chip easy to mass produce, ligand compatible

Supplementary Table 1 : Main chip versions

5.2. Pattern V9

The 8 first patterns will not be discussed in this thesis because they were made in 2016 during the internship prior to the thesis. The pattern V9 (Supp. Fig. 1) was used as reference at the end of the internship.



Supplementary Figure 3 : Design Version 9.

This scheme (a) shows the Solidworks plan for the V9 pattern and two zooms (b) & (c) focusing on the traps. It is made of two cross serving as target for the punching ; a long vertical channel, that separate the plug in from the traps ; the traps series at the center, composed of 2 sets of 6 rows made of 30 traps made to block the crystals, as seen in the microfluidic material and methods chapter ; and a delimitation rectangular shaped pattern of 15mm*30mm made to help cutting the chip to fit the chip holder. The image in yellow (d) shows a zoom in of a microfluidic chip using the V9 pattern. The circle around the pattern is the border of the 100 µm / 25µm kapton thin window of the chip (see chapter absorption studies).

5.3. *Pattern V11 : high trap density*

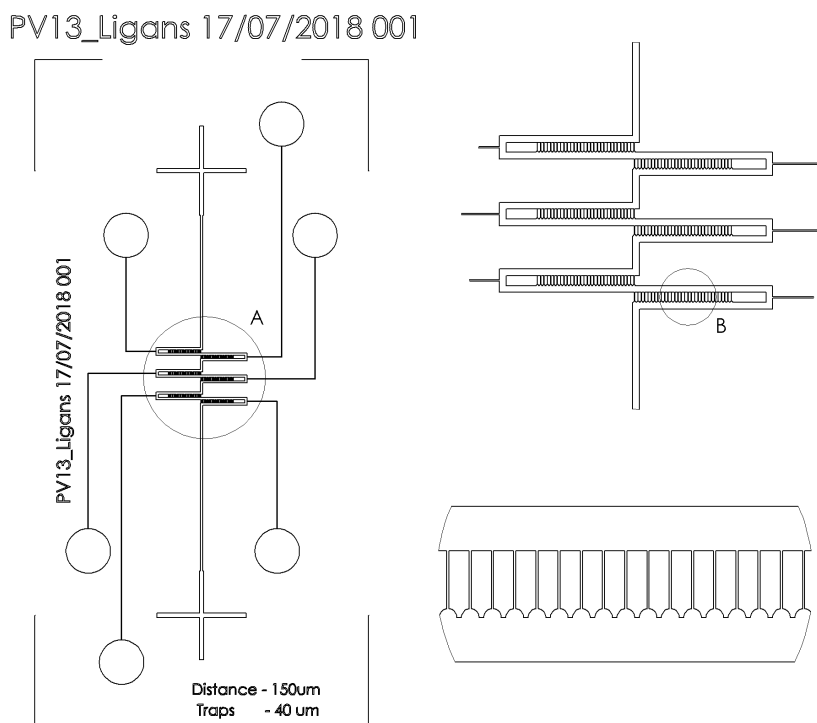
The version 11 of the chip reduces the space between the rows in order to improve the number of traps to 2*4*30 traps in the beamline easily accessible area. But the bonding efficiency of the chip was reduced in the trap zone as the bonded area was reduced. This effect leads to a smaller chip made over chip created. The trap density did not reach its limit, leading possibly to more traps in the chip, but because the number of traps is not currently crucial, the implementation of high density traps was set aside for now.

5.4. *Pattern V12 : variation in trap size*

The version 12 is made of two versions made to adapt the traps and the channels for 20 μm crystals and 100 μm crystals. The recess made to isolate the crystal from the liquid flow was made circular and with a diameter of 20 μm or 100 μm depending on the chip. The main channels of the Big version were enlarged to 200 μm . After experimenting, it appears that the recess size impact mostly with the accumulation of micron sized small objects of semi solid objects that may aggregate in the trap without blocking the stream.

5.5. Pattern V13 : in-chip ligand injection

The version 13 adds naming and helping to record the trap version with the version number, the date of the pattern creation and traps information (Supp. Fig. 2). The ligand designs were made to trap the crystals then filling selectively ligands into the traps. In order to make the first tests, a simplifier design with 4 traps per row was made, more detail in the tests and the results in the ligand chapter. If the ligand outlets are not plugged, the pressure of the channel non used will push out the liquid and act as if they do not exist. The chip can be used as a non-ligand chip.

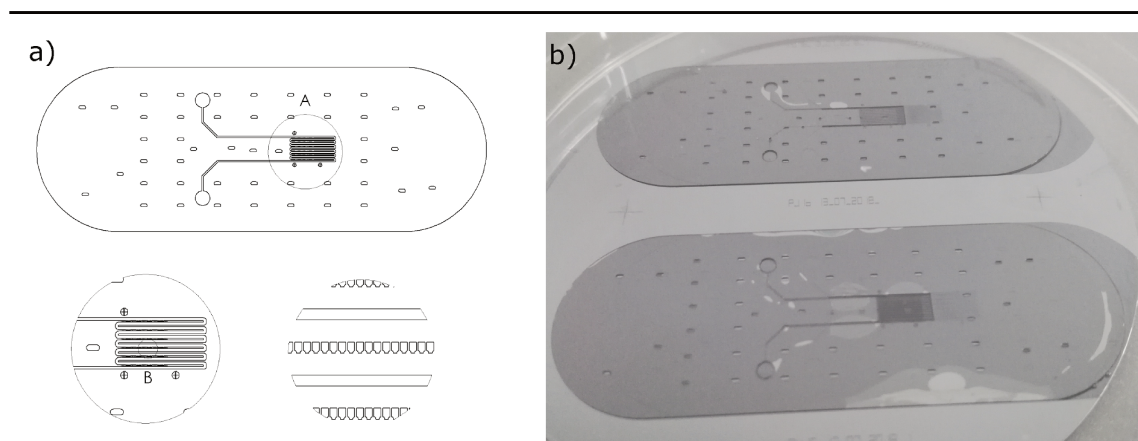


Supplementary Figure 4 : Design version 13_Ligans.

The figure shows the solidworks plan of the first layer of the otromer chip and two zooms focusing on the traps. The chip is composed of 6 supplementary channels linked to independant inlets.

5.6. Pattern V14-V17 : ostromer-kapton chips

The versions 14 to 17 implies adaptations to make ostromer-kapton chips, see the ostromer chips chapter. The chips were designed as positive layers, where the channels are placed in empty spaces of the mold and the chip material will be present where the SU-8 is present, contrary to the negative layers made previously. The laserwriter properties linked with the diffusion of the laser in the pattern lead to difficulties to write small positive channels. In order to make the chip, a PDMS mold is made and then an ostromere resin is injected into the mold. In order to prevent leaks during the ostromere injection, the PDMS mold is pressed on a kapton sheet. The chip had to ensure the injection ostromère injection while sustaining the pressure. In order to sustain the pressure without collapsing, pillars were placed in the large areas. The chip was made with two layers, the traps and the corners at both extremities of the rows were only one layer thick in order to permit the ostromer to fill the gap. The outlets were moved to the side to improve the filling of the resin. Three crosses are visible around the traps (Supp. Fig. 3) these are alignment crosses made for aligning the chip on the beamline.



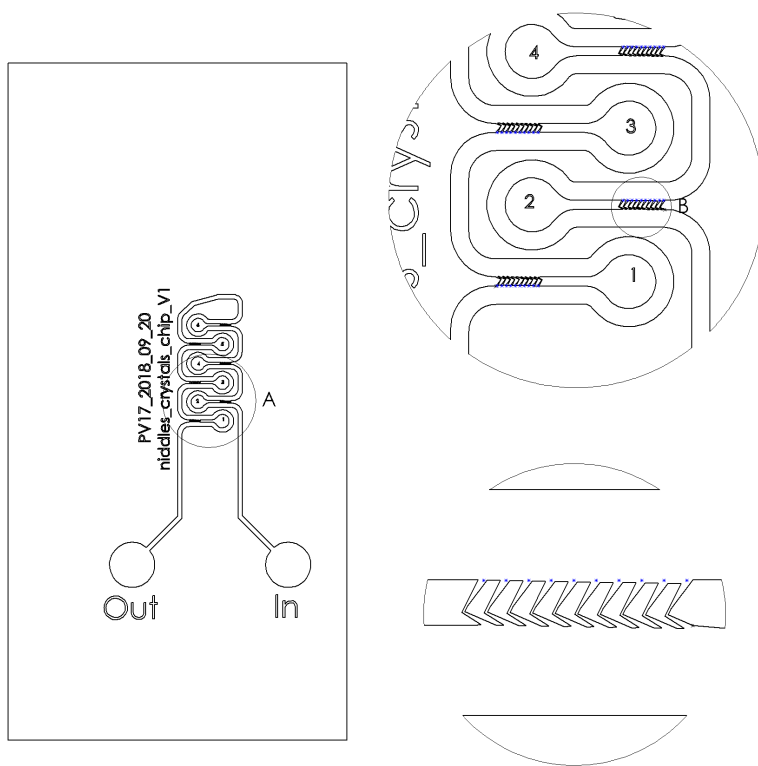
Supplementary Figure 5 : Design version 17 : Ostromer-kapton chip.

The figure (a) shows the solidworks plan of the first layer of the ostromer chip and two zooms focusing on the traps. The picture (b) shows two chips printed in a 3 inch wafer

Between the V14 and V17, the improvements were mostly made to optimise the ostromere injection during the chip making. Furthermore, between the versions, the pillars placement has been improved and the length of the chip has been reduced.

5.7. Pattern V18 : adaptation for needle objects

The version 18 is designed to trap needle shape crystals. The supplementary figure 4 highlights the evolutions. The chip design was never used. Experiments with *hQr2* crystals highlighted the trapping efficiency of the V9 traps for needle crystals. Therefore molds of this version were never printed.

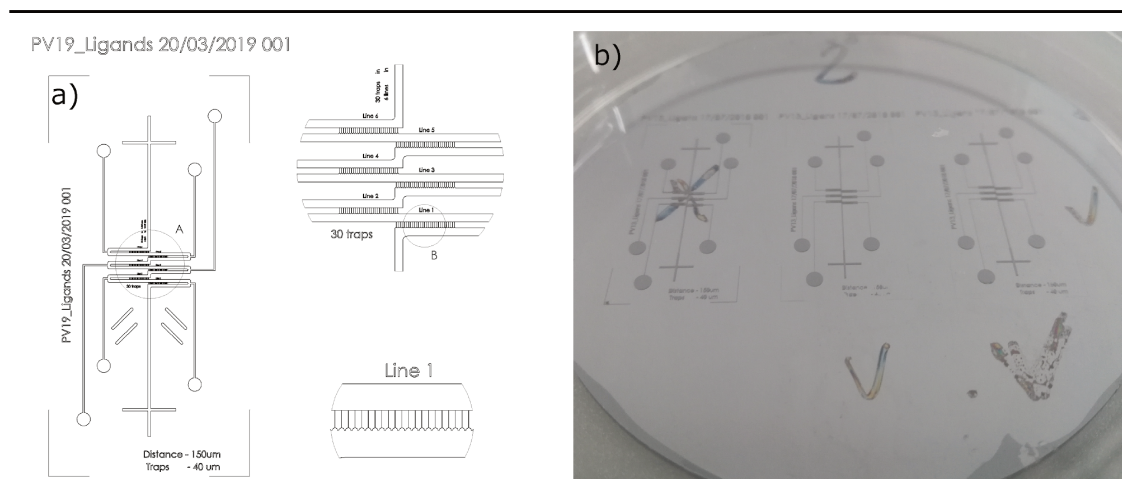


Supplementary Figure 6 : Design version 18 : needle blocking chips.

The figure shows the solidworks plan of the chip and two zooms focusing on the traps. The modifications with the original design consist in channels with a radius of curvature superior than 300 μm , to prevent crystal blocking in the channel curves and traps with a 90° angle to block the needles crystals. the numbers of traps have been reduced to 6 rows of 10 traps.

5.8. Pattern V19 : standardisation of the chip

The version 19 implied a standardization of the chip with further in chip information like a line number, trap information and visual inlet / outlet differentiation. two versions exist, with and without the six peripheral outlet made to inject ligand. The version with ligand is shown in supplementary figure 5.

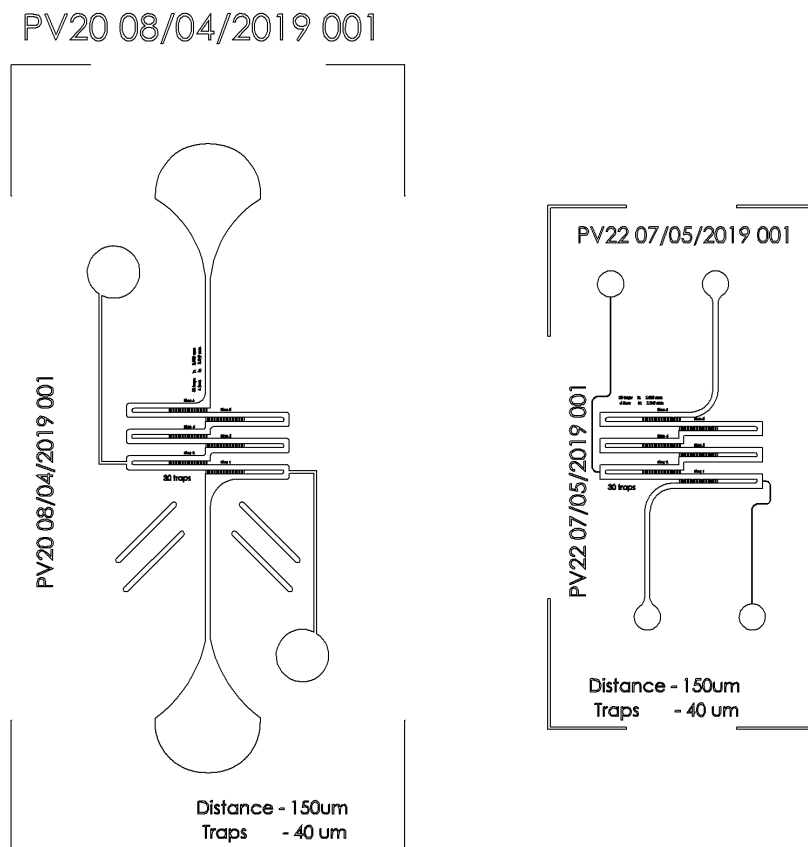


Supplementary Figure 7 : Design Version 19.

The figure (a) shows the solidworks plan of the chip and two zooms focusing on the traps. The four 45° lines are made to differentiate with the naked eye the inlet and the outlet (here inlet at the bottom). The picture (b) shows 3 designs printed in a wafer with marks made to recognise the ones well printed.

5.9. Patterns V20-V22 : design optimisation

The version 20 was made to reduce the clogging chances in the main channel by adding 300 mm radius of curvature at two places it was recorded, the outlet and the first turn (Supp. Fig. 6). When the chip was made, the inlets collapsed during the bonding step blocking the chip. The blockage can be circumvented by plugging the tubes at the entrance of the outlet.



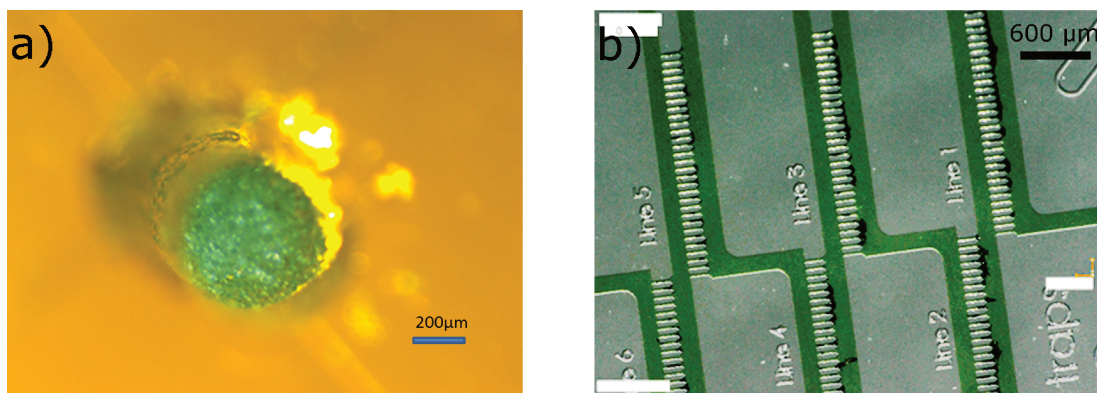
Supplementary Figure 8 : Designs version 20 and 22.

The figure shows the solidworks plan of the two chips at scale (15x30 mm for the version 20 and 10x20 mm for the version 22).

With the arrival of a new microfluidic experience at soleil thanks to Ramakrishna Vasireddi, a method to bond thin PDMS layer was added to the project. With this implementation, the distance between the traps and the inlets can be reduced. This leads to the reduction of the chip size and the augmentation of the numbers of chips on the silicium wafer from 3 to 11.

Only two ligand inlets are present on these chips. It permits to make ligand injection tests and keeping the chip simple for non ligand use.

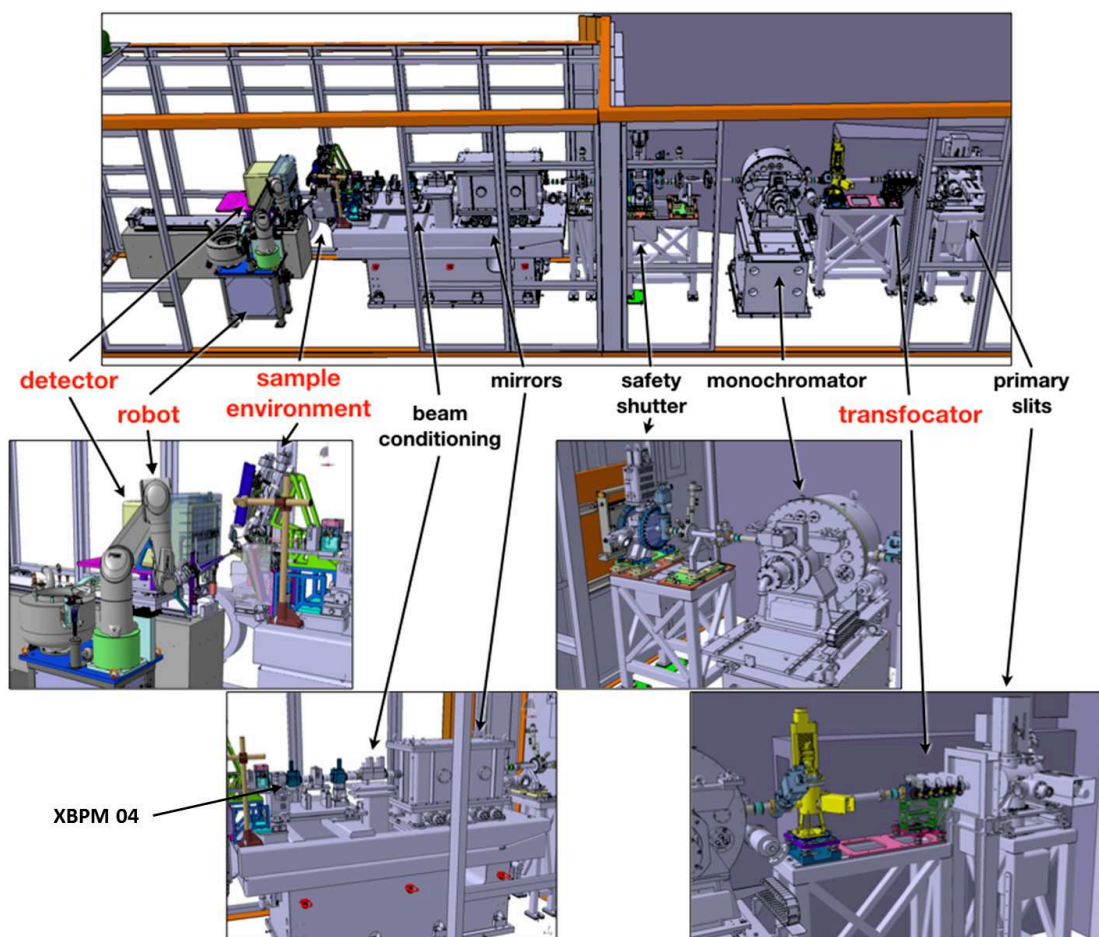
6. Injections difficulties during chemical tests



Supplementary Figure 9 : Injection difficulties during chemical tests.

(a) Closed view of the connectic of the chip with 100 μm to 50 μm marbles clogging (in blue) during an injection test using water and glass marbles at the entrance of the chip. (b) a chip injected with AmmoSO₄ and green food coloring. The two components interaction create a dark semi-solid component clogging in the traps.

7. Proxima-1 beamline technical overview



Supplementary Figure 10 : 3D view of the optical elements of the PROXIMA-1 beamline.

A 3D overview of the proxima-1 beamline with the different elements highlighting the place of the XBPM 04 between the optical experiment and the head of the beamline.

LIST OF FIGURES

1.1	PDB data distribution by experimental methods	11
1.2	Overall view of a classical sample preparation pipeline	12
1.3	Gas-dynamic virtual nozzle liquid jet for serial crystallography at XFELs	13
1.4	Design of the micro-patterned silicon chip and data collection strategy	15
1.5	A microfluidic trap array for protein crystals	17
2.1	A schematic drawing of a protein crystallisation phase diagram based on two of the most commonly screened parameters: proteins and precipitant concentrations	22
2.2	Illustration of the Bragg's law	24
2.3	Simplified scheme of a classical synchrotron layout	27
2.4	Sketch of the SmarGon goniometer with the different rotation axis	29
2.5	PROXIMA-1 sample environment	32
2.6	Scheme of the trapping principle	37
2.7	Illustration of filling strategy of KloéDesign	40
2.8	Film thickness over spin-coating speed	42
2.9	Illustration of the different steps of the chip making	44
2.10	Design of the ChipX3	50
2.11	Mechanism behind <i>in-chip</i> ligand soaking	51
2.12	Design version 13 for Ligand soaking	52
2.13	Two and three layers trapping designs and printed results	54
2.14	Design of the one lane cell placing chip	55
2.15	Chip handling by the CATS robot	56
2.16	Alignment challenges using motorisation located before the rotation axis	59
2.17	MXCuBE interface as of March 2019	62
2.18	MXCuBE I.G.O.R. scanning Selection windows	63

3.1	Chip design V22	65
3.2	Covers for creating a window on the chip	66
3.3	Handling of thinner chips	67
3.4	Chip support frame	69
3.5	PDMS chip absorption studies at PROXIMA-1	71
3.6	Impact of the beam on the chip	72
3.7	Beam / PDMS interaction depending of the angle in the cross sectional view of the chip	74
3.8	Methyl viologen in a windowed chip model V9	78
3.9	Anaerobic tests on ChipX3	79
3.10	Ligands injection cycle	81
4.1	<i>hQr2</i> crystals in drops before and after sampling	84
4.2	Filling of a chip during injection	86
4.3	Filling the traps of a chip during the preloading	87
4.4	Large bubbles trapped in the largest channels	89
4.5	Crystal channel clogging	90
4.6	MXCuBE PX1 preferences widget	92
5.1	Lysozyme crystals grown in batch	94
5.2	Lysozyme crystal trapping	95
5.3	In situ Lysozyme crystal structure	96
5.4	Insulin crystals grown in batch	98
5.5	Insulin crystal trapping	99
5.6	In situ Insulin SAD anomalous information compared to molecular replacement structure obtained	102
5.7	HEK cells with fluorescent crystal	104
5.8	<i>In-cellulo</i> grown XPA crystal trapped in a V22 Pattern chip	105
5.9	Diffraction Pattern obtained with the <i>In-cellulo</i> grown XPA collected <i>in-situ</i>	106
5.10	Experimental results of the line cell placing chip injection	108

5.11	<i>Ta</i>Ribosome crystals in the crystallisation plates	110
5.12	<i>Ta</i>Ribosome crystals trapped in a V19 chip	111
5.13	X-ray diffraction from Ribosome crystals	112
5.14	<i>h</i>Qr2:ligand complex crystal packing	113
5.15	human Quinone Reductase II crystallisation	116
5.16	Crystals of human Quinone Reductase II trapped in microfluidic chips	117
5.17	In situ human Quinone Reductase II crystal structure	118
Sup. 1	Chip Transmittance of the different chips	130
Sup. 2	Chip Transmittance depending on the placement	131
Sup. 3	Design Version 9	133
Sup. 4	Design version 13_Ligans	135
Sup. 5	Design version 17 : Ostromer-kapton chip	136
Sup. 6	Design version 18 : needle blocking chips	137
Sup. 7	Design Version 19	138
Sup. 8	Designs version 20 and 22	139
Sup. 9	Injection difficulties during chemical tests	140
Sup. 10	3D view of the optical elements of the PROXIMA-1 beamline	141

LIST OF TABLES

1.1	Advantages and drawbacks of Roedig <i>et al.</i> in chip serial crystallography	14
1.2	Sample delivery methods for serial crystallography experiments	16
2.1	PROXIMA-1 beamline compared to other representative beamlines	28
3.1	Absorption and bonding quality of different materials	71
3.2	Validation process of the chips	73
3.3	Summary of the chemical validation of the PDMS chips.	77
5.1	Lysozyme data processing and refinement statistics	96
5.2	Insulin data processing and refinement statistics using data replacement	100
5.3	Insulin data processing and refinement statistics using SAD	101
5.4	human Quinone Reductase II data processing and refinement statistics using data replacement	118
Sup. 1	Main chip versions	132

BIBLIOGRAPHY

- [1] Abdallah, B.G., *et al.* Microfluidic sorting of protein nanocrystals by size for X-ray free-electron laser diffraction. *Structural Dynamics* **2**, 041719 (2015). doi:[10.1063/1.4928688](https://doi.org/10.1063/1.4928688)
- [2] Ascone, I., *et al.* Proxima 1, a new beamline on the third generation SR source SOLEIL combining PX and single-crystal BioXAS. *AIP Conf. Proc.* **882**, 872 (2007). doi:[10.1063/1.2644688](https://doi.org/10.1063/1.2644688)
- [3] Benjdia, A., *et al.* Post-translational modification of ribosomally synthesized peptides by a radical SAM epimerase in *Bacillus subtilis*. *Nature chemistry* **9.7** 698 (2017). doi:[10.1038/nchem.2714](https://doi.org/10.1038/nchem.2714)
- [4] Bentley, G., *et al.* Structure of insulin in 4-zinc insulin. *Nature* **261.5556** 166-168 (1976). doi:[10.1038/261166a0](https://doi.org/10.1038/261166a0)
- [5] Bingel-Erlenmeyer, R., *et al.* SLS Crystallization Platform at Beamline X06DA A Fully Automated Pipeline Enabling in Situ X-ray Diffraction Screening. *Crystal growth & design* **11.4** 916-923 (2011). doi:[10.1021/cg101375j](https://doi.org/10.1021/cg101375j)
- [6] Boudes, M., *et al.* A pipeline for structure determination of in vivo-grown crystals using in cellulose diffraction. *Acta Cryst.* **D72**, 8-15 (2016). doi:[10.1107/S2059798316002369](https://doi.org/10.1107/S2059798316002369)
- [7] Boutin, J. A., *et al.* S29434, a Quinone Reductase 2 inhibitor: Main biochemical and cellular characterization. *Molecular pharmacology* **95.3** 269-285 (2019). doi:[10.1124/mol.118.114231](https://doi.org/10.1124/mol.118.114231)
- [8] Bowler, M.W., *et al.* MASSIF-1: a beamline dedicated to the fully automatic characterisation and data collection from crystals of biological macromolecules. *J Synchrotron Radiat.* **22**, 1540-1547 (2015). doi:[10.1107/S1600577515016604](https://doi.org/10.1107/S1600577515016604)
- [9] Chapman, H., *et al.* Femtosecond X-ray protein nanocrystallography. *Nature* **470**, 73-77 (2011). doi:[10.1038/nature09750](https://doi.org/10.1038/nature09750)
- [10] Chaussavoine, I. Realisation of microfluidic chips for macromolecular X-ray crystallography. Master thesis (2016).
- [11] Cohen, A. unipuck website platform. http://smb.slac.stanford.edu/robosync/Universal_Puck/, 2004.
- [12] Chayen, N.E. Comparative studies of protein crystallisation by vapour-diffusion and microbatch techniques. *Acta Cryst.* **D54**, 8-15 (1998). doi:[10.1107/s0907444997005374](https://doi.org/10.1107/s0907444997005374)
- [13] DePonte, D. P., *et al.* Gas dynamic virtual nozzle for generation of microscopic droplet streams. *J. Phys. D: Appl. Phys.* **41**, 195505 (2008). doi:[10.1088/0022-3727/41/19/195505](https://doi.org/10.1088/0022-3727/41/19/195505)
- [14] Desjardins, K., *et al.* X-ray position-sensitive duo-lateral diamond detectors at SOLEIL. *Journal of synchrotron radiation* **25.2** 399-406 (2018). doi:[10.1107/S1600577517016769](https://doi.org/10.1107/S1600577517016769)
- [15] Dhoub, K., *et al.* Microfluidic chips for the crystallization of biomacromolecules by counter-diffusion and on-chip crystal X-ray analysis. *Lab on a Chip* **9.10** 1412-1421 (2009). doi:[10.1039/B819362B](https://doi.org/10.1039/B819362B)
- [16] Doye, J.P.K. and Poon, W.C.K. Protein crystallisation in vivo. *Curr. Opin. Coll. Interf. Sci* **11**, 40-46 (2006). doi:[10.1016/j.cocis.2005.10.002](https://doi.org/10.1016/j.cocis.2005.10.002)

- [17] Drenth, J. Principles of protein X-ray crystallography. Springer-Verlag New York (2007). doi:[10.1007/0-387-33746-6](https://doi.org/10.1007/0-387-33746-6)
- [18] Duran, D., *et al.* PROXIMA 2A – A New Fully Tunable Micro-focus Beamline for Macromolecular Crystallography. J. Phys.: Conf. Ser. **425**, 012005 (2013). doi:[10.1088/1742-6596/425/1/012005](https://doi.org/10.1088/1742-6596/425/1/012005)
- [19] Gabadinho, J., *et al.* MxCuBE: a synchrotron beamline control environment customized for macromolecular crystallography experiments. J Synchrotron Radiat. **17**, 700-707 (2010). doi:[10.1107/S0909049510020005](https://doi.org/10.1107/S0909049510020005)
- [20] Gerard, C. JJ, *et al.* Crystallization via tubing microfluidics permits both in situ and ex situ X-ray diffraction. Acta Crystallographica Section F: Structural Biology Communications **73.10** 574-578 (2017). doi:[10.1107/S2053230X17013826](https://doi.org/10.1107/S2053230X17013826)
- [21] Gerard, C. JJ, *et al.* "A chemical library to screen protein and protein–ligand crystallization using a versatile microfluidic platform." Crystal Growth & Design **18.9** 5130-5137 (2018). Doi: <https://doi.org/10.1021/acs.cgd.8b00572>
- [22] Grünbein, M. L., *et al.* Sample delivery for serial crystallography at free-electron lasers and synchrotrons. Acta Cryst. Struct. Biology **75.2** 178-191 (2019). doi:[10.1107/S205979831801567X](https://doi.org/10.1107/S205979831801567X)
- [23] Henniker plasma. Hpt-100 benchtop plasma treater reference. <https://plasmatreatment.co.uk/wp-content/uploads/2015/11/Henniker-plasma-product-brochure-HPT-100.pdf>.
- [24] Hasegawa, H. Simultaneous induction of distinct protein phase separation events in multiple subcellular compartments of a single cell. Exp. Cell Res **379**, 92-109 (2019). doi:[10.1016/j.yexcr.2019.03.010](https://doi.org/10.1016/j.yexcr.2019.03.010)
- [25] Hudson, S.D. Poiseuille flow and drop circulation in microchannels. Rheol Acta **49**, 237-243 (2010). doi:[10.1007/s00397-009-0394-4](https://doi.org/10.1007/s00397-009-0394-4)
- [26] Hall, D.B., *et al.* Spin coating of thin and ultrathin polymer films. Polymer Engineering and Science **38**, 2039-2045 (1998). doi:[10.1002/pen.10373](https://doi.org/10.1002/pen.10373)
- [27] Hilgart, M.C., *et al.* Automated sample-scanning methods for radiation damage mitigation and diffraction-based centering of macromolecular crystals. J Synchrotron Radiat. **18**, 717-722 (2011). doi:[10.1107/S0909049511029918](https://doi.org/10.1107/S0909049511029918)
- [28] Jacquamet, L., *et al.* Upgrade of the CATS sample changer on FIP-BM30A at the ESRF: towards a commercialized standard. J Synchrotron Radiat. **16**, 15-21 (2009). doi:[10.1107/S0909049508031105](https://doi.org/10.1107/S0909049508031105)
- [29] Jollès, J., *et al.* La structure chimique du lysozyme de blanc d'oeuf de poule: étude détaillée. Biochimica et Biophysica Acta **78** 668-689 (1963). doi:[10.1038/nchem.2714](https://doi.org/10.1038/nchem.2714)
- [30] Kabsch, W. XDS. Acta Cryst. **D66**, 125-132 (2010). doi:[10.1107/S0907444909047337](https://doi.org/10.1107/S0907444909047337)
- [31] Karplus, P.A. and Diederichs, K. Linking crystallographic model and data quality. Science **336**, 1030-1033 (2012). doi:[10.1126/science.1218231](https://doi.org/10.1126/science.1218231)
- [32] Klebe, G. Virtual ligand screening: strategies, perspectives and limitations. Drug Discov Today **11**, 580-594 (2006). doi:[10.1016/j.drudis.2006.05.012](https://doi.org/10.1016/j.drudis.2006.05.012)
- [33] Legrand, P. xdsme github platform. <https://github.com/legrandp/xdsme>, 2017

- [34] Le Maire, Albane, *et al.* In-plate protein crystallization, in situ ligand soaking and X-ray diffraction. *Acta Crystallographica Section D: Biological Crystallography* **67.9** 747-755 (2011). doi: [10.1107/S0907444911023249](https://doi.org/10.1107/S0907444911023249)
- [35] Lim, C.T., *et al.* Novel Dome-Shaped Structures for High-Efficiency Patterning of Individual Microbeads in a Microfluidic Device. *Small* **3**, 573-579 (2007). doi: [10.1002/sml.200790014](https://doi.org/10.1002/sml.200790014)
- [36] Lyubimov, A.Y., *et al.* Capture and X-ray diffraction studies of protein microcrystals in a microfluidic trap array. *Acta Cryst.* **D71**, 928-940 (2015). doi: [10.1107/S1399004715002308](https://doi.org/10.1107/S1399004715002308)
- [37] Madden, J.T., *et al.* Integrated nonlinear optical imaging microscope for on-axis crystal detection and centering at a synchrotron beamline. *Journal of synchrotron radiation* **20.4** 531-540 (2013). doi: [10.1107/S160057751601612X](https://doi.org/10.1107/S160057751601612X)
- [38] Martiel, I, *et al.* Strategies for sample delivery for femtosecond crystallography. *Acta Cryst.* **75.2** (2019). doi: [10.1107/S2059798318017953](https://doi.org/10.1107/S2059798318017953)
- [39] MicroChem. Su-8 2000 processing guidelines. https://kayakuam.com/wp-content/uploads/2019/09/SU-82000DataSheet2000_5thru2015Ver4.pdf
- [40] Moreno, A. Advanced Methods of Protein Crystallization. *Methods Mol Biol* **1607**, 51-76 (2017). doi: [10.1007/978-1-4939-7000-1_3](https://doi.org/10.1007/978-1-4939-7000-1_3)
- [41] Murshudov, G.N. *et al.* REFMAC5 for the refinement of macromolecular crystal structures. *Acta Cryst.* **D67** 355-367 (2011). doi: [10.1107/S0907444911001314](https://doi.org/10.1107/S0907444911001314)
- [42] Neutze, R., *et al.* Potential for biomolecular imaging with femtosecond X-ray pulses. *Nature* **406**, 752-757 (2000). doi: [10.1038/35021099](https://doi.org/10.1038/35021099)
- [43] Nierhaus, K.H. and Wilson, D.N. Protein synthesis and ribosome structure: translating the Genome. Wiley-VCH Verlag GmbH & Co (2004). doi: [10.1002/3527603433](https://doi.org/10.1002/3527603433)
- [44] Oh, K.W., *et al.* Design of pressure-driven microfluidic networks using electric circuit analogy. *Lab Chip*. **12**, 515-545 (2012). doi: [10.1039/c2lc20799k](https://doi.org/10.1039/c2lc20799k)
- [45] Olympus. BX43 Upright Microscope reference. <https://www.olympus-lifescience.com/en/microscopes/upright/bx43/>
- [46] Osserman, E. (Ed.). (2012). *Lysozyme*. Elsevier.
- [47] Pellegrino, S., *et al.* The Amaryllidaceae alkaloid haemanthamine binds the eukaryotic ribosome to repress cancer cell growth. *Structure* **26.3** 416-425 (2018). doi: [10.1016/j.str.2018.01.009](https://doi.org/10.1016/j.str.2018.01.009)
- [48] Protein Data Bank. website data distribution. <https://www.rcsb.org/stats/summary>
- [49] Ren, Z, *et al.* Crystal-on-crystal chips for in situ serial diffraction at room temperature. *Lab on a Chip* **18.15** 2246-2256 (2018). doi: [10.1039/c8lc00489g](https://doi.org/10.1039/c8lc00489g)
- [50] Roedig, P., *et al.* High-speed fixed-target serial virus crystallography. *Nat Methods* **14**, 805-810 (2017). doi: [10.1038/nmeth.4335](https://doi.org/10.1038/nmeth.4335)
- [51] Roessler, C.G., *et al.* Acoustic Injectors for Drop-On-Demand Serial Femtosecond Crystallography. *Structure* **24**, 631-640 (2016). doi: [10.1016/j.str.2016.02.007](https://doi.org/10.1016/j.str.2016.02.007)
- [52] Romoli, F., *et al.* SPINE-compatible ‘carboloops’: a new microshaped vitreous carbon sample mount for X-ray and neutron crystallography. *Acta Cryst.* **F70**, 681-684 (2014). doi: [10.1107/S2053230X14005901](https://doi.org/10.1107/S2053230X14005901)
- [53] Sandy, J., *et al.* Recent developments on beamline I02 at the Diamond Light Source. *Acta Cryst* **A69**, s149 (2013). doi: [10.1107/S0108767313098747](https://doi.org/10.1107/S0108767313098747)
- [54] Schönherr, R., *et al.* Protein crystallisation in living cells. *Biol Chem* **399**, 751-772 (2018). doi: [10.1515/hsz-2018-0158](https://doi.org/10.1515/hsz-2018-0158)

- [55] Sierra, R. G., *et al.* Nanoflow electrospinning serial femtosecond crystallography. *Acta Cryst.* **D68**, 1584-1587 (2012). doi:[10.1107/S0907444912038152](https://doi.org/10.1107/S0907444912038152)
- [56] SmarAct GmbH. Smargon website platform. <https://www.smaract.com/smargon>, 2020.
- [57] Sochol, R.D., *et al.* Hydrodynamic resettability for a microfluidic particulate-based arraying system. *Lab Chip*. **12**, 5051-5056 (2012). doi:[10.1039/C2LC40704C](https://doi.org/10.1039/C2LC40704C)
- [58] SOLEIL Synchrotron. website informations. <https://www.synchrotron-soleil.fr/en/about-us/what-soleil/soleil-3-questions>, 2016.
- [59] Tsutsui, H., *et al.* A diffraction-quality protein crystal processed as an autophagic cargo. *Mol. Cell* **58**, 186-193 (2015). doi:[10.1016/j.molcel.2015.02.007](https://doi.org/10.1016/j.molcel.2015.02.007)
- [60] Wampler, R. D., *et al.* Selective detection of protein crystals by second harmonic microscopy. *Journal of the American Chemical Society* **130**.43 14076-14077 (2008) doi:[10.1021/ja805983b](https://doi.org/10.1021/ja805983b)
- [61] Weierstall, U., *et al.* Lipidic cubic phase injector facilitates membrane protein serial femtosecond crystallography. *Nat Commun* **5**, 3309 (2014). doi:[10.1038/ncomms4309](https://doi.org/10.1038/ncomms4309)
- [62] Wijn, R., *et al.* A simple and versatile microfluidic device for efficient biomacromolecule crystallization and structural analysis by serial crystallography. *IUCrJ*. **6**, 454-464 (2019). doi:[10.1107/S2052252519003622](https://doi.org/10.1107/S2052252519003622)
- [63] Yano, J., *et al.* X-ray free electron lasers: applications in materials, chemistry and biology. Royal Society of Chemistry (2017). doi:[10.1039/9781782624097](https://doi.org/10.1039/9781782624097)
- [64] Zhang, S., *et al.* Versatile Microfluidic Approach to Crystallization. *Org. Process Res. Dev* **19**, 1837-1841 (2015). doi:[10.1021/acs.oprd.5b00122](https://doi.org/10.1021/acs.oprd.5b00122)
- [65] Zhang, W.Y., *et al.* Elastomer-supported cold welding for room temperature wafer-level bonding. 17th IEEE International Conference on Micro Electro Mechanical Systems. Maastricht MEMS 2004 Technical Digest, 741-744 (2004). doi:[10.1109/MEMS.2004.1290691](https://doi.org/10.1109/MEMS.2004.1290691)
- [66] Zhu, Z., *et al.* A Versatile Bonding Method for PDMS and SU-8 and Its Application towards a Multifunctional Microfluidic Device. *Micromachines* **7**, 230 (2016). doi:[10.3390/mi7120230](https://doi.org/10.3390/mi7120230)

Titre : Mise en place d'un système de mesures de données de diffractions *in-situ* à haut débit sur des échantillons biologiques

Mots clés : microfluidique, diffraction, synchrotron, cristallographie, *in-situ*

Résumé : Dans le domaine de la cristallographie biologique, la solution communément utilisée pour protéger les échantillons fragiles du faisceau de rayon x, est la congélation des échantillons. Un traitement chimique empêche la cristallisation de l'eau et de ce fait la destruction des échantillons, mais peut être un frein à la cristallisation de molécules sensibles. Pour contourner cette difficulté, les expériences sont effectuées à température ambiante dite *in-situ* en utilisant des données provenant d'un grand nombre d'échantillons pour contourner les difficultés de dommages de radiations. Les méthodes actuellement utilisés, dite de *serial crystallography*, récupèrent une fraction infime des données requises sur chacun des cristaux, ce qui amène à une forte consommation d'échantillon difficiles à se procurer. Cette thèse présente une approche, utilisant la microfluidique, permettant de placer et collecter automatiquement les cristaux biologiques sur un angle permettant de réduire drastiquement l'utilisation d'échantillon. Le but des travaux présentés est de mettre en place un système de mesures *in-situ* à haut débit, en tirant avantage des nouvelles avancées en développements de puces mi-

crofluidiques adaptées à des échantillons biologiques cristallins, en complément des approches robotiques mises en places sur la ligne PROXIMA-1. Les puces devront être munies de qualités particulières qui devront favoriser un chargement d'échantillons cristallins avec un minimum de stress externe ; supporter les environnement chimiques des échantillons ; disposer de manière périodique les cristaux tout au long de la puce ; être usinée dans un matériau permettant la prise de collectes de clichés de diffraction avec un minimum d'absorption et de diffusion en bruit de fond ; être adaptées au robot de changement d'échantillons opérationnel sur la ligne. Les travaux présentés vérifient les capacités de la puce à répondre à certaines difficultés actuelles de la cristallographie, comme la sensibilité de certains échantillons ou l'acquisition expérimentale de la phase, et examine les apports directs que cette technologie pourrait avoir sur le domaine, comme le trempage automatique de ligands, le confinement des échantillons, ou permettre une acquisition de donnée de diffraction sur des échantillons *in-cellulo*.

Title : Establishment of high-throughput *in-situ* diffraction data measurement methods applied to biological samples

Keywords : microfluidic, diffraction, *in-situ*, crystallography, synchrotron

Abstract : In the field of biological crystallography, the solution commonly adopted to protect fragile samples from the X-ray beam is the freezing of the samples. Chemical treatment prevents water crystallisation, therefore the destruction of samples, but can be an obstacle to the crystallization of sensitive molecules. To circumvent this difficulty, the experiments are carried out at room temperature called *in-situ* using data coming from a large number of samples to circumvent the difficulties of radiation damage. The methods currently used, called serial crystallography, recover a tiny fraction of the data required on each of the crystals, which leads to a high consumption of rare samples. This thesis presents an approach, using microfluidics, allowing to automatically place and collect biological crystals on an angle allowing to dras-

tically reduce the sample consumption. The aim of the work presented is to set up a high-throughput *in situ* measurement system, taking advantage of new advances in the development of microfluidic chips adapted to crystalline biological samples, in addition to the robotic approaches implemented on the PROXIMA-1 beamline. The chips will have to be provided with particular qualities which will favor a loading of crystalline samples with a minimum of external stress; withstand the chemical environment of the samples; periodically arranging the crystals throughout the chip; be machined from a material allowing the taking of diffraction collections with a minimum of absorption and background noise diffusion; be adapted to the operational sample changing robot on the line. The work presented verifies the capabilities of the chip to respond to certain current difficulties in crystallography, such as the sensitivity of certain samples or the experimental acquisition of the phase, and examines the direct contributions that this technology could have on the field, such as automatic soaking of ligands, confinement of samples, or allow acquisition of diffraction data on *in-cellulo* samples.